NANYANG TECHNOLOGICAL UNIVERSITY

CHARACTERISTICS OF HYDRAULIC RESISTANCE AND VELOCITY PROFILE IN VEGETATED OPEN-CHANNEL FLOWS

NGUYEN HOAI THANH

SCHOOL OF CIVIL AND ENVIRONMENTAL ENGINEERING

2012

CHARACTERISTICS OF HYDRAULIC RESISTANCE AND VELOCITY PROFILE IN VEGETATED OPEN-CHANNEL FLOWS

NGUYEN HOAI THANH

School of Civil and Environmental Engineering

A thesis submitted to the Nanyang Technological University
in fulfilment of the requirements for the degree of
Doctor of Philosophy

2012

ACKNOWLEDGEMENTS

First and foremost, I wish to express my sincere gratitude to my supervisor, Associate Professor Cheng Nian Sheng, for his valuable supervision, encouragement and enthusiasm throughout the entire years.

I am also grateful to all the staff members of CEE Hydraulics Laboratory, especially to Mr. Foo Shiang Kim and Mr. Lim Kok Hin for their devoted time and assistance in my experimental setup. Thanks are also due to my seniors and fellow research students in the hydraulics lab and DHI-NTU Centre who made my stay here joyful.

I cannot miss the chance to acknowledge the enduring love and moral support from my family. Their expectation and encouragement on me constitute the major source of my persistence on the long and winding road over the years.

Finally, the scholarship awarded by Nanyang Technological University for this research project is grateful acknowledged.

TABLE OF CONTENTS

ABSTRACT

The presence of vegetation in open-channel flow has significant influences on flow resistance, turbulence structures and sediment transport. This thesis sets out aims to evaluate the flow resistance and scale velocity profile in depth-limited flow conditions. It carries out flume experiments with arrays of cylinders to simulate rigid vegetation under emergent and submerged flow conditions. The thesis investigates the impact of vegetation on the flow resistance under emergent flow conditions. The resistance induced by simulated emergent vegetation in open channel flows has been interpreted differently in the literature, largely due to different definitions of friction factors or drag coefficients and due to different Reynolds numbers. By drawing analogies between pipe flows and vegetated channel flows, the thesis proposes a new friction function with a new Reynolds number which is defined using a vegetation-related hydraulic radius. This relation is useful for consolidating various experimental data across a wide range of vegetation density. Experimental results clearly show a monotonic decrease of the drag coefficient using the new Reynolds number, which is qualitative comparable to other drag coefficients for non-vegetated flows. A procedure for correcting sidewall and bed effects while evaluating vegetation drag is also proposed.

In addition, the thesis deals with the representative roughness height of submerged vegetation which is important factor to evaluate resistance in

submerged vegetated flows. By transforming the concept of hydraulic radius, a representative roughness height is proposed by considering the relative blockage caused by submerged vegetation which is related to stem diameter and vegetation density. The formula to estimate the average flow velocity and resistance coefficients for both cases of rigid and flexible vegetation was proposed by this study which results in more accurate flow rate predictions, especially for the case of low flow rates. The thesis shows that different formulas from previous studies, under certain conditions, share a general form.

Finally, the thesis proposes a length scale metric that normalises velocity profiles of depth-limited open channel flows with submerged vegetation using the plane mixing layer analogy. It considers the case of rigid vegetation submerged in shallow flows, of which the flow depth remains not greater than twice the vegetation height. The proposed scaling is better than those based on the logarithmic, velocity-defect and power laws in collapsing the velocity profiles, which is shown in experiments conducted in this thesis and also in those reported in the literature for a variety of flow and vegetation configurations. A simple viscosity model is developed to justify the scaling argument.

Keywords: vegetation, open channel flow, drag coefficient, roughness height, resistance, friction, Reynolds number, hydraulic radius, Manning coefficient, velocity profile, scaling, roughness sublayer, similarity, half-thickness.

LIST OF TABLES

LIST OF FIGURES

LIST OF SYMBOLS

A	=	frontal area of the vegetation stem;
B	=	channel width;
C_B	=	bed drag coefficient;
C_D	=	drag coefficient of vegetation;
C_{Dv}	=	drag coefficient [$= 2F_D/(\rho dHV_v^2)$];
c_p	=	Turbulence intensity, height-averaged over the vegetation height;
d	=	stem diameter;
d_{50}	=	median grain diameter;
D_f	=	total horizontal diffusivity;
D_{tl}	=	turbulent diffusion in the emergent vegetated flow;
D_{ul}	=	turbulent diffusion in the shear layer;
f	=	friction factor ($= 8grS/ V_v^2$);
F_D	=	vegetation-induced drag;
Fr	=	Froude number;
f_p	=	friction factor for the packed bed;
f_b	=	bed friction factor;
f_v	=	vegetation friction factor ($= 8gr_vS/V_v^2$);
f_w	=	sidewall friction factor;
f_{wS}	=	smooth-sidewall friction factor;
f_{wR}	=	rough-sidewall friction factor;
g	=	gravitational acceleration;
H	=	flow depth ($= h_s + h_v$);
h_*	=	flow depth corresponding to the maximum Reynolds stress;
h_{log}	=	lower limit of log-law zone;
h_p	=	penetration depth;
h_s	=	thickness of the flow above vegetation or surface layer;
h_v	=	height of vegetation;
k	=	constant;

K	=	coefficient of permeability;
k_s	=	equivalent roughness size;
k_{sb}	=	bed roughness height;
k_{sw}	=	sidewall roughness height;
k_T	=	turbulent kinetic energy per unit mass;
L	=	length of vegetation zone;
L_*	=	dimensionless void scale;
m	=	exponent;
N	=	number of vegetation elements per unit area of bed;
n	=	Manning roughness coefficient;
p	=	wetted perimeter;
p_b	=	bed-related wetted perimeter;
p_v	=	vegetation-related wetted perimeter;
p_w	=	sidewall-related wetted perimeter;
P_1,P_2	=	streamwise pressure forces exerting on the control volume;
Q	=	flow discharge;
q	=	flow discharge per unit width;
Re	=	Reynolds number;
Re_p	=	Reynolds number for flow through the packed bed;
Re_v	=	vegetation Reynolds number (= $V_v r_v / \nu$);
r	=	hydraulic radius;
r_b	=	bed-related hydraulic radius;
r_v	=	vegetation-related hydraulic radius;
r_{v*}	=	dimensionless vegetation-related hydraulic radius;
r_{vm}	=	corrected vegetation-related hydraulic radius;
r_w	=	sidewall-related hydraulic radius;
S	=	energy slope;
s	=	stem spacing;
t	=	time;
t_{ml}	=	shear layer thickness;

u_*	=	shear velocity (= $\sqrt{grS}$)
U	=	mean flow velocity ;
$u(z)$	=	flow velocity at the depth of z;
U_p	=	superficial velocity or flow through the packed bed;
U_s	=	average velocity in the surface layer;
U_v	=	average velocity in the vegetation layer;
u_{hv}	=	slip velocity at a distance $z = h_v$;
u_{max}	=	maximum flow velocity at the free surface;
u_{rms}	=	velocity fluctuation;
u_{s0}	=	characteristic constant flow velocity in non-submerged vegetation;
u_v	=	flow velocity in the vegetation layer;
u_ε	=	average velocity passing through the pore space;
u^*	=	friction velocity (wall friction velocity);
u^+	=	$(u-U_v)/(g\zeta_{1/2}S)^{1/2}$;
$-\overline{u'w'}$	=	Reynolds stress;
V	=	average flow velocity [$=Q/(BH)$];
V_a	=	average velocity approaching the stem;
V_v	=	average pore velocity [$=V/(1-\lambda)$] for emergent case;
w	=	vertical flow velocity;
W	=	weight of the control volume;
w_{rms}	=	vertical velocity fluctuation;
x, y, z	=	Cartesian coordinates;
z_1	=	lower limit of the shear layer;
z_2	=	upper limit of the shear layer;
α	=	exponent;
β	=	exponent;
δ_e	=	penetration of shear-scale turbulence into the canopy;
ΔP	=	pressure drop through a column of packed grains;
ΔU	=	$u_{max} - u_{z1}$;

$\Delta\eta$	=	zero-plane displacement;
ε	=	apparent turbulence viscosity;
ε^{+}	=	$\varepsilon/[(gS)^{1/2}(\zeta_{1/2})^{3/2}]$;
η	=	distance measured upwards from the edge of vegetation;
η_o	=	hydrodynamic roughness length;
κ	=	von Karman constant close to 0.4;
λ	=	vegetation density or fraction of vegetation-occupied volume;
ν	=	kinematic viscosity of fluid;
ν_t	=	eddy viscosity;
μ	=	dynamic viscosity;
θ	=	momentum thickness;
ρ	=	density of fluid;
τ	=	shear stress;
τ_0	=	bed-shear (bottom shear) stress;
τ_w	=	wall stress;
ζ	=	distance measured downwards from the free surface;
$\zeta_{1/2}$	=	half-thickness;

CHAPTER

1

INTRODUCTION

1.1 Background

Vegetation in rivers has significant influences on flow resistance, flow structures and sediment transport. Vegetated zones are important aspects in environmental and river management. They stabilize the habitat and ecology of natural and artificial systems. Therefore, understanding the hydrodynamics and sediment transport processes in vegetated open-channel would provide valuable scientific means to assess the impacts of vegetation on river flows. However, flow characteristics and associated transport processes for vegetated shallow flow conditions have received limited attention and are not yet well understood.

Open channel flows, once vegetated, the vegetation-induced drag increases the resistance and reduces the flow discharge in channels. The reduction in the mean velocity exerts significant changes on physical and biological processes in aquatic environments, and also leads to morphological changes of the floodplain. This explains why most of previous works on river hydrodynamics and mechanics of vegetated flows focused on the evaluation of flow structures

and resistance (Kouwen et al. 1969, Nepf and Vivoni 2000, Carollo et al. 2002, Jarvela 2002, Nezu and Sanjou 2008). Although these topics has been studied for decades, there still remains difficulties in evaluating vegetation resistance, particularly limited to the qualitative description of relevant flow phenomena. For example, the vegetation drag and its related Reynolds number have been defined in several different forms, leading to inconsistent conclusions even for simple cases, such as the emergent case. The roughness length scale is also an important factor when considering submerged vegetation in open channel flows, but it is still difficult to estimate. As a result, hydraulic engineers are undecided concerning the question of how to describe velocity profile and how to evaluate flow resistance and sediment transport rates, in the presence of vegetation.

The complexity in determining flow resistance under emergent and submerged flow conditions means that modeling flow distribution in vegetated open-channels becomes difficult. Although the flow velocity distribution in vegetated open-channel has been studied experimentally and analytically in the literature, it cannot be simply quantified for a large variety of flows and vegetation configurations, especially depth-limited vegetation flows. Previous works used logarithmic law or power-law distribution to describe the velocity profile of the zone above the vegetation. However, in shallow flow conditions, the major portion of the flow above vegetation may be characterized more appropriately as a roughness sublayer rather than an inertial sublayer where logarithmic law

applies. Within a roughness layer, local imbalance between production and dissipation of turbulent transport invalidates of logarithmic profiles (Nepf et al. 2007). Moreover, although important for characterizing vegetated open channel flows, the effect of interfacial transport and turbulence transfer has not been fully considered in scaling velocity profiles.

The works presented in this thesis are motivated by the above-mentioned gap in the literature.

1.2 Objectives

This work sets out to investigate the effect of vegetation on the flow resistance and mean flow properties in open-channel flow. It considers rigid vegetation submerged in shallow flows. More specifically, the thesis aims to:

1) Observe flow velocity profiles and turbulence characteristics affected by emergent and submerged vegetation in shallow flow condition.
2) Find more accurate velocity and length scales used for evaluating the flow resistance in emergent and submerged flow conditions.
3) Investigate how velocity profiles in vegetated open channel flows could be scaled for depth-limited flow conditions.

1.3 Layout of the thesis

The remaining of this thesis is organized as follows:

Chapter 2 reviews the literature on flows over vegetated open-channel flows. Methodologies, results and shortfalls of relevant works are categorized into groups of theoretical frameworks, experimental investigations and analytical studies.

Chapter 3 introduces the experimental setups and procedures, together with preliminary analysis.

Chapter 4 presents a proposed vegetation-related hydraulic radius and a redefined Reynolds number for vegetated open channel flows. Experiments are then carried out over emergent rigid vegetation in order to evaluate drag coefficients using the new Reynolds number.

Chapter 5 proposes a representative roughness height for quantifying the effect of submerged vegetation on flow resistance in the surface layer. It describes a new approach for estimating the average flow velocity and resistance coefficients for both cases of rigid and flexible vegetation. The new approach is compared against other formulas available in the literature.

Chapter 6 investigates how the velocity profile in vegetated open channel flows could be scaled for depth-limited conditions. A simple viscosity model is presented that helps to justify the scaling argument.

Chapter 7 concludes the thesis.

CHAPTER

2

LITERATURE REVIEW

2.1 Introduction

This chapter review related works on flow structures and resistance in vegetated open-channel flows. It also surveys common theories on open-channel flows.

2.2 Mean velocity in open-channel flows

Consider a two-dimensional (2-D) uniform open-channel flow over a channels without vegetation, shown in Fig. 2-1, where *u*, *w* denote the components of mean velocity and *u'*, *w'* are the velocity fluctuation. The shear stress in this flow is given by:

$$\tau = -\rho\overline{u'w'} + \mu\frac{\partial u}{\partial z} \tag{2.1}$$

where ρ is the fluid density, μ is the coefficient of dynamic viscosity, and *z* is the vertical coordinate. The bed stress, τ_b, and the related friction velocity u_* are defined as

$$\frac{\tau_b}{\rho} = u_*^2 = gHS \tag{2.2}$$

where g is the gravitational acceleration, *H* is the flow depth and *S* is the energy slope.

Prandtl (1925) applied the mixing-length concept to derive the mean velocity distribution over the channels without vegetaiton. The velocity distribution in the turbulent region close to the wall region is logarithmic,

$$\frac{u}{u_*} = \frac{1}{\kappa}\ln\left(\frac{zu_*}{\nu}\right) + A \tag{2.3}$$

where κ is the Karman constant with the value close to 0.40, ν is the kinematic viscosity of fluid, and *A* is a constant.

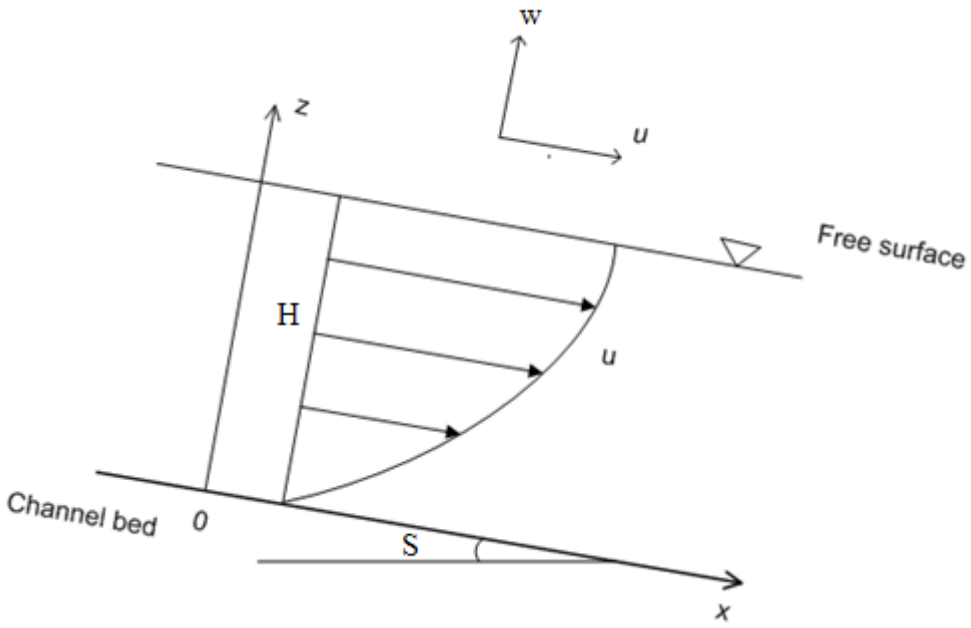

Fig. 2-1. Velocity distribution in uniform open-channel flow.

Flow resistance in open-channel flows

In open-channel flows, different methods have been developed for estimating energy losses caused by channel roughness. Chezy (1796) proposed the well-known formula for uniform flow:

$$V = C\sqrt{RS} \tag{2.4}$$

where V is the cross-sectional average velocity, R is the hydraulic radius, and C is a factor of flow resistance called Chezy's C.

In 1889, Manning presented a formula for fully rough flows, which was later modified to its present well-known form

$$V = \frac{1}{n} R^{2/3} S^{1/2} \tag{2.5}$$

where n is the coefficient of roughness (Chow 1959). There are many factors contributing to Manning's roughness coefficient, including surface roughness, vegetation and channel irregularity. Chow (1959) suggested for selecting n values in the form of surface photographs.

Turbulent flows over rough beds are important in hydraulic engineering, because almost all river beds contain large-scale roughness and complicated bed configurations. By modifying Prandtl's log law, Nikuradse (1933) used the equivalent sand roughness k_s to represent the effective height of the irregularities forming the roughness elements. In particular, k_s was taken as the

mean diameter of the sand grains. The velocity distribution over roughness beds can be shown as follows:

$$\frac{u}{u_*} = \frac{1}{\kappa}\ln\left(\frac{z}{k_s}\right) + B \tag{2.6}$$

where B is an adjustment parameter, which is shown to be equal to 8.5.

The location of the theoretical wall level at which $z = 0$ can be set at a distance δ below the top of the roughness elements. Nezu and Nakagawa (1993) showed that the range of δ/k_s is from 0.15 to 0.3.

2.3 Effects of vegetation on open-channel flows

Vegetation's influences on the flow characteristics have long been of interest to hydraulicians. The presence of vegetation on an open-channel flow affects velocity distributions, turbulence structures, and sediment transport. There have been numerous attempts in analyzing the vegetation's effect on flow, which can be categorized into two different approaches. One group used real vegetation as experimental media to collect data for developing empirical results, which can then be used under similar conditions. The other group conducted experiments in the laboratory flumes using rigid cylinders or flexible strips arranged in fixed patterns, in order to simulate the vegetation (Tsujimoto and Kitamura 1990, Nepf 1999, Carollo et al. 2002, Nezu and Sanjou 2008). The laboratory-based results have been found useful in helping to understand the basic mechanics of flow through vegetation.

2.3.1 Velocity distribution and flow resistance in vegetated open-channel flows

In normal open-channel flows, vertical velocity distributions have been assumed to be logarithmic (e.g. Chow 1959; Nezu and Nakagawa 1993). However, the presence of vegetation in channels induces drag to the flow and causes considerable changes in the velocity profile inside and above the canopy. In the cases of emergent vegetation, the velocity profile is mostly uniform over the depth (Tsujimoto and Kitamura 1990, Stone and Shen 2002). In the cases of submerged vegetation, the velocity profile is S-shaped (Kouwen et al. 1969, Temple 1986, Ikeda and Kanazawa 1996, Carollo et al. 2002). In all cases, the flow velocity inside the vegetation layer is significant smaller than that in the surface layer. Due to the interaction between surface and vegetation layers, the submerged condition becomes more complex than the emergent condition (Stone and Shen 2002).

To compare the velocity profile between emergent and submerged flow conditions, Liu et al. (2008) experimented with rigid dowels, using a Dantec one-dimensional laser Doppler velocimeter (LDV) to measure the flow velocity at multiple locations within the canopy (Fig. 2-2). The results indicated that flow characteristics inside the arrays of submerged canopy are similar to those observed in the emergent cases. A near-constant velocity dominates inside vegetation layer, which increases near the interface (Fig. 2-3). However, in both emergent and submerged cases, the flow velocity is strongly dependent on

vegetation density and varies significantly with different locations. In a low-density canopy, the velocity does change much, but in denser arrays, its variability much more observable in different locations. An important property is that under the fully submerged conditions, the velocity increases near the interface characterized by an inflection point.

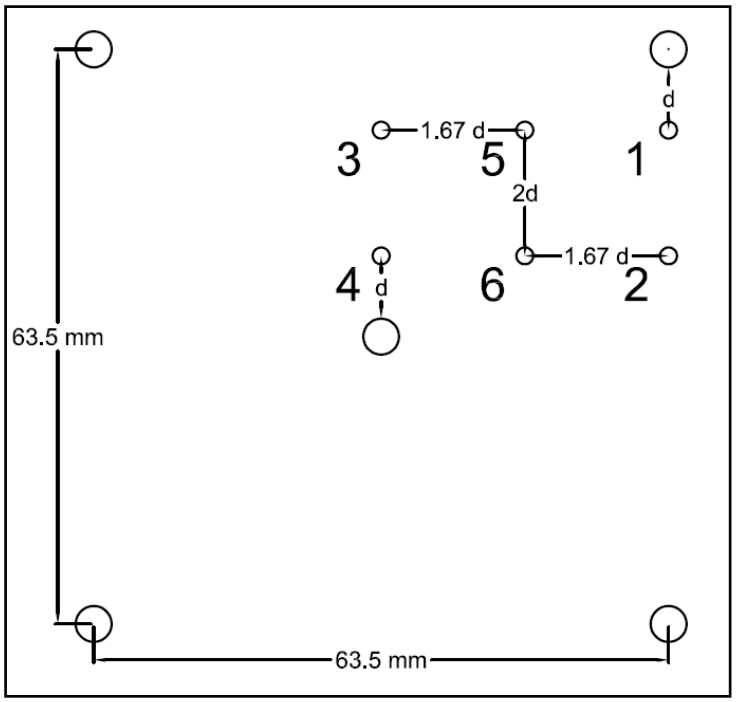

Fig. 2-2. Measurement locations for Liu et al.'s (2008) experiments. Flow direction is from top of page to bottom.

In submerged flow conditions, the velocity profile above the canopy is often assumed to be logarithmic. Kouwen et al. (1969) carried out flume experiments and analytical analysis to investigate velocity distributions over natural and artificial flexible roughness. The results indicated that flow field can be divided into two areas: one flow above the vegetation and another inside it (Fig. 2-4). They showed that the flow velocity outside the vegetation varies in proportion

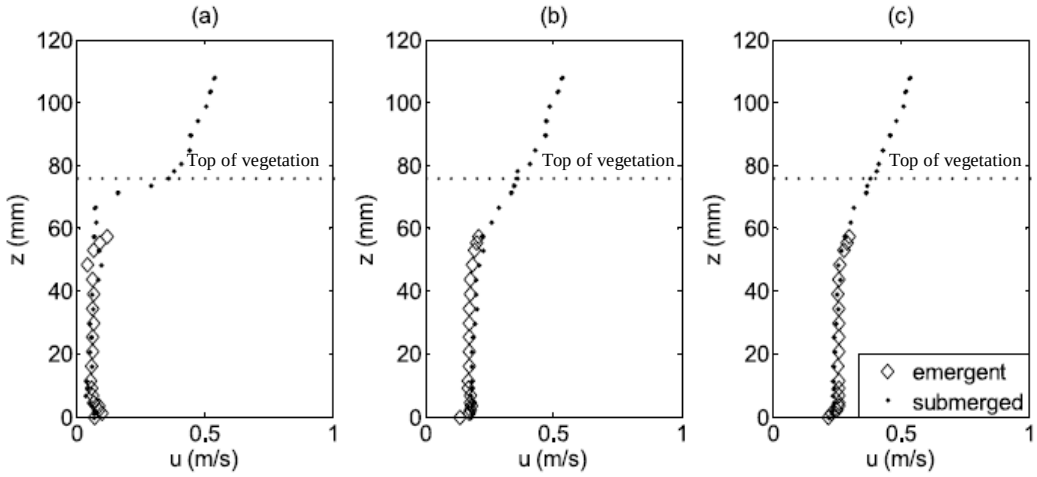

Fig. 2-3. Comparison between the emergent and fully submerged velocity profiles of Liu et al.'s (2008) experiments at (a) location 1, (b) location 3, and (c) location 5.

to the logarithm of the distance from the channel bed, which can be represented by the following equation:

$$\frac{u}{u_*} = \frac{u_{h_v}}{u_*} + \frac{1}{\kappa}\ln\left(\frac{z}{h_v}\right) \tag{2.7}$$

where u is the velocity at a distance, z, from the channel bed, h_v is the height of vegetation, and u_{hv} is a slip velocity taken at $z = h_v$.

Kouwen and Unny (1973) performed a series of experiments using plastic strips to simulate vegetation. The results suggested that the logarithmic velocity profile (2.7) is applicable above the reference distance ($z = h_v$).

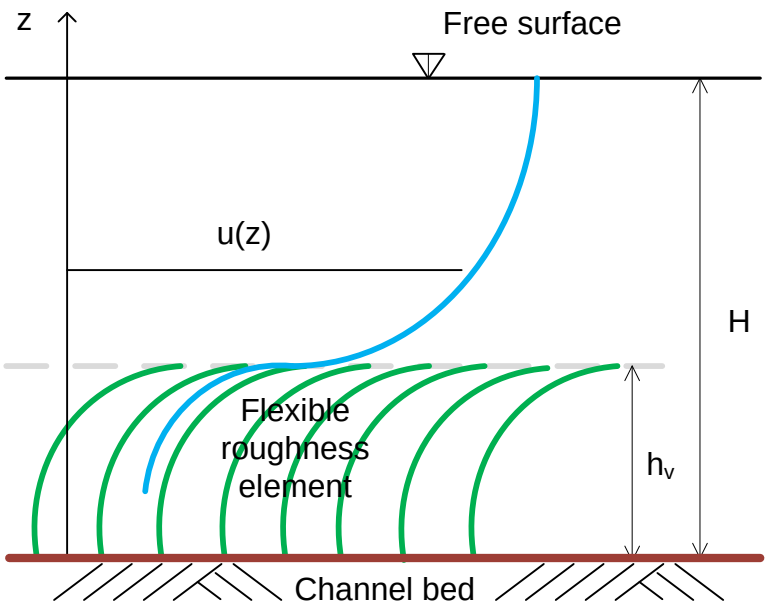

Fig. 2-4. Typical velocity profile above flexible artificial roughness observed by Kouwen et al. (1969).

Gourlay (1970) showed that for an energy slope less than 0.05, there are three distinct layers of flow: one with virtually constant low velocity near the bed, another with rapidly increasing velocity in the upper vegetation layer, and one with less rapidly increasing velocity above the vegetation. It was showed that the discontinuity between layer two and three occurs at the top of vegetation, and all vegetation bending occurs in layer two. The velocity in the bottom layer was found to be proportional to shear velocity, u_*. When $S \geq 0.05$, layer two and layer three merge to form a two layer appearance.

Christensen (1985) used the log law to calculate flow over the canopy as follows

$$\frac{u}{u_*} = \frac{1}{\kappa}\ln\left(\frac{z-(h_v - k_s/29.7)}{k_s}\right) + 8.5 \tag{2.8}$$

Carollo et al. (2002) studied the flow over flexible bottom vegetation by measuring flow velocity using a 2-D ADV. They analyzed the influence of the depth/vegetation height ratio, H/h_v, and the vegetation concentration (λ) on the velocity profiles. The velocity distributions are S-shaped comprised of three zones (Fig. 2-5):

(i) Zone I, $z < z_1 < h_v$, where the velocities are small but show a increasing trend.

(ii) Zone II, for $z_1 \leq z \leq z_2$, where the velocity profile is logarithm. There exists an inflection point at which the maximum turbulence intensity occurs.

(iii) Zone III, for $z > z_2$, where there is a positive vertical velocity gradient which decreases until it becomes null near the free

A linear relationship between z_1/H and h_v/H, and between z_2/H and h_v/H were found to follow

$$\frac{z_1}{H} = 0.865\frac{h_v}{H} \tag{2.9}$$

$$\frac{z_2}{H} = 0.15 + 0.865\frac{h_v}{H} \tag{2.10}$$

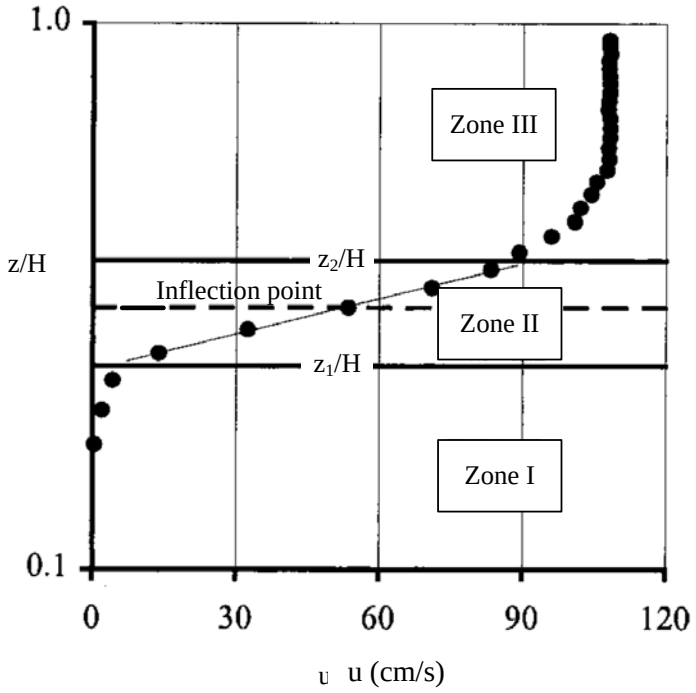

Fig. 2-5. Definition of three different zones by Carollo et al. (2002).

The relative depth z_1/H and z_2/H do not vary with the stem concentration λ. When λ decreases, the flow velocity increases inside and decreases above the vegetation.

Stephan and Gutknecht (2002) used flume experiments to study flow structures over flexible vegetation. The log-law was modified for the velocity above vegetation as follows:

$$\frac{u}{u_*} = \frac{1}{\kappa}\ln\left(\frac{z-h_v}{h_v}\right)+8.5 \tag{2.11}$$

To apply Eq. (2.11) in computing velocity profile, the shear velocity was calculated from the Reynolds stress $-\overline{u'w'}$.

This work has recently been extended by Jarvela (2005). It was shown that the approach was successful to represent flow structure above flexible vegetation. In addition, the shear velocity u_* can be evaluated using four different methods:

$$u_{*1} = \sqrt{gHS} \tag{2.12}$$

$$u_{*2} = \sqrt{g(H - h_v)S} \tag{2.13}$$

$$u_{*3} = \sqrt{g(H - h_*)S} \tag{2.14}$$

$$u_{*4} = \sqrt{-(\overline{u'w'})_{\max}} \tag{2.15}$$

where h_* is the flow depth corresponding to the maximum value of $-\overline{u'w'}$. The shear velocity u_{*2} found more practical compared to the other.

Two-layer approach

In the two-layer approach, the flow in and above the vegetation are treated separately. The shear stress gradient is derived from the momentum balance of the flow in the vegetation layer:

$$\frac{\partial \tau(z)}{\partial z} = F_D(z) - \rho g S \tag{2.16}$$

where τ is the shear stress and F_D is the drag force due to the drag around the cylinders within the stem layer. The shear stress depends on the turbulence near the bed, which is affected by water depth, vegetation properties and bed roughness. Inside the vegetation, turbulence is assumed to be mainly the wake turbulence. However, this assumption might not be valid in the case of vegetation with a low density, for the region near the top of the vegetation, or

for the near-bed region (Baptist et al. 2007). The turbulent shear stress is then described by a Boussinesq-type equation:

$$\tau(z) = \varepsilon \frac{du}{dz} \tag{2.17}$$

where ε is the turbulent viscosity that equals to ρv_t , and v_t is the eddy viscosity. The drag force F_D acting on the vegetation is defined as:

$$F_D(z) = NdC_D \frac{1}{2} \rho u(z)^2 \tag{2.18}$$

where N is the number of vegetation elements per unit area of bed, d is the diameter of the stem, and C_D is the drag coefficient of vegetation.

Klopstra et al. (1997) assumed that v_t is characterized by the product of velocity scale and a length scale of the large scale turbulence, that is responsible for the vertical transport of momentum. The characteristic length scale α is assumed to be independent of z. The turbulent shear stress (2.17) is then defined as:

$$\tau(z) = \rho \alpha u(z) \frac{du}{dz} \tag{2.19}$$

The flow velocity profile in the vegetation layer is given by

$$u_v = \sqrt{C_1 e^{-z\sqrt{2A}} + C_2 e^{z\sqrt{2A}} + u_{s0}^2} \qquad (0 < z < h_v) \tag{2.20}$$

where C_1 and C_2 are the integration constants, and u_{s0} is the characteristic constant flow velocity in non-submerged vegetation,

$$A = \frac{NdC_D}{2\alpha} \tag{2.21}$$

and

$$u_{s0} = \sqrt{\frac{2gS}{C_D Nd}} \tag{2.22}$$

C_1 and C_2 in (2.20) using boundary conditions are derived as

$$C_1 = \frac{-2gS(H - h_v)}{\alpha\sqrt{2A}(e^{k\sqrt{2A}} + e^{-k\sqrt{2A}})} \tag{2.23}$$

$$C_2 = -C_1 \tag{2.24}$$

For the surface layer, the log-law of Prandtl (1925) is applied:

$$\frac{u}{u_*} = \frac{1}{\kappa}\ln\left(\frac{z - (h_v - \delta_s)}{k_s}\right) \qquad (z \geq h_v) \tag{2.25}$$

where δ_s is the vertical shift of the virtual zero-level of the logarithmic profile and k_s is the length scale of the virtual bed roughness of the surface layer. Using the continuity condition, both the value and gradient of the flow velocity of the vegetation and the surface layer should be equal at the vegetation edge ($z = h_v$). The values of δ_s and k_s are:

$$\delta_s = g\frac{1 + \sqrt{1 + \frac{4.E^2\kappa^2(H - h_v)}{g}}}{2.E^2\kappa^2} \tag{2.26}$$

$$k_s = \delta_s e^{-F} \tag{2.27}$$

where

$$E = \frac{\sqrt{2.A}C_3 e^{h_v\sqrt{2A}}}{2.\sqrt{C_3 e^{h_v\sqrt{2.}} + u_{v0}^2}}$$

$$F = \frac{\kappa\sqrt{C_3 e^{h_v\sqrt{2A}} + u_{v0}^2}}{\sqrt{g(H-(h_v-\delta_s))}} \qquad (2.28)$$

$$C_3 = \frac{C_2}{S}$$

$$u_{v0} = \frac{u_{s0}}{\sqrt{S}}$$

With (2.20) and (2.25), the velocity profile of flow in and above vegetation is established. The unknown parameter is the α. Using physical model tests, Klopstra et al. (1997) showed a correlation between α and flow and vegetation characteristics:

$$\alpha = 0.0793 h_v \ln\frac{H}{h_v} - 0.00090 \quad \text{and} \quad \alpha \geq 0.001 \qquad (2.29)$$

which is later confirmed by using Meijer and Van Velzen's (1998) flume experiments with prototype scale and confirmed the applicability of the Klopstra et al.'s model for field conditions. It was also reported that α is independent of the vegetation density and flow conditions. More specifically

$$\alpha = 0.0144\sqrt{Hh_v} \qquad (2.30)$$

Baptist et al. (2007) derived the velocity profile inside and above the canopy analytically. Unlike Klopstra et al. (1997) who used α to determine the eddy viscosity v_t, Baptist et al. (2007) employed mixing-length theory:

$$\nu_t(z) = lk_T = c_p l u(z) \tag{2.31}$$

where l is the mixing length determined by the space between the vegetation, k_T is the turbulent kinetic energy per unit mass, and c_p is the turbulence intensity. The value of c_p is estimated by

$$c_p = \frac{(1/h_v)\int_0^{h_v}\sqrt{h_v(z)}dz}{(1/h_v)\int_0^{h_v}\sqrt{u(z)}dz} \tag{2.32}$$

Solving the momentum balance equation (2.16**)**, arrives at:

$$u_v = \sqrt{u_{s0}^2 + ae^{z/L} + be^{-z/L}} \tag{2.33}$$

where a, b are the integration coefficients, and u_{s0} is uniform velocity in non-submerged vegetation which is calculated by

$$u_{s0} = \sqrt{\frac{2gS}{C_D N d}} \tag{2.34}$$

and L is the length scale given by

$$L = \sqrt{\frac{c_p l}{C_D N d}} \tag{2.35}$$

Equation (2.33) consists of two exponential parts, one near the top, described by $ae^{(z/L)}$ and the other near the bed, described by $be^{(-z/L)}$. Thus, the values of the integration constants a and b determine the shape of the profile. To estimate the depth-averaged velocity through the vegetation, a constant value for b was assumed to be negligible. This means that there is a decrease of the velocity

from the top of the vegetation downward, until (for sufficiently high vegetation) the uniform flow velocity u_{s0} is reached, as shown in Fig. 2-6.

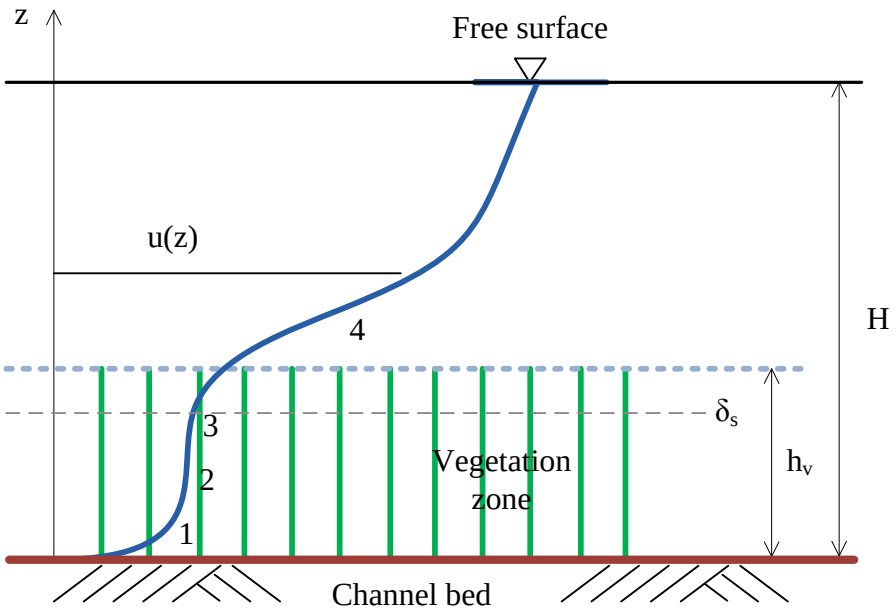

Fig. 2-6. Four zones in the vertical profile for horizontal velocity through and over vegetation by Baptist et al. (2007).

Finally, the equation describing the velocity profile inside vegetation is simplified as:

$$u_v = \sqrt{S\left(u_{v0}^2 + a_v e^{z/L}\right)} \tag{2.36}$$

where

$$u_{v0} = \sqrt{\frac{2g}{C_D N d}}$$
$$a_v = \frac{2Lg(H - h_v)}{c_p l e^{h_v/L}} \tag{2.37}$$

For the velocity profile above the vegetation, Baptist et al. (2007) assumed a logarithmic profile that included a zero-plane displacement δ_s:

$$\frac{u}{u_*} = \frac{1}{\kappa}\ln\left(\frac{z-\delta_s}{k_s}\right) \tag{2.38}$$

δ_s corresponds to the vertical position of the centroid of momentum absorption. It was calculated using the formula proposed by Thom (1971):

$$\delta_s = \frac{\int_0^{h_v} \frac{d\tau(z)}{dz} z dz}{\int_0^{h_v} \frac{d\tau(z)}{dz} dz} \tag{2.39}$$

The roughness height k_s was calculated using the boundary condition at the top of the vegetation that the flow velocity of the vegetation profile, $u_v(h_v)$, equals the flow velocity of the overlying logarithmic profile, $u_o(h_v)$. Thus:

$$\delta_s = h_v - L(1-e^{-h_v/L}) \tag{2.40}$$

$$k_s = (h_v - \delta_s)e^{\left(-\kappa\sqrt{\frac{2L}{c_p l}\left(1+\frac{L}{H-h_v}\right)}\right)} \tag{2.41}$$

where the turbulence intensity c_p is given by:

$$c_p = \frac{1}{20}\frac{H-h_v}{l} \tag{2.42}$$

The two-layers approach has been used to evaluate the average velocities for vegetated open-channel flows, for example Stone and Shen (2002), Defina and Bixio (2005), and Huthoff et al. (2007). By describing the bulk behavior of

flows, Stone and Shen (2002), and Huthoff et al. (2007) avoided the necessity of integration over depth and the associated complexity of depth-dependent turbulence intensities. The model can be used to quickly evaluate mean velocity in field applications. The values of δ_s and k_s were discussed by Defina and Bixio (2005) and Huthoff et al. (2007).

Huthoff et al. (2007) developed an analytical model for determining the depth-average velocity in submerged flow conditions. Vegetation was simulated using cylindrical stems, while the flow field was divided into two layers (Fig. 2-7). The results were compared against laboratory experiment data. The average velocity in the resistance layer, U_v, *is* determined by considering a balance between the streamwise component of the gravitational force, bed resistance, form drag, and shear stress due to flow over the vegetation. Particularly:

$$U_v = \sqrt{\frac{2bgS}{1+\frac{2b}{H}f}} \qquad \text{for emergent condition, } H \le h_v \tag{2.43}$$

$$U_v = \sqrt{\frac{2bgS}{1+\frac{b}{32h_v}\left(\frac{k_s}{H}\right)^{1/3}}} \qquad \text{for submerged condition, } H \ge h_v \tag{2.44}$$

where f is the bed resistance function, and b is the drag length:

$$b = \frac{1}{C_D N d} \tag{2.45}$$

In addition, the scaling equation for the average velocity in the surface layer is

$$\frac{U_s}{U_v} \sim \left(\frac{H - h_v}{l} \right)^{\frac{2}{3}\left(1 - \left(\frac{H}{h_v}\right)^{-\alpha}\right)} \tag{2.46}$$

where l is the scaling length and α is the transition exponent.

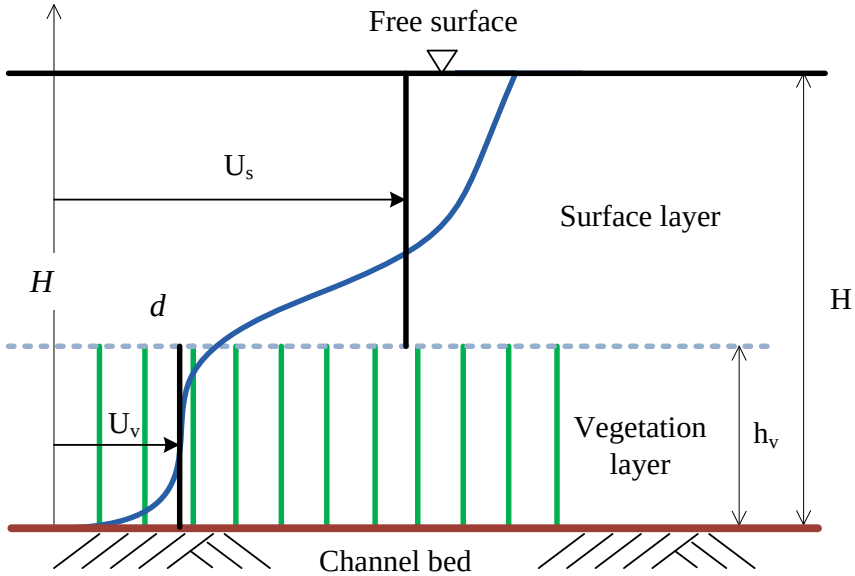

Fig. 2-7. The two-layer approach for flow with submerged vegetation (Huthoff et al., 2007).

Summary of two-layer approach

Table 2-1 summaries two-layer approaches. In general, the flow velocity inside the canopy depends on the vegetation characteristics, i.e. d, N, h_v, the flow depth H, the energy gradient S, and most importantly the drag coefficient C_D. Above vegetation, most of the related works simulate the flow distribution using log-law. In cases, the flow velocity profile for the zone above vegetation also depends on C_D. Therefore, the validation of the predicted velocity profile is predicated on the selection of C_D.

Table 2-1. Summary of two-layer approach for vegetated open-channel flows.

Investigator	**Year**	**Results**	**No. of Equation**
Kouwen et al.	1969	$\frac{u}{u_*}=\frac{u_{h_v}}{u_*}+\frac{1}{\kappa}\ln\left(\frac{z}{h_v}\right)$	(2.7)
Christensen	1985	$\frac{u}{u_*}=\frac{1}{\kappa}\ln\left(\frac{z-(h_v-k_s/29.7)}{k_s}\right)+8.5$	(2.8)
Stephan and Gutknecht	2002	$\frac{u}{u_*}=\frac{1}{\kappa}\ln\left(\frac{z-h_v}{h_v}\right)+8.5$	(2.11)
Klopstra et al.	1997	For the emergent case, $u_{s0}=\sqrt{\frac{2gS}{C_D N d}}$	(2.22)
		For the submerged case, $u_v=\sqrt{C_1 e^{-z\sqrt{2A}}+C_2 e^{z\sqrt{2A}}+u_{s0}^2}$ for $(z<h_v)$ $\frac{u}{u_*}=\frac{1}{\kappa}\ln\left(\frac{z-(h_v-h_s)}{k_s}\right)$ for $(z\geq h_v)$	(2.20) (2.25)

Table 2-1. Summary of two-layer approach for vegetated open-channel flows (cont.).

Investigator	**Year**	**Results**	**No. of Equation**
Baptist et al.	2007	$u_v = \sqrt{S\left(u_{v0}^2 + a_v e^{z/L}\right)}$ for ($z < h_v$) $\frac{u}{u_*} = \frac{1}{\kappa}\ln\left(\frac{z-\delta_s}{k_s}\right)$ for ($z \geq h_v$)	(2.36) (2.38)
Huthoff et al.	2007	$\frac{u}{u_*} = \frac{1}{\kappa}\ln\left(\frac{z-\delta_s}{k_s}\right)$ for ($z \geq h_v$) For submerged condition, $H \geq h_v$: $U_v = \sqrt{\frac{2bgS}{1+\frac{b}{32h_v}\left(\frac{k_s}{H}\right)^{1/3}}}$ The scaling equation for the average velocity in the surface layer: $\frac{U_s}{U_v} \sim \left(\frac{H-h_v}{l}\right)^{\frac{2}{3}\left(1-\left(\frac{H}{h_v}\right)^{-\alpha}\right)}$	(2.38) (2.44) (2.46)

2.3.2 Turbulence structures in vegetated open-channel flows

Aquatic plants affect flow characteristics such as the mean and turbulence structure, and mixing dynamics. Similar results are found when studying air flow over forest, e.g., Raupach (1986) and Raupach et al. (1996). Raupach et al. (1996) observed that the mean streamwise velocity profile of wind over vegetation canopy is similar to that of a plane mixing layer, leading to

proposing a mixing layer analogy for atmospheric canopy flows. The plane mixing layer is the turbulent shear flow formed in the region between two coflowing streams of different velocities. This region contains a strong inflection point in the mean velocity profile (Fig. 2-8) which leads to the creation of coherent eddies and hydrodynamic instability processes.

Fig. 2-8. The plane mixing layer, showing the vorticity thickness δ_w by Roupach et al. 1996.

For flow through flexible vegetation, Nepf and Vivoni 2000 showed a strong shear layer developing at the top of the canopy. The flow on the canopy is driven mainly by turbulent stress caused by the vertical transport of momentum from the overlying flow, with negligible contribution from pressure gradients. The phenomena was explained clearly by exploring the transition from the emergent to the submerged regime. First, the flow force within the canopy shifts from pressure-driven to stress-driven. Second, the primary source of turbulence production shifts from stems wakes to the shear layer at the top of

the canopy. Third, the principal mechanism for momentum exchange with the surrounding water column shifts from longitudinal advection to vertical turbulent exchange. In the case of submerged vegetation, the mean velocity profile has an inflection point near the vegetation edge causing the significant shear instability and the maximum turbulence intensity (Ikeda and Kanazawa 1996, Nepf and Vivoni 2000, Carollo et al. 2002, Jarvela 2002, Nezu et al. 2006, Nezu and Sanjou 2008). In such the condition, the drag discontinuity at the interface and the momentum transfered from the over-canopy layer toward the bed are obstructed by vegetation elements. This leads to Reynolds stress peaking just below the top of the canopy and decaying downwards (Nepf and Vivoni 2000, Nezu and Sanjou 2008). In the emergent case, the Reynolds stress is negligible because there is no vertical transport of momentum from the over-canopy layer.

Thompson and Roberson (1976) defined three zones of the velocity distribution:

- A viscous sublayer of height δ' occurring adjacent to the channel bottom.

- A zone below the top of the roughness elements of height h_v, and above the viscous sublayer. This is considered to be influenced by intensive turbulence mixing.

- A zone above the top of the roughness elements, which is considered free of local vortex effects.

The term “penetration depth” was first used by Nepf and Vivoni (2000), in which the Reynolds stress $-\overline{u'w'}$ decays to 10% of its maximum value. It was suggested that the vegetated flow could be divided into two regions, above and below the penetration depth, as shown in Fig. 2-9. The lower canopy is called the “longitudinal exchange zone”, and the upper canopy is called the “vertical exchange zone”. Within the longitudinal exchange zone, the vertical transport of momentum is negligibly small, and the flow is determined by a balance of pressure gradient and vegetative drag. These conditions are considered the same in an emergent canopy condition ($h_p = H$).

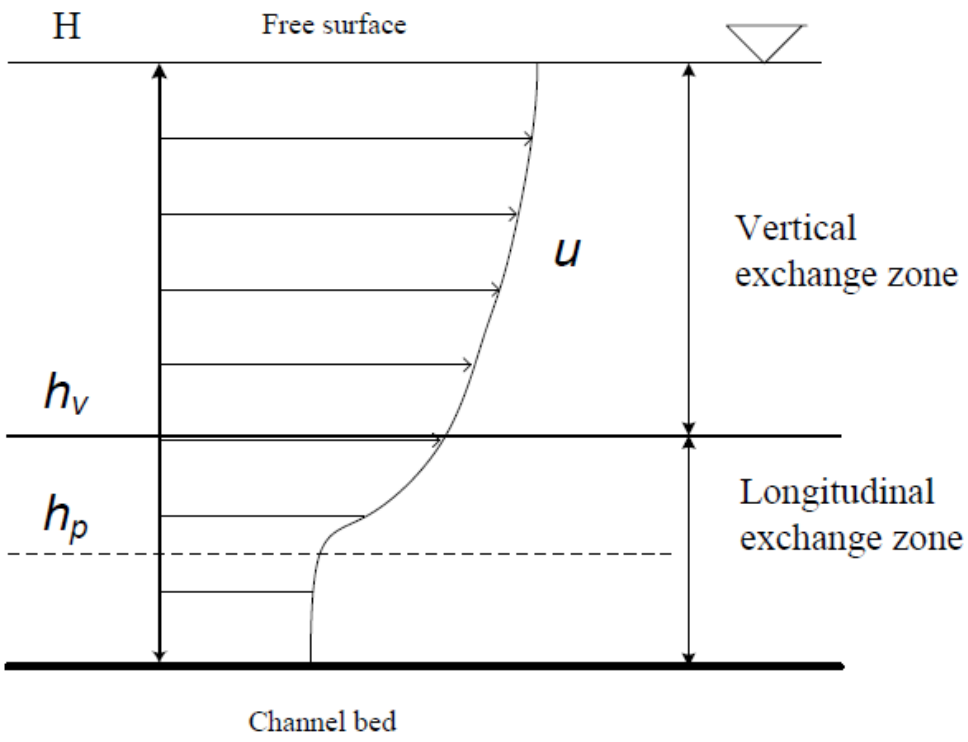

Fig. 2-9. Schematized flow model for aquatic canopy flow by Nepf and Vivoni, 2000.

Within the vertical exchange zone ($z > h_p$) turbulent stress contributes to the momentum balance within the canopy. The pressure gradient and associated longitudinal transport are present, but become less important as the depth of submergence increases. When the canopy becomes submerged, the zone appears at the top of the canopy and deepens into the canopy as the depth of submergence increases. Nepf and Vivoni (2000) observed that a logarithmic velocity profile exists for $H/h_v > 1.25$ and h_p depends on the drag coefficient C_D and the canopy density.

Poggi et al. (2004) modeled the effect of vegetation density on the canopy sub-layer. It was showed that the flows within and just above the foliage behave as a perturbed mixing layer due to the presence of an extensive and dense canopy. The canopy sub-layer was divided into three zones (Fig. 2-10). In the first zone ($z/h_v << 1$), the flow field is dominated by small vortices connected with von Kármán vortex streets. The second zone, which spans the canopy top, is a superposition of attached eddies and Kelvin–Helmholtz waves produced by inflectional instability in the mean longitudinal velocity profile. In the third zone ($z/h_v >> 2$), the flow's behavior fits in the classical surface-layer similarity theory.

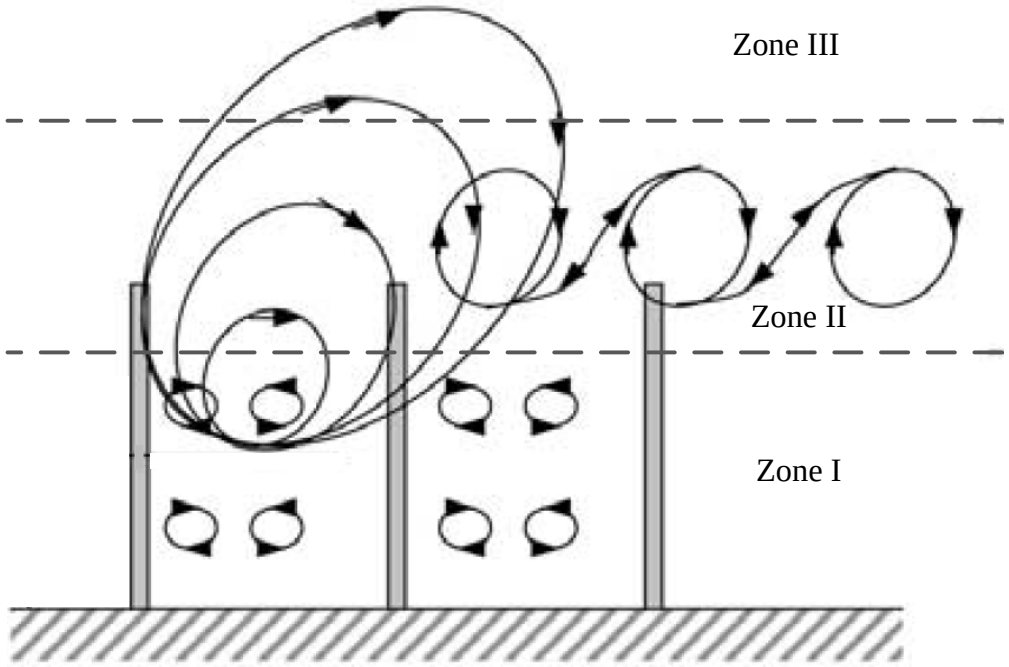

Fig. 2-10. Schematized flow structure by Poggi et al. (2004).

Finnigan et al. (2009) proposed a phenomenal model to explain the differences between turbulence in the canopy and the inertial sublayer above, which agrees with a large set of observations from real and model canopies.

Ghisalberti and Nepf (2004, 2006) used flume experiments with rigid and flexible model vegetation to study vertical mass transport and the structure of coherent vortices in vegetated shear flows. Regarding turbulent vertical momentum transport, the flow region was divided into two sub-zones, as shown in Fig. 2-11. The upper region ($z_1 < z < H$) is called the “exchange zone”, while the lower region ($0 < z < z_1$) is called the “wake zone”. The upper limit z_1 of a wake zone occours where the shear layer vortices from above have negligible

effects. In a wake zone with negligible shear and limited water renewal, the turbulence length scale and intensities are diminished. Assuming that vertical transport in the wake zone is dominated by stem wakes, the diffusivity is an order of magnitude lower than that in the exchange zone. The upper limit of the shear layer z_2, occurs where $-\overline{u'w'}$ has decayed to zero. The shear layer thickness is represented by t_{ml} (= $z_1 - z_2$) and the total shear by $\Delta U / t_{ml}$.

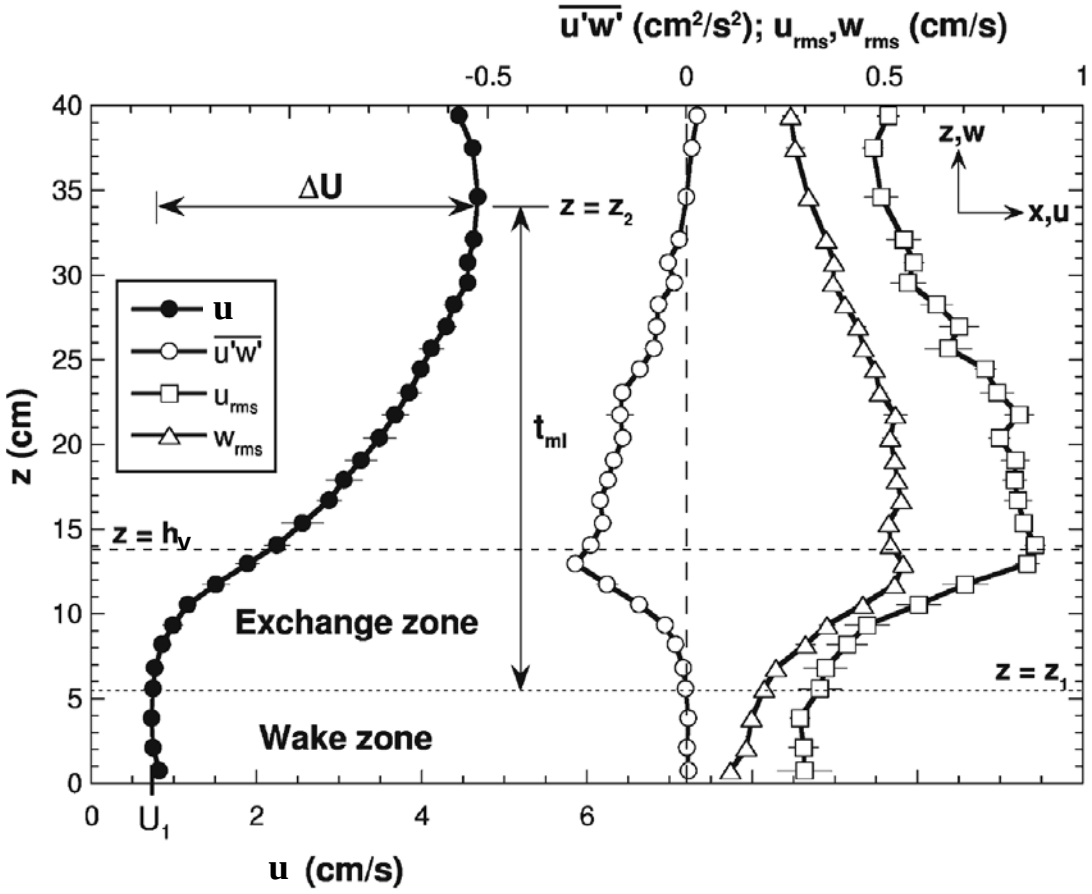

Fig. 2-11. Definition of the shear layer variables (Ghisalberti and Nepf, 2006).

Nepf and Ghisalberti (2008) parameterized δ_e as the penetration of shear-scale turbulence into the canopy. The shear layer, which induced by canopy generates

shear vortices, penetrates a distance δ_e into the canopy. Taking into account the turbulent kinetic energy budget at the shear-layer scale, δ_e can be derived as:

$$\frac{\delta_e}{h_v} = \frac{0.23 \pm 0.06}{C_D a h_v} \tag{2.47}$$

where a is the frontal area per canopy volume.

According to Nepf et al. (2007), in the case of small values of canopy drag ($C_D a h_v < 0.2$), the vortex penetrates to the bed, i.e., $\delta_e = h_v$. The scaling (2.47) breaks down when $(C_D a)^{-1}$ approaches the scale of the canopy elements d.

Ghisalberti (2009) studied of the hydrodynamic similarities among different obstructed shear flows that are partially obstructed by a permeable medium (e.g. submerged vegetation, sediment bed and urban canopy). The similarities are expected if Kelvin-Helmholtz instability dominates the interfacial layer. Due to the discontinuous drag at the top of the canopy, a shear layer is generated and dominated by the mixing process. The main velocity profile reveals a clear point of inflection, and therefore, is inviscidly unstable to perturbation. In the shear layer, the Kelvin-Helmholtz vortices govern interfacial transport and create instabilities.

Nezu and Sanjou (2008) used the penetration concept to model canopy flows. The flow region is divided into the three sub-zones: emergent zone ($0 \leq z \leq h_p$), mixing-layer zone ($h_p \leq z \leq h_{log}$), and log-law zone ($h_{log} \leq z \leq H$) (Fig. 2-12) . In the emergent zone, the flow velocity is almost constant due to strong wake effects of vegetation stems, leading to the flow structure in this region to

resemble that of an emergent canopy. This zone is similar to the ‘‘longitudinal exchange zone’’ (Nepf and Vivoni 2000) in which the vertical transport of momentum is negligibly small.

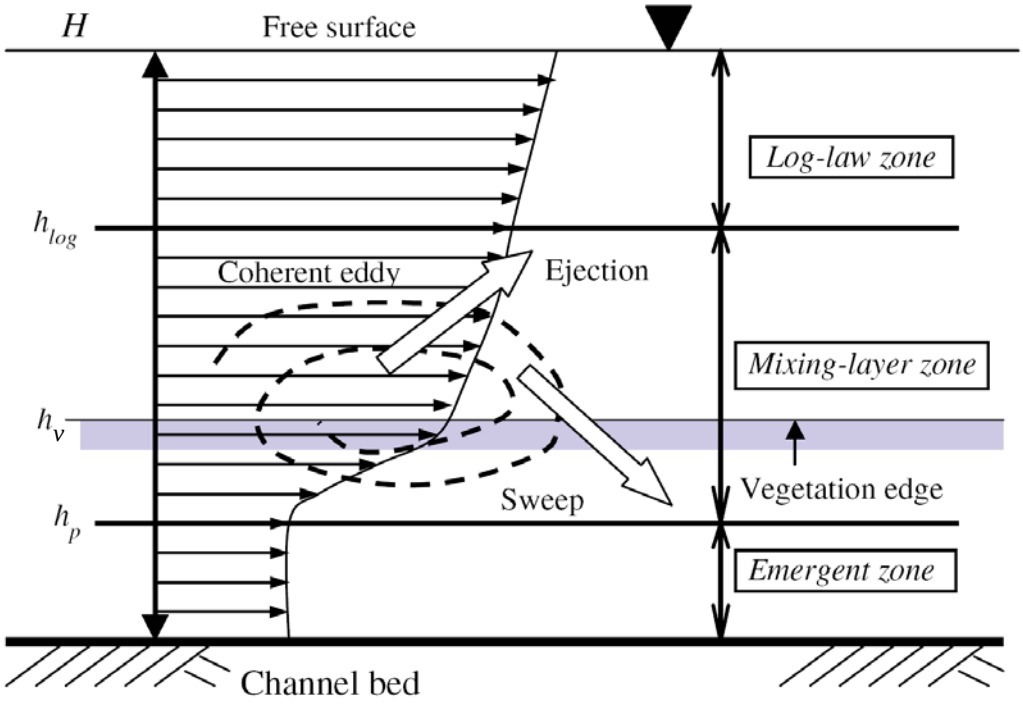

Fig. 2-12. Schematized flow model for aquatic canopy flow (Nezu and Sanjou, 2008).

While Nepf and Vivoni (2000) and Ghisalberti and Nepf (2006) considered the whole upper zone as the exchange zone, Nezu and Sanjou (2008) divided it into two zones: the “mixing-layer” zone and “log-law” zone. In the latter zone ($h_{log} \leq z \leq H$), the turbulence structure is similar to that in boundary layers and open-channel flows with rough beds. Hence, the log-law for rough beds could be applicable for describing vegetated flows. Experimental results indicated that if submergence becomes low, the thickness of the log-law zone, i.e., $H - h_{log}$,

becomes smaller and disappears at the critical depth where $H/h_v = h_c/h_v \approx 1.5$ - 2.0. The value of h_c may be dependent on aquatic vegetation density and flexibility. The relationship between the thickness of the mixing-layer zone (δ) with the momentum thickness (θ) of the mixing layer is such that δ normalized by θ is constant of 5.0 - 6.0. θ can be determined by using the hyperbolic tangent-type profile [Raupach et al. (1996), Ghisalberti and Nepf (2002)] as follows:

$$\frac{u-\overline{U}}{\Delta U} = \frac{1}{2}\tanh\left(\frac{z-\bar{z}}{2\theta}\right) \tag{2.48}$$

where ΔU is the velocity difference of the mixing layer ($\Delta U = U_2 - U_1$), U_1 and U_2 are the margin velocity at the lower and upper margins h_p and h_{log} of the mixing layer, respectively. Furthermore, $\overline{U} = (U_2 - U_1)/2$ and $\bar{z} = (h_{log} + h_p)/2$.

Table 2-2. Summary of turbulence structure in vegetated open-channel flows.

Investigator	**Results**
TURBULENT CHARACTERISTICS IN VEGETATED OPEN-CHANNEL FLOWS	
Ikeda and Kanazawa (1996), Nepf and Vivoni (2000), Carollo et al. (2002), Juha (2002), Nezu et al. (2006), Nezu and Sanjou (2008)	The mean velocity profile has an inflection point near the vegetation edge, which causes the significant shear instability and the maximum turbulence intensity.
Nezu and Sanjou (2008)	The horizontal turbulent intensity, u_{rms}, attains maximum just above the canopy. The vertical turbulence intensity, w_{rms}, attains maximum just below the canopy.
Nepf and Vivoni (2000), Nezu and Sanjou (2008)	The Reynolds shear stress peaks just below the top of the canopy and decays downwards
Nepf and Vivoni (2000)	The term “penetration depth”: h_p was defined at which the Reynolds stress $-\overline{u'w'}$ decays to 10% of its maximum value.

Table 2-2. Summary of turbulence structure in vegetated open-channel flows (cont.).

Investigator	**Results**
THE DIVISION OF FLOW REGION	
Nepf and Vivoni (2000)	The flow region was divided into two zones (Fig. 2-9). - Longitudinal exchange zone: $z \leq h_p$ - Vertical exchange zone: $z > h_p$
Poggi et al. (2004)	The flow region was divided into three zones (Fig. 2-10). - Zone I: $z/h_v << 1$ - Zone II is spanning the canopy top - Zone III: $z/ h_v >> 2$
Ghisalberti and Nepf (2004, 2006)	The flow region was divided into two zones (Fig. 2-11). - Wake zone: $0 < z < z_1$ - Exchange zone: $z_1 < z < H$
Nezu and Sanjou (2008)	The flow region was divided into three zones (Fig. 2-12). - Emergent zone: $0 \leq z \leq h_p$ - Mixing-layer zone: $h_p \leq z \leq h_{log}$ - Log-law zone: $h_{log} \leq z \leq H$

2.3.3 Drag and diffusion

Drag coefficient

In vegetated open-channel flows, the drag comprises three components, grain roughness, form roughness, and vegetative roughness. For most vegetated channels, the drag caused by vegetation contributes most to the flow resistance. It particularly reduces the mean flow within the vegetated zone (Nepf 1999). The flow depth and residence time also increase with the drag of vegetation. (Nepf 1999; Nepf 2000; Poggi et al. 2004; Takemura and Tanaka 2007; Nezu and Sanjou 2008; Wu et al. 2008; Kothyari et al. 2009; Poggi et al. 2009) used force equilibrium to evaluate the drag of the vegetal, while others (e.g. Li and Shen 1973; Stone and Shen 2002) modeled vegetative drag based on cylinders drag.

Nepf (1999) modeled the drag, turbulence, and diffusion for flow through emergent vegetation using laboratory experiments with cylindrical stems. Assuming that the production of turbulence within stem wakes (P_w) balances the viscous dissipation ε for emergent vegetation, relationship of the bulk drag coefficient, $\overline{C_D}$, and a dimensionless population density of vegetation, $ad = d^2/\Delta S$ (where ΔS is the mean spacing between cylinders) can be described as follows

$$\frac{\sqrt{k_t}}{u} = \alpha_1 \left(\overline{C_D} ad\right)^{1/3} \tag{2.49}$$

where α_1 is a scale coefficient and k_t is the turbulent kinetic energy per unit mass. It can be seen that the turbulence intensity increases with the bulk drag coefficient and population intensity. In contrast, since, using the force balance,

$$(1 - C_v d) C_B u^2 + \frac{1}{2} \overline{C_D} ad \left(\frac{H}{d}\right) u^2 = gH \frac{\partial h}{\partial x} \tag{2.50}$$

where C_B is the bed drag coefficient, the bulk drag coefficient decreases when the population density of vegetation (ad) increases. For ad > 0.01 at the emergent condition, the diffusion is reduced within the stems due to the reduction in eddy scale. The total horizontal diffusivity D_f is:

$$\frac{D_f}{ud} = \alpha \left(\overline{C_D} ad\right)^{1/3} + \left(\frac{\beta^2}{2}\right) ad \tag{2.51}$$

where α and β are scale factors.

Nepf and Vivoni (2000) observed that, in flexible canopy, $C_D(z)$ increases toward the bed, reflecting the increasing viscous effects with decreasing plant-scale Reynolds number, $Re_p = du/v$. Above the bed, the value C_D aproximates 1 in emergent flow condition. The decrease of C_D towards the interface is due to the relaxation of form drag as the flow bleeds around the free end (Fig. 2-13).

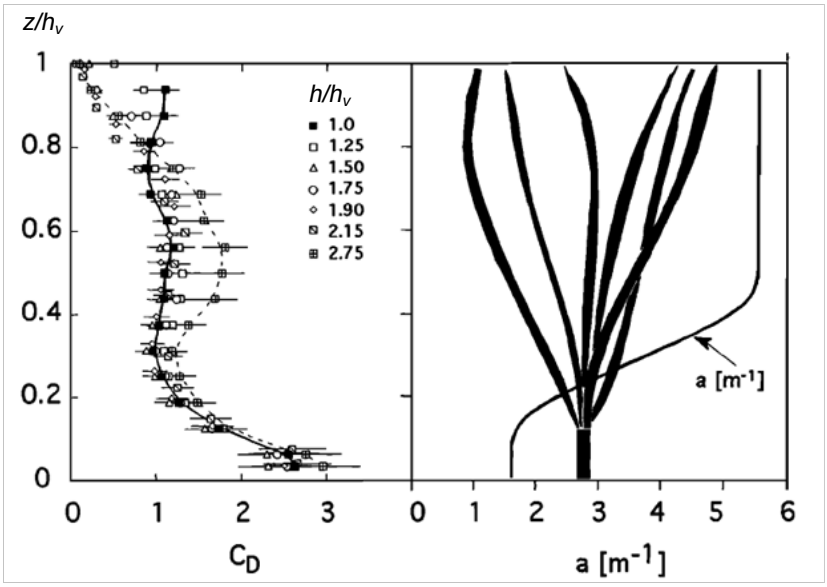

Fig. 2-13. Profile of vegetative drag (Nepf and Vivoni, 2000).

Poggi et al. (2004) combined the aerodynamic force per unit volume in the mean momentum equation in order to estimate drag coefficient as:

$$C_D(z,\mathrm{Re},a) = -2\left(\frac{d\overline{u'w'}}{dz}+\frac{d\overline{p}}{dx}\right)\left(au^{-2}\right)^{-1} \tag{2.52}$$

where p is the kinematic pressure. It was showed that C_D decreases from the bed and with the increasing vegetation density and Reynolds number. Other works confirmed these results (e.g. Tanino and Nepf 2008; Nezu and Sanjou 2008).

The drag coefficient has also been studied using cylinder drag by Li & Shen (1973) and Stone & Shen (2002). Li and Shen (1973) considered a group of cylinders with various setups in non-submerged flow conditions. Experimental results indicated that flow depend heavily on by patterns or groupings. Four

contributing factors to the drag coefficient were identified: the flow turbulence, non-uniform velocity profile, free surface effects, and effect of blockage. Stone & Shen (2002) investigated the hydraulic resistance using cylindrical roughness and showed that the drag coefficient C_{Dm} based on the constricted cross-sectional velocity U_c is more accurate than C_D since it is closer to the drag coefficient of single cylinder. The relationship between C_D and C_{Dm} is:

$$C_D = C_{Dm} \frac{U_c^2}{U_l^2} \tag{2.53}$$

where U_l is the apparent vegetation layer velocity and U_c is the surface layer velocity (Fig. 2-14), moreover,

$$U_l = \left(1 - \sqrt{\frac{4\lambda}{\pi}}\right) \sqrt{\frac{g(1-\lambda l^*)\pi d}{2\lambda l^* C_D}} \sqrt{S} \tag{2.54}$$

where l^* is h_v/H.

Fig. 2-14. Definitions of U_c and U_l in the vegetation layer.

Diffusion in vegetated open-channel flows

Vegetation also affects the flow regime, and hence the vertical transport which tends to increase vertical diffusivity above the canopy and reduce it within the canopy (Ghisalberti and Nepf 2005). (Nepf and Vivoni 2000; Poggi et al. 2004; Nepf and Ghisalberti 2008) showed that vegetation drag restricts the penetration of the Kelvin-Helmholtz vortices, and the flow field can be split into two zones with different turbulent characteristics. In the emergent vegetated flow, as in the lower region of submerged condition, the stem diameter d and the velocity U_l controlling the turbulent diffusion follows the equation:

$$D_{tl} = (0.17 \pm 0.08) U_l d \tag{2.55}$$

For the upper region ($z > h_v - \delta_e$), the vertical turbulent diffusion scales on the size of the Kelvin-Helmholtz vortices (Ghisalberti and Nepf 2005; Nepf and Ghisalberti 2008). The average diffusivity in the upper canopy is

$$D_{tu} = (0.019 \pm 0.003) \Delta U t_{ml} \tag{2.56}$$

Similar to the Reynolds' stress, the turbulent diffusivity peaks at the top of the canopy where $D_{tu}(z = h_v) \approx 0.032 \Delta U t_{ml}$.

Double averaged methodology has been developed to study the complex interaction between subdivisions of the flow rather than the simple partition into mean and turbulence. Double averaging method was originally developed for the atmospheric boundary layer flows (e.g. Finnigan, 2000) and defined for aquatic ecosystems (e.g. Nikora et al., 2007). Double-averaging is needed for

obtaining representative spatially averaged flow measurements which is a practical impossibility in a real plant canopy. The double-averaging procedure gives the continuity, momentum, advection-diffusion, energy and other high order equations for the fluid phase, which are averaged in both time and space domains. Double averaged equations explicitly contain important terms such as form-induced and fluxes, and for the flow region below roughness tops, form and viscous drag terms, wake and waving production terms.

2.4 Summary

Flow resistance induced by vegetation in open channels flows has been a subject of extensive research. However, the conclusion drawn are often inconsistent, which calls for a general formula for calculating drag coefficient or the roughness height. Consequently, describing velocity profile and evaluating flow resistance in the presence of vegetation, still remain an open question.

The velocity profile of flows over submerged vegetation could be divided into two or three layers. However, this has not been considered sufficiently for depth-limited vegetation flow condition. Some works demonstrated that the logarithmic law can present the velocity profile measured in the surface layer, but such profile exists only high above the canopy. In addition, within the vegetation and some distance above it, a local imbalance between production

and dissipation of turbulent transport invalidates the use of logarithmic profiles (Nepf et al. 2007). Besides that, the length scale associated with roughness size used in the log law is still difficult to calculate. Therefore, an issue raised here is how to describe properly velocity profiles under depth-limited flow with submerged vegetation.

CHAPTER 3

EXPERIMENTAL SET-UP AND PROCEDURE

3.1 Introduction

This chapter details the experiments, describing the flow system, artificial vegetation arrays, measuring techniques, experimental procedure and data collection approaches.

All the experiments are carried out in a straight flume with a rectangular cross section at the Hydraulics Laboratory of Nanyang Technological University. Uniform flows with six sets of artificial vegetation arrays are considered. The chosen flow depths for each experiment represent both emergent and submerged vegetation conditions. They are not greater than twice the vegetation height, so that the velocity profile in submerged shallow flow conditions can be examined. The streamwise and vertical components of flow velocity are measured using a two-dimensional Laser Doppler Anemometer (LDA) and a two-dimensional Electromagnetic Current Meter (EMCM).

3.2 Flume system

The flume used in the experiments is a rectangular flume (12 m length, 0.3 m wide, and 0.45 m deep), with glass walls and a steel bottom. There is a flow straightener device placed at the entrance section of the flume to minimize entrance effects on flows at the section tested. At the end of the flume, a reservoir is connected to a tailgate that that can be used to adjust the flow depth. The flume resides on an I-beam supported by a hinged platform at one end and a screw jack at the other. The jack can be adjusted to change the flume slope. Fig. 3-1 and Fig. 3-2 are the photographs and schematic drawing of the facility, respectively.

Water is circulated by a water pump, passing through the pipelines, head and tail tank. The maximum flow rate of the pump is 45 L/s, which is monitored with a flow meter and controlled with two valves, one manual and one electronic.

Fig. 3-1. Photographs of the flume.

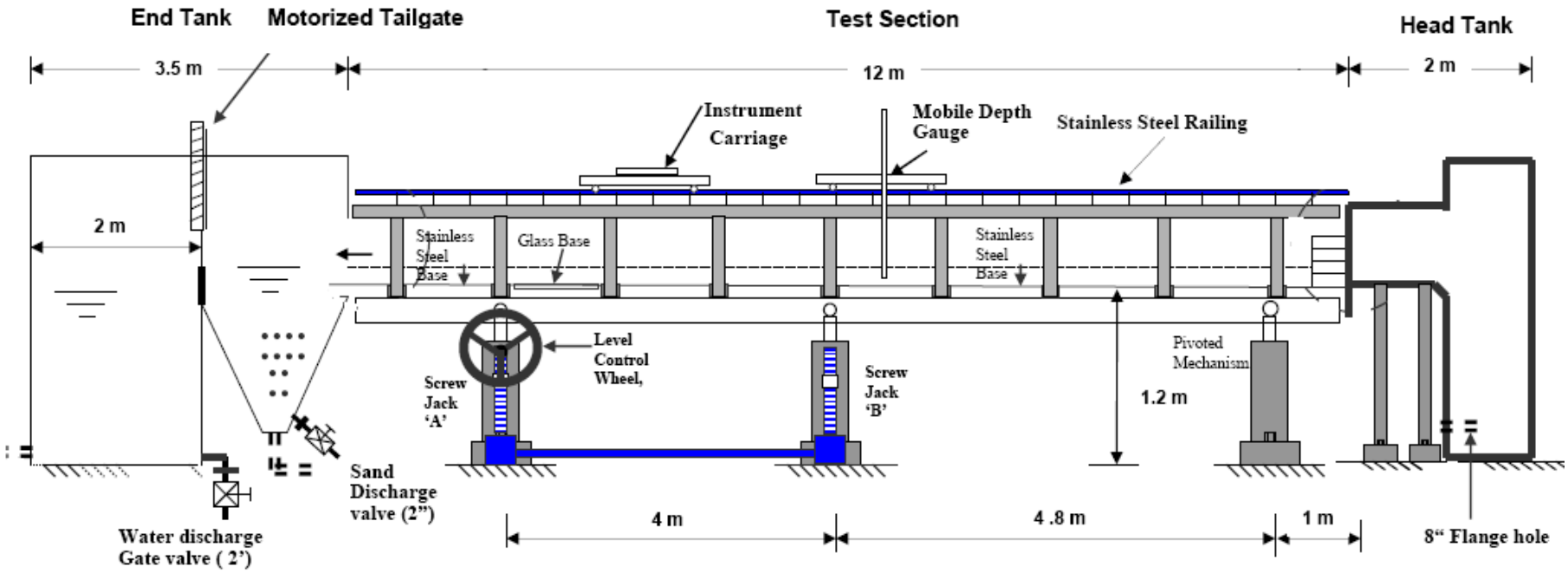

Fig. 3-2. Schematic of the flume system.

3.3 Vegetation configuration

The vegetation is assumed to consist of shoots with cylindrical morphology, and therefore could be modeled as an array of circular cylinders. The rigid cylinder array is ideal for modeling the flow-vegetation interaction, as it provides a reasonable morphological approximation of the stem region. Six arrays of rigid rods were set on PVC plates and placed at the flume bottom to simulate the vegetation. The artificial vegetation covered a 9.6 m long portion of the flume (Fig. 3-1).

Six vegetation configurations were tested in the experiments. The rods were arranged in staggered pattern and labeled in the form of A (B or C) + number. Here, A, B, and C represent different diameters of rods, and the number is the distances between any two neighboring rods (in mm). The arrangement is shown in Table 3-1. The rods had a uniform length of 100 mm (Fig. 3-3). Various flow depths H were set to cover both cases of emerge and submerged vegetation. For submerged flow conditions, the flume slope was fixed at 0.004 (see Table 3-3), which was calculated from the longitudinal flow depth variations measured using a point gauge accurate to 0.1 mm while water in the flume remained stationary. Different slopes were used to simulate emergent flow conditions. The flow depths along the flume were measured to ensure that experiments are in uniform flow conditions. The Reynolds number (defined as VR/ν) varied from 1.0×10^3 to 1.5×10^5, and the Froude number (defined as $V/(gH)^{0.5}$) varied from 0.07 to 0.25, where $V = Q/(BH)$, Q is the flow discharge,

B is the channel width, H is the flow depth, $R = BH/(B+2H)$ and ν is the kinematic viscosity of fluid. Table 3-2 and Table 3-3 show a summary of experimental conditions for emergent and submerged flow conditions respectively.

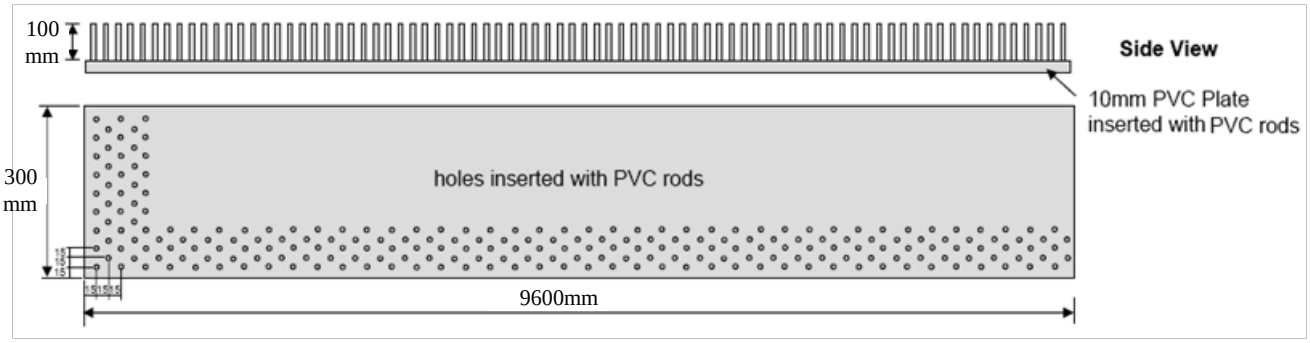

Fig. 3-3. Vegetation model.

Table 3-1. Vegetation configurations.

Model	***d* (mm)**	**N (Rods/m^2)**	
A60	3.2	556	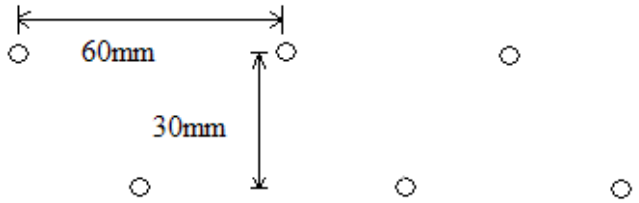
B60	6.6	556	
C60	8.3	556	
A30	3.2	2222	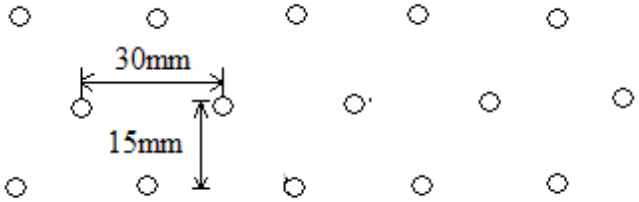
B30	6.6	2222	
C30	8.3	2222	
Note: N is the number of stem per unit area of bed			

.

Table 3-2. Summary of experimental conditions for emergent cases.

Model	Stem diameter d (mm)	Vegetation density λ	Energy slope S	H (cm)								
				2	3	4	5	6	7	8	9	10
				Q (l/s)								
A60	3.2	0.0043	0.00950	0.52	0.74	1.11	1.41	1.65	1.93	2.27	2.58	2.75
			0.00186	0.71	1.14	1.58	2.00	2.47	2.84		3.74	4.12
			0.00047			0.69	0.86	1.16	1.34	1.39	1.48	1.61
B60	6.6	0.0192	0.00122		0.53	0.66	0.83	1.08	1.28	1.41	1.59	1.84
			0.00196	0.49	0.68	0.96	1.26	1.49	1.81	2.07	2.22	2.51
			0.00410	0.64	0.97	1.41	1.74	2.13	2.54	2.95	3.29	3.80
			0.00811	1.06	1.40	1.97	2.58	3.19	3.75	4.29	4.84	5.45
C60	8.3	0.0298	0.00100			0.61		0.97		1.35	1.31	1.43
			0.00200		0.62	0.75		1.22		1.74	1.89	2.21
			0.00400		0.83	1.07		1.71		2.83	2.74	3.19
A30	3.2	0.0173	0.00100			0.60		0.94		1.25	1.46	1.60
			0.00200		0.63	0.86		1.30		1.68	1.93	2.12
			0.00400		0.90	1.20		1.92		2.56	2.76	2.90
B30	6.6	0.0769	0.00100		0.24	0.28		0.42		0.60	0.66	0.71
			0.00200				0.58	0.64	0.69	0.79	0.94	1.02
			0.00374				0.74	0.87	1.04	1.26	1.38	1.59
			0.00750		0.67	0.81	1.06	1.29	1.55	1.79	2.08	2.34
C30	8.3	0.1189	0.00103						0.47	0.58	0.63	0.66
			0.00197					0.46	0.54	0.62	0.68	0.82
			0.00386			0.50	0.62	0.71	0.84	0.97	1.11	1.26
			0.00808			0.64	0.84	1.03	1.18	1.39	1.64	1.80

Note: λ is the vegetation density ($\lambda = N\pi d^2 / 4$).

Table 3-3. Experimental data collected for submerged cases.

Run	Discharge Q (m^3/s)	Channel width B (m)	Flow depth H (m)	Energy slope S	Vegetation density λ (%)	Stem diameter d (m)	Vegetation height h_v (m)	Number of stems per unit area N ($/m^2$)
A30-13	0.0056	0.3	0.13	0.004	1.73	0.0032	0.1	2221
A30-15	0.0076	0.3	0.15	0.004	1.73	0.0032	0.1	2221
A30-17	0.0111	0.3	0.17	0.004	1.73	0.0032	0.1	2221
A30-20	0.0152	0.3	0.20	0.004	1.73	0.0032	0.1	2221
A60-13	0.0099	0.3	0.13	0.004	0.43	0.0032	0.1	556
A60-15	0.0128	0.3	0.15	0.004	0.43	0.0032	0.1	556
A60-17	0.0161	0.3	0.17	0.004	0.43	0.0032	0.1	556
A60-20	0.0205	0.3	0.20	0.004	0.43	0.0032	0.1	556
B30-13	0.0038	0.3	0.13	0.004	7.69	0.0066	0.1	2221
B30-15	0.0059	0.3	0.15	0.004	7.69	0.0066	0.1	2221
B30-17	0.0079	0.3	0.17	0.004	7.69	0.0066	0.1	2221
B30-20	0.0095	0.3	0.2	0.004	7.69	0.0066	0.1	2221
B60-13	0.0062	0.3	0.13	0.004	1.92	0.0066	0.1	556
B60-15	0.0096	0.3	0.15	0.004	1.92	0.0066	0.1	556
B60-17	0.0123	0.3	0.17	0.004	1.92	0.0066	0.1	556
B60-20	0.0161	0.3	0.20	0.004	1.92	0.0066	0.1	556
C30-13	0.0030	0.3	0.13	0.004	11.90	0.0083	0.1	2221
C30-15	0.0046	0.3	0.15	0.004	11.90	0.0083	0.1	2221
C30-17	0.0072	0.3	0.17	0.004	11.90	0.0083	0.1	2221
C30-20	0.0114	0.3	0.20	0.004	11.90	0.0083	0.1	2221
C60-13	0.0059	0.3	0.13	0.004	2.98	0.0083	0.1	556
C60-15	0.0079	0.3	0.15	0.004	2.98	0.0083	0.1	556
C60-17	0.0116	0.3	0.17	0.004	2.98	0.0083	0.1	556
C60-20	0.0154	0.3	0.20	0.004	2.98	0.0083	0.1	556

3.3.1 Laser Doppler Anemometer (LDA)

Flow velocities were measured using a 2-D Laser Doppler Anemometer (LDA) manufactured by DANTEC. Mean velocity components *u* and *w* correspond to the stream-wise (*x*) and vertical (*z*) directions, respectively. The system comprises an integrated four beams, two-component laser-optic unit, laser generator and signal processor, and a traversing system, together with a PC installed with the application software.

The working principles of Laser Doppler Anemometry are shown in Fig. 3-4. The LDA measures velocities at a point in a flow with optical access to the measurement point provided that micro-sized seeding particles present. The measurements are performed at the intersection of two laser beams, where there is an interference fringe pattern of alternating light and dark planes. Seeding particles scatter the light, which appears to flash, as the particles pass through the bright planes of the interference pattern. The back-scattered light is captured by the FlowLite transmission/receiving optics. A photomultiplier then converts the light intensity fluctuations to electrical signals, and then into velocity information in the BSA processor. The frequency of the flashing light (Doppler frequency) is proportional to the flow velocity at the measurement point. The results are processed by BSA Flow Software. Two components of the velocity vector can be acquired simultaneously. The analysis also can produce other statistics, such as RMS values or cross moments which allow for the calculation of Reynolds stresses.

The LDA probe was mounted on an automated traversing system that could move within ±0.1 mm in three orthogonal directions (see Fig. 6-5). The seeding particles [Titanium (IV) oxide TiO2 powder, less than 5 µm in diameter] were used to trace flows with a satisfied sampling rate, i.e. 100-300 Hz.

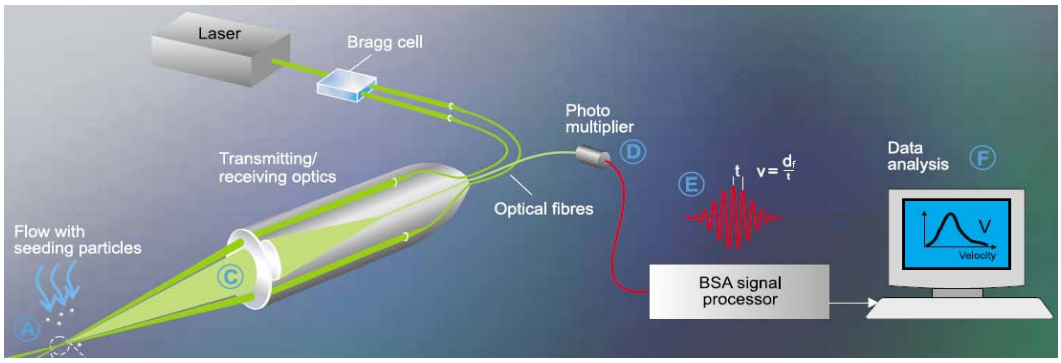

Fig. 3-4. The principles of Laser Doppler Anemometry (LDA) (Dantec, 2000).

Fig. 3-5. Laser Doppler Anemometry (LDA) system.

3.3.2 Electromagnetic Current Meter (EMCM)

This intrusive Current Meter is developed by utilizing Faraday's law i.e. the voltage induced across a conductor as it moves at right angles through a magnetic field is proportional to the velocity of the conductor. The Faraday's formula is $E = VBD$, where E is the voltage generated in a conductor, V is the velocity of the conductor, B is the magnetic field strength, and D is the length of the conductor. In wafer-style magnetic flowmeters, a magnetic field is created throughout the entire cross-section of the flow tube (Fig. 3-6). If this field is considered as the measuring element of the magnetic flowmeter, then it is exposed to the hydraulic conditions throughout the entire cross-section of the flowmeter. With insertion-style flowmeters, the magnetic field radiates outward from the inserted probe.

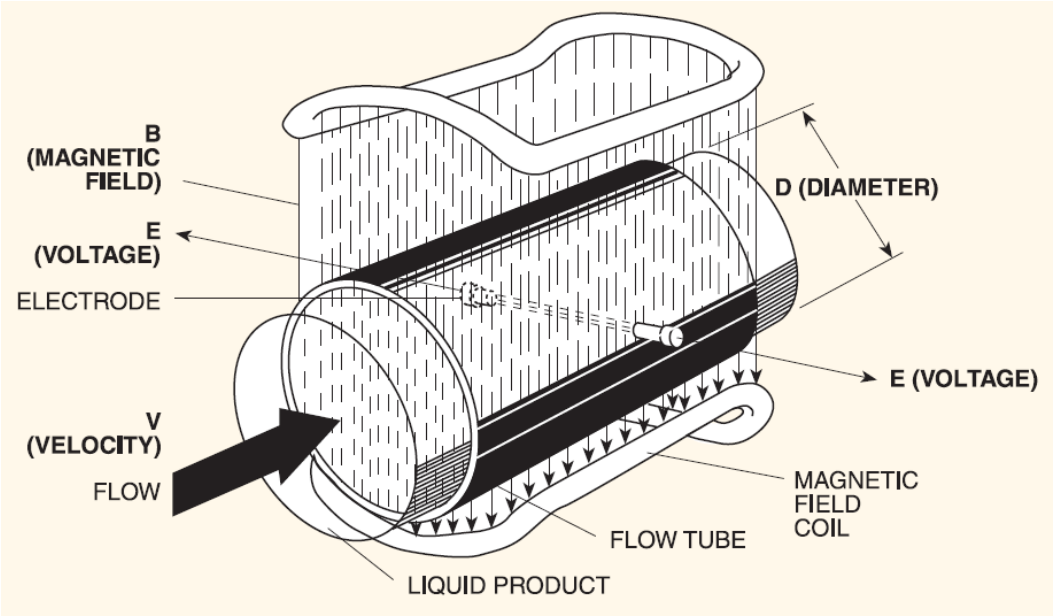

Fig. 3-6. The principles of Electromagnetic Current Meter (Omega n.d.)

This meter is the combination of VM-802H Main Unit and VMT2-200-04PL Detector (Fig. 3-7). The diameter and length of the sensor are 4 mm and 18 mm respectively. Longitudinal and vertical flow velocities are in the range of ±200 cm/s and can be divided into 4 scale ±25 cm/s, ±50 cm/s, ±100 cm/s, ±200 cm/s. The accuracy of this EMCM is ±2% of Full Scale. The voltage output is then transpated to digital output through Labview system (National Instrument) and converted into flow velocities with the frequency of 100 Hz.

Fig. 3-7. Electromagnetic Current Meter system

3.3.3 Experimental procedure

All the experiments were conducted under uniform flow conditions, with varying configurations of the vegetation model. First, the flume slope was carefully adjusted. Next, vegetation plates were glued to the flume bed with planned alignment, making sure that the base of vegetation plate was aligned flat with the flume bottom. Then, the pump and tailgate were adjusted to obtain uniform flow conditions in the flume at the designed flow depth. The flow

discharge was recorded using a built-in electromagnetic flow meter. Seeding powders were added into the flow to enable high sampling rates. Finally, flow velocities were measured using the LDA and EMCM. The measuring location (show in Fig. 3-8) of the velocity profile was at the centre of the flume, so that the sidewall effects were minimized. The measuring location always fell into the range of 6.0 – 8.0 m from the upstream of the flume since the flow was considered to be fully developed.

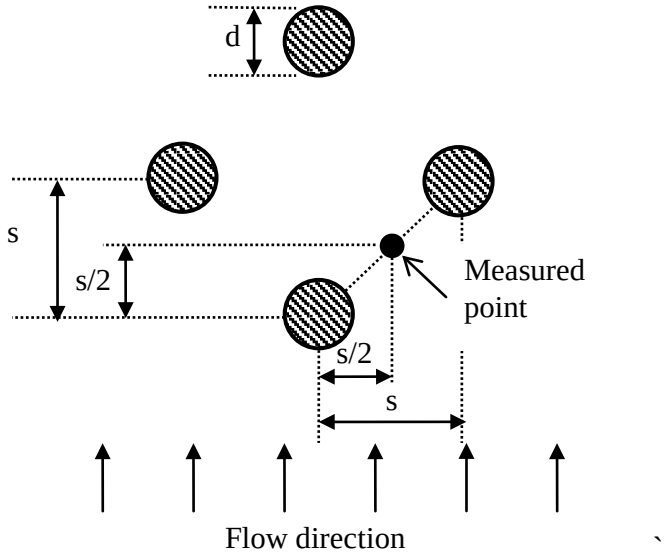

Fig. 3-8. Velocity measuring location.

Flow velocities were recorded every 5 mm from the flume bottom to the free surface. To better understand the flow field near the vegetation interface, the velocities were sampled every 2 mm in the range of 25 mm below and above the interface. Due to the settings of EMCM, the upper most 7 mm of the flow could not be sampled. Velocities were recorded for 1 to 2 minutes for each

point with a sampling frequency of 100-300 Hz. Using LDA, the sampling rate is when it is close to the bed. However, a minimum of 5000 realizations for each point-velocity measurement has been archived (Dantec, 2000). The instantaneous velocities were examined together with the information of seeding particle's arrival and transit time. The analysis yielded the mean velocities and other statistics.

3.4 Comparison of LDA and EMCM measurements

The measurement accuracies of LDA and EMCM are compared against each other.

Fig. 3-9 (a), (b), (c), (d), and (e) compare the horizontal and vertical velocity distributions measured with EMCM and LDA for case B30, in which H = 10, 13, 15, 17, and 20 cm, respectively. It can be seen that the data points agree with each other for the flow velocity above the vegetation. However, the difference becomes more obvious inside the canopy and for emergent cases. LDA is more accurate in vertical velocity measurement than EMCM, since the vertical velocities obtained by LDA are mostly close to zero, which is not the case for EMCM. The differences can also be attributed to the following:

- LDA and EMCM cannot be employed together at the same time. Therefore, variation between two measurements might be a contributing factor.

- The size of EMCM's detector may limit accuracy. In some cases with high vegetation density, this causes difficulty in selecting measurement locations.
- The accuracy of EMCM ranges from ±0.5-2 cm/s, which is quite high comparing to the near-zero value of the vertical velocity in uniform flow conditions. Thus, it is recommended that EMCM should not be chosen to study the vertical velocity.
- The changing of measurement locations of EMCM is manual, which introduces errors to the data.

In this thesis, the measured data were used for different purposes, which are listed as follows:

- Chapter 3 used the longitudinal and vertical velocities which measured by both LDA and EMCM to verify the measurement accuracies. The velocity profiles u and w, as well as the turbulent intensities u_{rms} and w_{rms} measured by LDA were used in the preliminary analysis.
- Chapter 4 used flow depth and discharge data to evaluate the drag coefficient in emergent vegetation flow conditions. The vertical velocity profiles w were used for confirming the uniformity of velocity distributions in the vertical direction.
- Chapter 5 used flow depth and discharge data to work out the representative roughness height for submerged vegetation.

- In Chapter 6, the longitudinal velocity profiles *u* measured by LDA were scaled under depth-limited flow conditions with submerged vegetation.

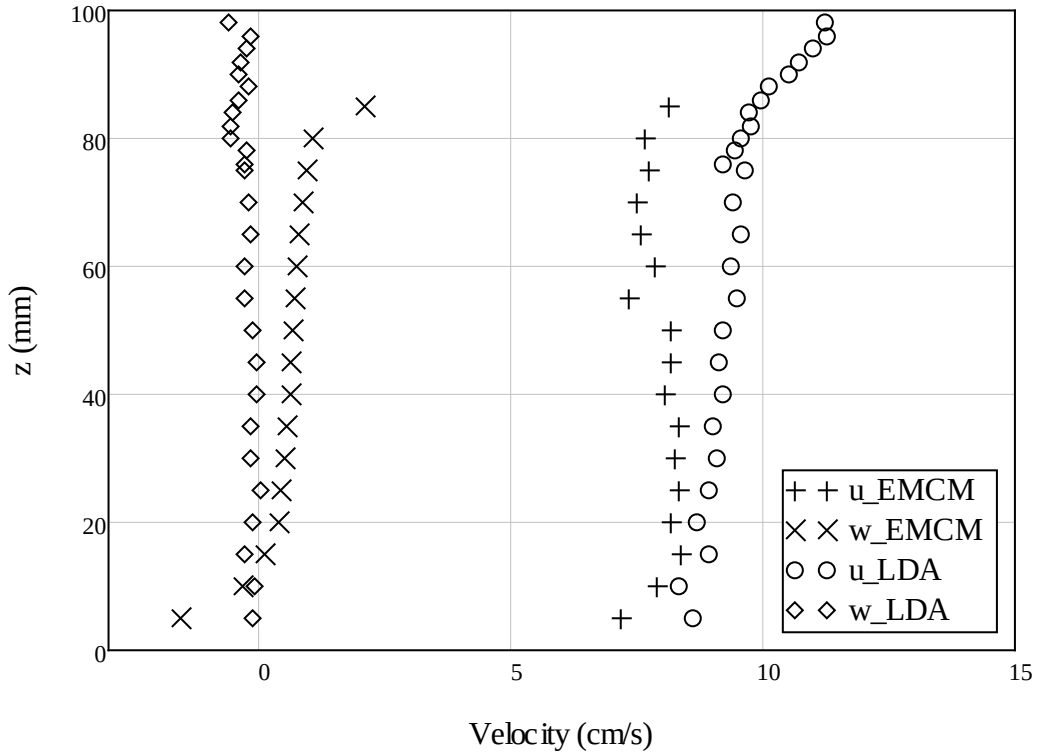

Fig. 3-9 (a). Comparison of velocity distribution (case B30, H = 10 cm).

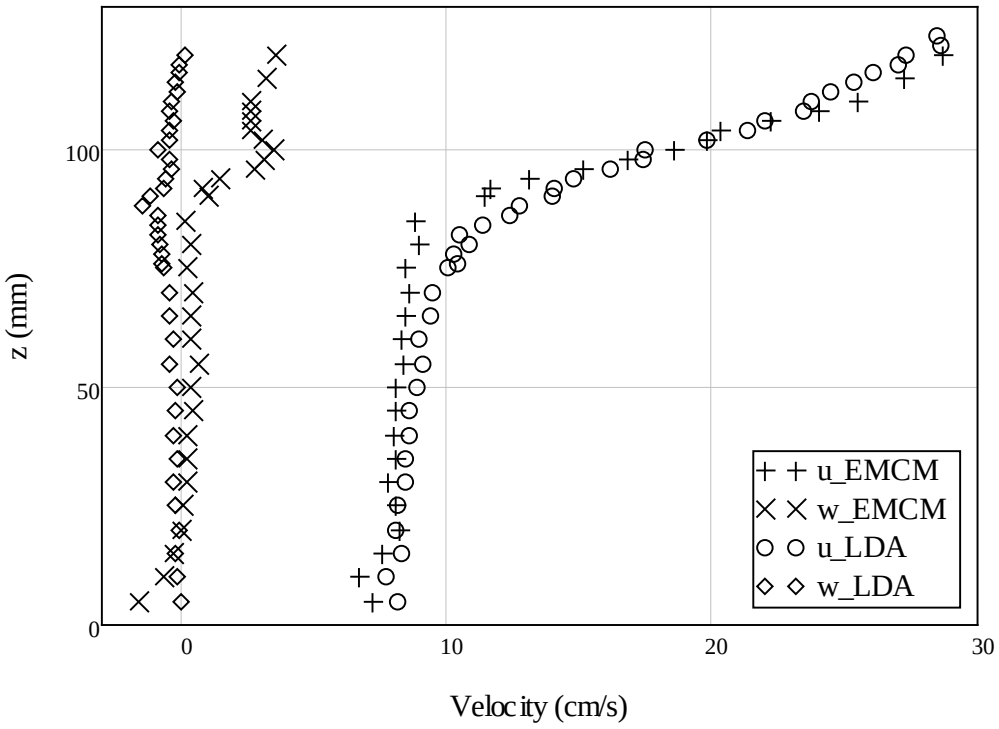

Fig. 3-9 (b). Comparison of velocity distribution (case B30, *H* = 13 cm).

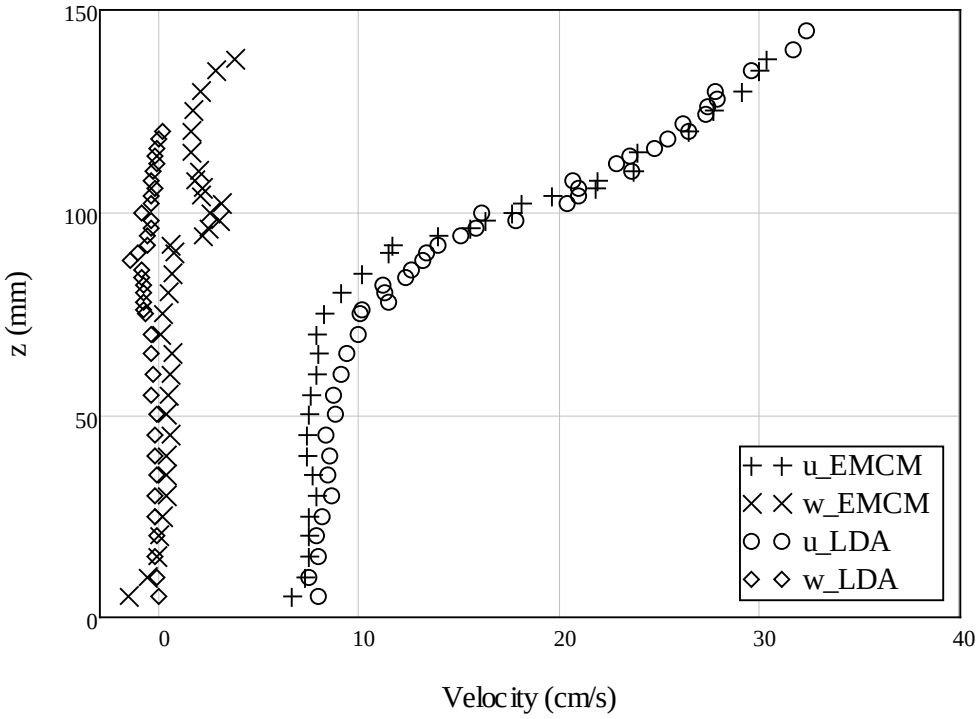

Fig. 3-9 (c). Comparison of velocity distribution (case B30, *H* = 15 cm).

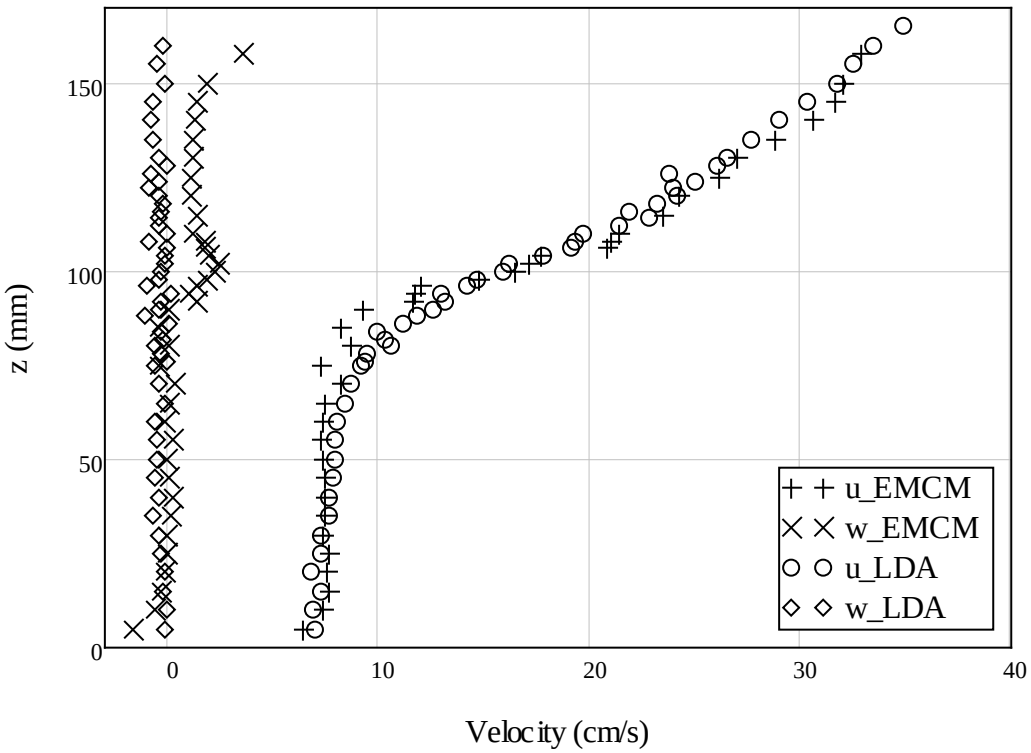

Fig. 3-9 (d). Comparison of velocity distribution (case B30, *H* = 17 cm).

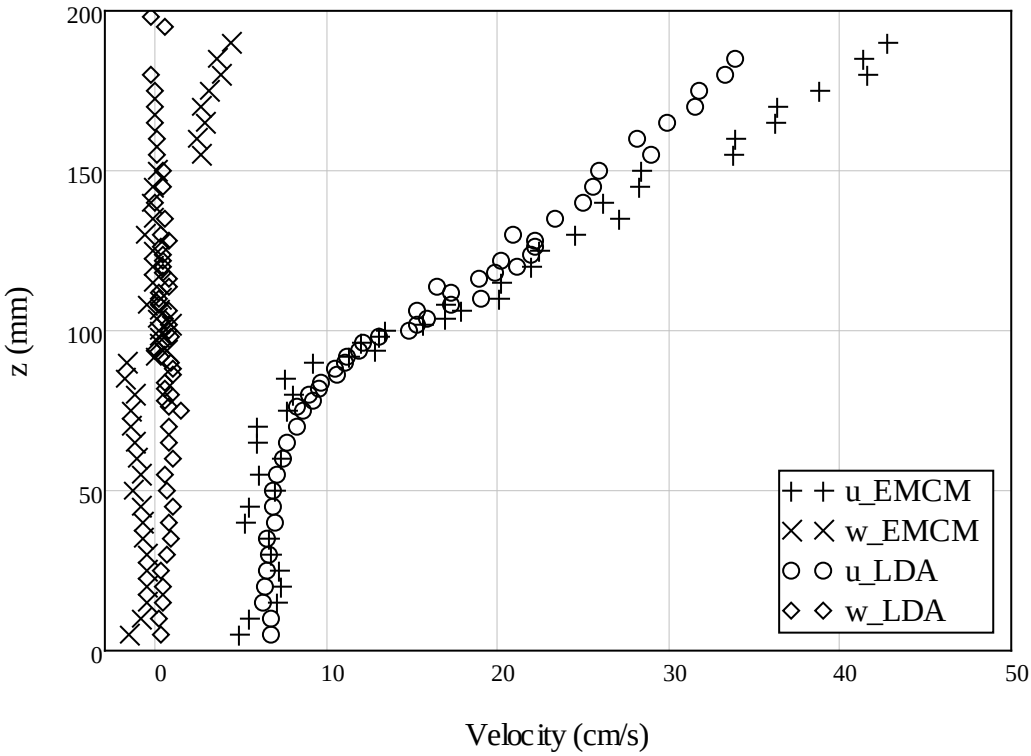

Fig. 3-9 (e). Comparison of velocity distribution (case B30, *H* = 20 cm).

3.5 Preliminary analysis of velocity profiles and turbulence intensities

Altogether, 24 runs of experiment with submerged flow conditions were carried out in order to analyze the influence of vegetation on the velocity profile of shallow open-channel flows. For emergent cases, 143 runs were conducted to study the flow resistance and the velocity profile affected by vegetation.

Preliminary analysis was carried out over the experimental data focusing on the variations in velocity profiles and turbulence intensities of vegetated open-channels flows. Fig. 3-10 shows the velocity distribution for a typical vegetation case, i.e. B60, while varying flow depths from 10 cm at the emergent condition to 20 cm (twice as the height of vegetation). It can be seen that flow velocities inside the canopy are small compared to those above the vegetation. There is a sudden change in the shape of the velocity profile near the top edge of vegetation.

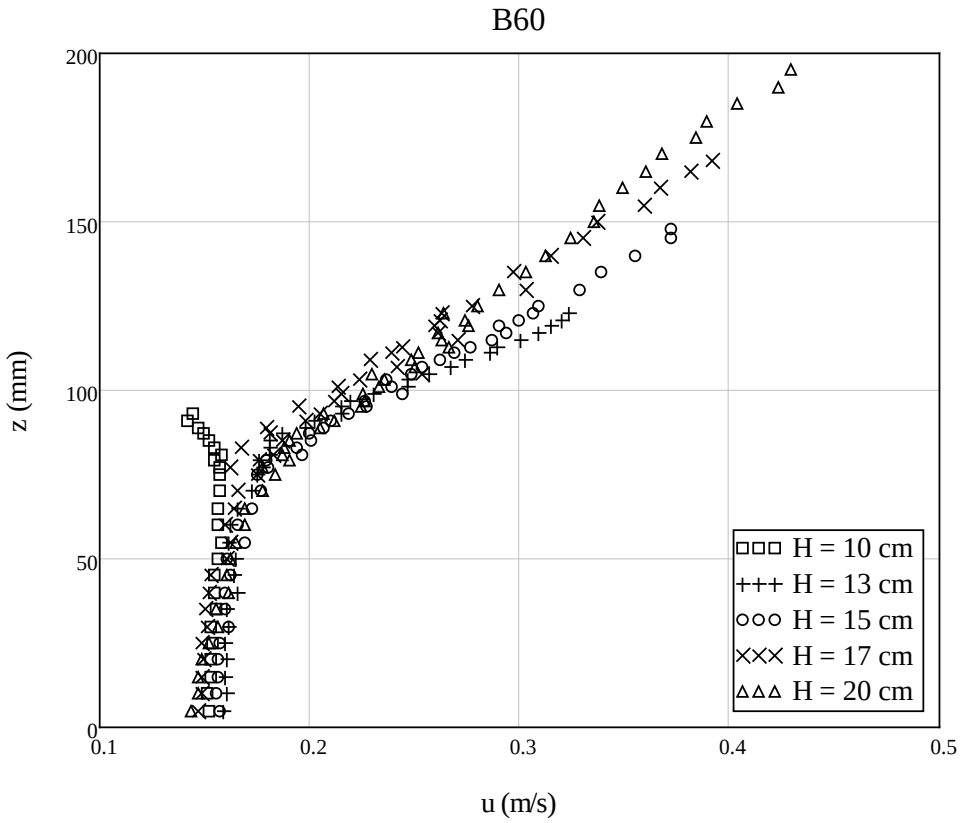

Fig. 3-10. Flow velocity profile for case B60.

Fig. 3-11 (a) and (b) illustrate the velocity profiles for different vegetation configurations. They indicate that higher values of vegetation concentration λ cause lower velocities in both emergent and submerged conditions.

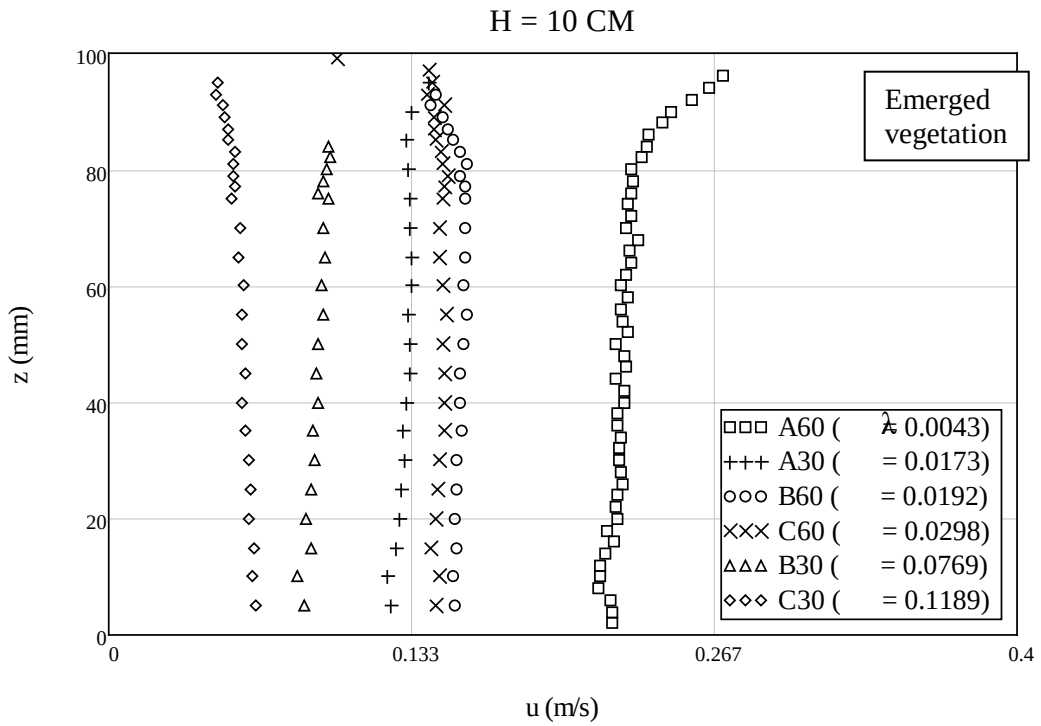

Fig. 3-11 (a). Flow velocity profiles for flow depth H = 10 cm.

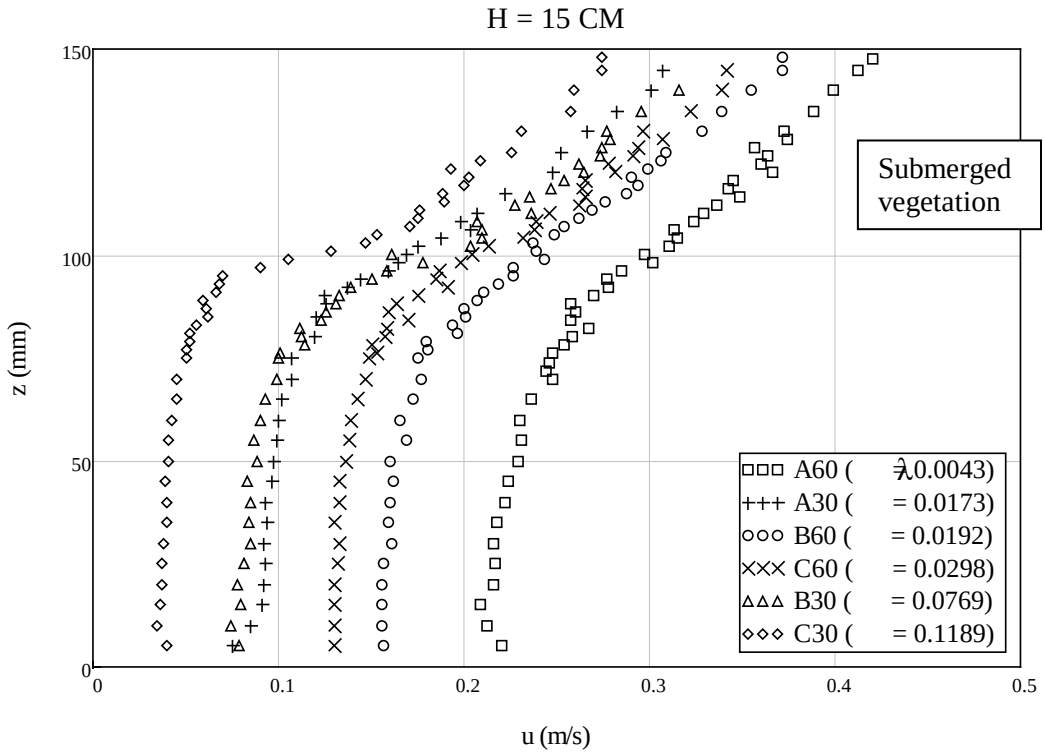

Fig. 3-11. (b). Flow velocity profiles for flow depth H = 15 cm.

The velocity profiles suggest a two-layer velocity distribution. In the vegetation layer, i.e. z ≤ h_v, the velocity is small but increasing in the upward direction. In the surface layer, i.e. z > h_v, it increases more.

Fig. 3-12 shows horizontal turbulent intensity u_{rms} and vertical turbulence intensity w_{rms} in which $u_{rms} \equiv \sqrt{\overline{u'^2}}$ and $w_{rms} \equiv \sqrt{\overline{w'^2}}$. u_{rms} attains its maximum value just above the canopy, whereas w_{rms} attains its maximum just below the canopy. These properties are also observed by Nezu and Sanjou (2008). In general, the value of u_{rms} is higher than w_{rms}. The changes in flow depth affect on turbulent intensities. In particular, u_{rms} and w_{rms} are higher with high flow depths and vice versa. With dense vegetation, within the canopy, u_{rms} and w_{rms} change only slightly with the flow depths.

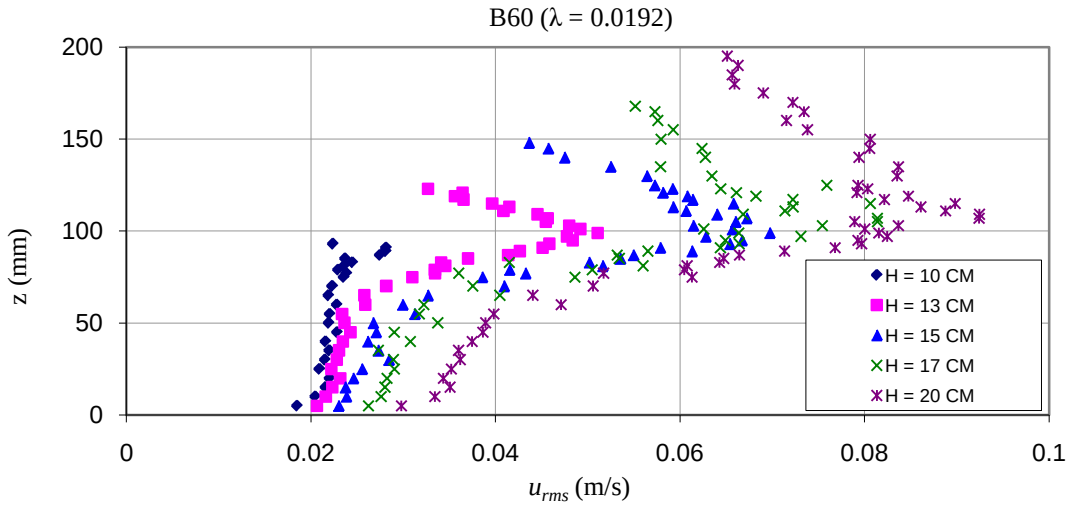

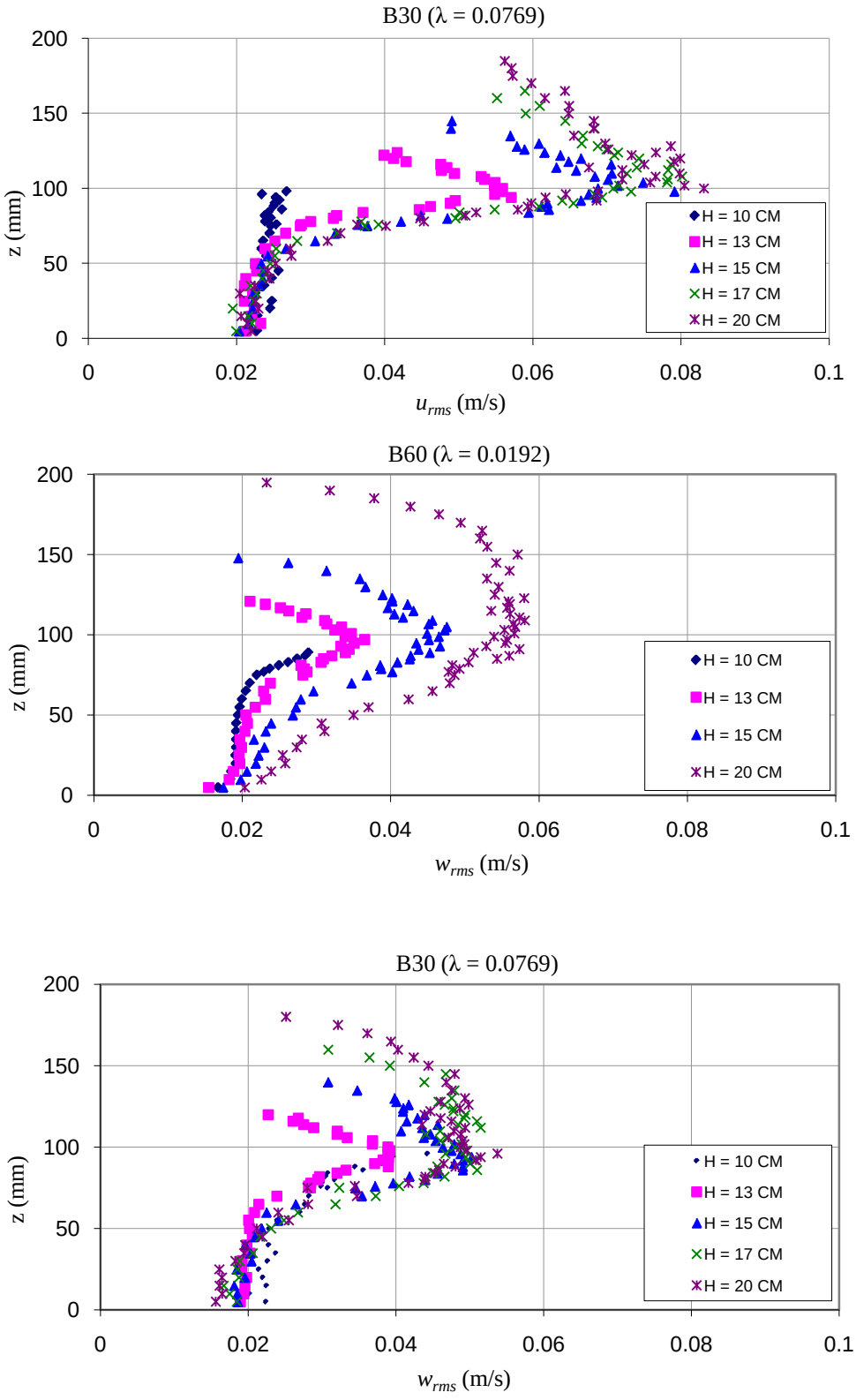

Fig. 3-12. Horizontal and vertical turbulent intensities of B30 and B60.

CHAPTER 4

HYDRAULIC RADIUS FOR EVALUATING RESISTANCE INDUCED BY EMERGENT VEGETATION

4.1 Introduction

The presence of emergent vegetation in wetlands and rivers has impacts on physical and biological processes in aquatic environments. The vegetation-induced drag reduces flow discharge in channels, and also helps in flood attenuation and sediment deposition. Open channel flows, once vegetated, are not only resisted by boundary shear but also the drag induced by stems and foliage. Therefore, the resistance to vegetated open channel flows generally depends on channel geometry, vegetation configuration and surface characteristics of both channel boundary and vegetation. In spite of the fact that the subject has been studied for decades, difficulties still exist in the evaluation of vegetation resistance, either using conventional formulas like Manning equation or others developed recently, because of the limited understanding of complex physics inherent in relevant flow phenomena (e.g. Yen 2002; Zima and Ackermann 2002).

For example, the vegetation drag and its relevant Reynolds number have been defined in several different forms, as reviewed in the subsequent section, and some definitions could be misleading because of improper use of length and velocity scales. As a result, conclusions drawn by different researchers are often inconsistent, and a general formula, similar to Manning's equation developed for regular open channel flows, is not available at present for evaluating resistance to vegetated open channel flows, even for the emergent case that is relatively simple.

In this study, we attempt to compare the resistance to vegetated open channel flows with that to pipe flows based on the concept of hydraulic radius. A vegetation-related hydraulic radius is then proposed to redefine the Reynolds number for vegetated open channel flows. Finally, it is shown that using the new Reynolds number, we are able to collapse drag coefficients across a wide range of stem density. For simplicity, all considerations here are limited to the case of emergent rigid vegetation simulated with circular cylinders.

4.2 Previous considerations

The vegetation-induced drag F_D can be described using the drag coefficient C_D,

$$F_D = C_D A \frac{\rho V_a^2}{2} \tag{4.1}$$

where A is the frontal area of the vegetation stem, ρ is the fluid density and V_a is the average velocity approaching the stem. Without considering effects of

vegetation configuration, several researchers simply replaced V_a with the bulk flow velocity V, the latter being the flow discharge divided by the total cross sectional area (e.g. Ishikawa et al. 2000; Lee et al. 2004; Wu et al. 1999). The use of V in place of V_a applies only for vegetation of low density. Noting that in the case of emergent vegetation, the longitudinal velocity does not vary much from the channel bed to the free surface (e.g. Liu et al. 2008), the depth-averaged pore velocity through the vegetation V_v [$= Q/(BH)/(1-\lambda) = V/(1-\lambda)$] is close to the actual approach velocity, where Q is the flow discharge, B is the channel width, H is the flow depth and λ is the vegetation density defined as the average volume fraction occupied by vegetation. Therefore, V_v can be used to be a good approximation of V_a (Kothyari et al. 2009; Tanino and Nepf 2008).

The drag coefficient is generally a function of Reynolds number. However, the definition of Reynolds number varies in the literature, which involves various length and velocity scales. By ignoring variations in the characteristics of vegetation, several studies simply used flow depth in the definition of Reynolds numbers (e.g. Wu et al. 1999). Lee et al. (2004) stated that other equivalent Reynolds numbers could be also formed using either stem diameter (d) or spacing (s). Table 4-1 provides examples of the Reynolds numbers used in some recent studies.

Table 4-1. Various definitions of Reynolds number for open-channel flows subject to emergent vegetation.

Investigator	Reynolds number	Characteristic velocity	Characteristic length	Note
Wu et al. (1999)	$\frac{VH}{\nu}$	bulk velocity, V	flow depth, H	$V = \frac{Q}{BH}$ $V_v = \frac{V}{1-\lambda}$ $r_v = \frac{\pi}{4}\frac{1-\lambda}{\lambda}d$
Ishikawa et al. (2000)	$\frac{Vd}{\nu}$	bulk velocity, V	stem diameter, d	
Lee et al. (2004)	$\frac{VH}{\nu}$; $\frac{Vs}{\nu}$; $\frac{Vd}{\nu}$	bulk velocity, V	flow depth, H; stem spacing, s; stem diameter, d	
Tanino and Nepf (2008)	$\frac{V_v d}{\nu}$	average pore velocity among stems, V_v	characteristic plant width or stem diameter, d	
Kothyari et al. (2009)				
Present study	$\frac{V_v r_v}{\nu}$	average pore velocity among stems, V_v	vegetation-related hydraulic radius, r_v	

The diversity in the definition of the drag coefficient and Reynolds number has resulted in a mixture of interpretations of the resistance results. For example, Wu et al. (1999) conducted experiments with rubberized horsehair mattress simulating bush-type vegetation, showing that the drag coefficient (defined as $2gS/V^2$, where S is the energy slope and g is the gravitational acceleration) was proportional to the Reynolds number (VH/ν) in the power form, $(VH/\nu)^{-k}$, where ν is the kinematic viscosity of fluid and k is a constant. They also reported that k was somehow independent of the vegetation density, but different k-value must be specified for particular data source. Such k-variations are understandable by noting that Wu et al.'s data analysis did not involve the vegetation density, which is an important variable for characterizing the

vegetation configuration but unfortunately was not measured in their experiments. Similar observations were also presented by Tsihrintzis (2001), who compared datasets provided by seven different studies and concluded that the *k*-value appears almost constant for each individual study but varies from 0.22 to 1.33.

Both Ishikawa et al. (2000) and Kothyari et al. (2009) used strain gauge to directly measure the drag force, F_D, exerted on a typical cylindrical stem placed in the middle of vegetation zone. By plotting the *V*-based drag coefficient $[2F_D/(\rho dHV^2)]$ against the Reynolds number (Vd/ν), Ishikawa et al. (2000) observed significant changes in the drag coefficient but unclear dependence of it on the Reynolds number (see Fig. 4-1). In comparison, Kothyari et al. (2009)'s results indicate that the V_v-based drag coefficient $[2F_D/(\rho dHV_v^2)]$ slightly varies with the Reynolds number ($V_v d/\nu$), but increases clearly with increasing vegetation density (see Fig. 4-2). It should be noted that Kothyari et al.'s experiments were conducted with a very short vegetation zone, which was 0.5 m wide and 1.8 m long. The short vegetation zone may not allow the vegetated flow to be fully developed, in particular, for the case of low vegetation density. We notice that the drag coefficients derived from Kothyari et al.'s experiments are generally overestimated in comparison to others observed in fully developed flows.

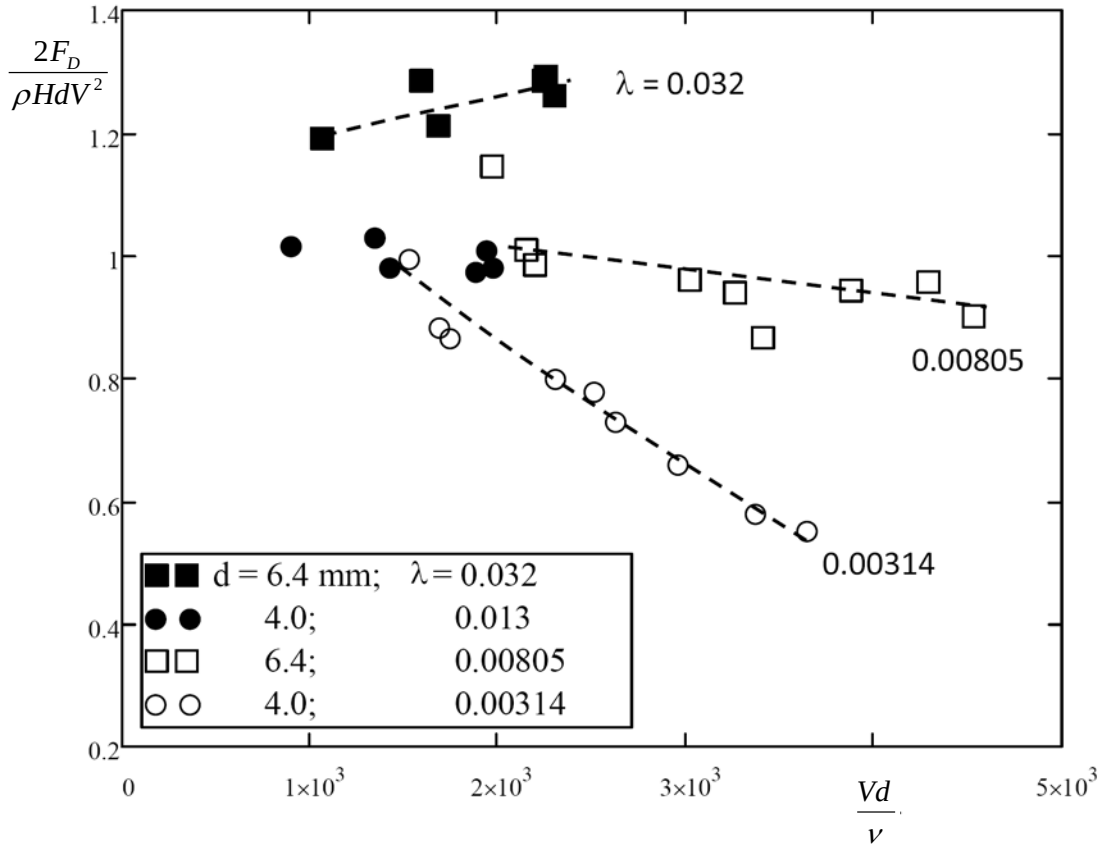

Fig. 4-1. Variations of V-based drag coefficient [= $2F_D/(\rho dHV^2)$] on Reynolds number (=Vd/ν) and vegetation density. The data are reproduced from Ishikawa et al. (2000).

Tanino and Nepf (2008) performed experiments in open channels with relatively dense, randomly distributed circular cylinders, and estimated the drag force from measured water surface slopes. They stated that the normalized drag, i.e. the ratio of the mean drag per unit cylinder length to the product of the viscosity and pore velocity, has a linear dependence on the Reynolds number, as shown in Fig. 4-3. This result seems to be consistent with Ergun equation developed for flows through packed beds (Ergun 1952). However, by

performing linear regression analysis, they also observed that both the gradient and intercept of the linear relation, though taken as constant in Ergun equation, vary clearly with the vegetation density.

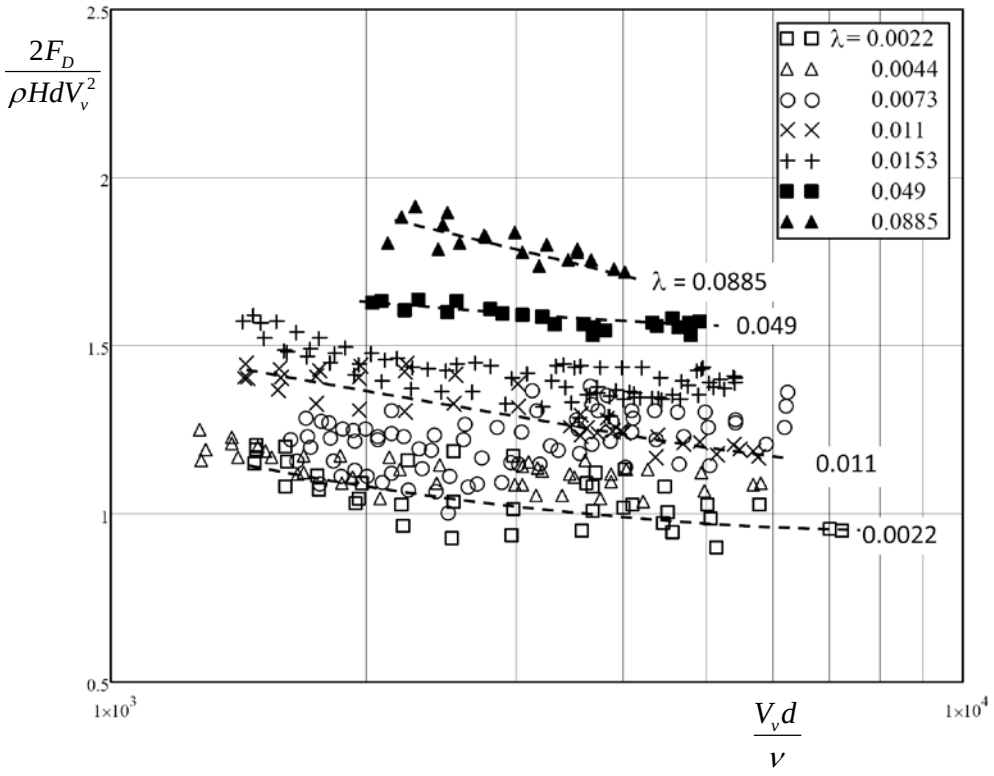

Fig. 4-2. Dependence of V_v-based drag coefficient [= $2F_D/(\rho d H V_v^2)$] on Reynolds number (=$V_v d/\nu$) and vegetation density. The data were provided by Kothyari et al. (2009).

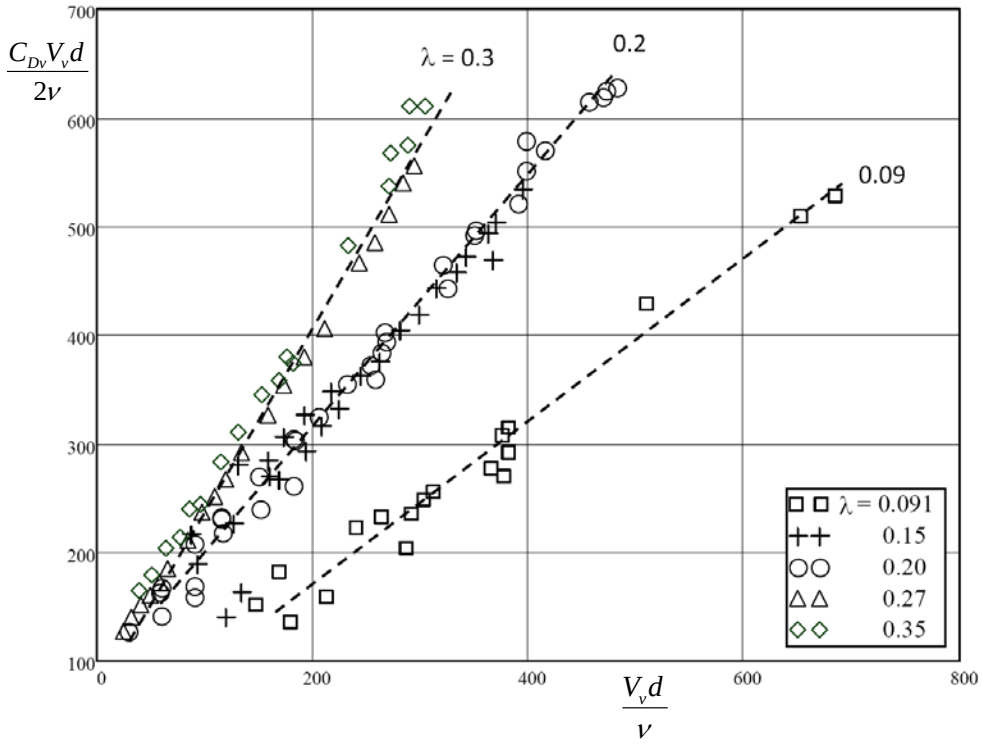

Fig. 4-3. Linear dependence of normalized drag ($0.5C_{Dv}V_v d/\nu$) on Reynolds number ($V_v d/\nu$). The data are reproduced from Tanino and Nepf (2008).

From the above examples, it follows that with different length and velocity scales, similar sets of vegetation drag data could be interpreted with inconsistent conclusions. Therefore, an immediate issue raised here is how to properly scale vegetated open channel flows by taking into account vegetation characteristics.

4.3 Length scale for characterizing vegetated channels

To select a reasonable length scale for characterizing the resistance induced by emergent vegetation to open channel flow, we first make a qualitative comparison of resistance between vegetated open channel and pipe flows. It is

well-known that the pipe friction factor f can be estimated from known Reynolds number and relative roughness height, e.g. using the Moody diagram or Colebrook-type function,

$$f = f\left[\mathrm{Re}, k_s/(4r)\right] \tag{4.2}$$

where $f = 8(u_*/V)^2$, $Re = 4Vr/\nu$, k_s is the equivalent roughness height, r is the hydraulic radius, u_* ($=\sqrt{grS}$) is the shear velocity, V is the cross-sectional average velocity and S is the energy slope. In terms of length scales, Eq. (4.2) also presents a relationship among ν/V, ν/u_*, k_s, and r. Here, both ν/u_* and k_s are boundary-related length scales, describing roughness effects in the sense of hydrodynamics. On the other hand, the hydraulic radius r serves as a measure of the dimension of flow domain or geometry. If the boundary is hydrodynamically smooth, then ν/V is related only to ν/u_* and r, or in the dimensionless form, V/u_* is related only to Re. Such relationships, though developed for pipe flows, have been successfully extended to open channel flows through the concept of the hydraulic radius.

In the following, we aim to develop a similar friction relationship for open channel flows in the presence of emergent vegetation. Therefore, the hydraulic radius needs to be redefined by taking into account the size and configuration of stems as well as the main channel geometry.

4.3.1 Vegetation-related hydraulic radius, r_v

As shown in Fig. 4-4, we consider emergent vegetation simulated with staggered rigid cylinders. For this case, the effective vegetation height is the same as the flow depth H, and the configuration of vegetation is solely governed by the stem diameter d and density λ. It is also assumed that the form drag induced by the vegetation is much more important than its skin friction.

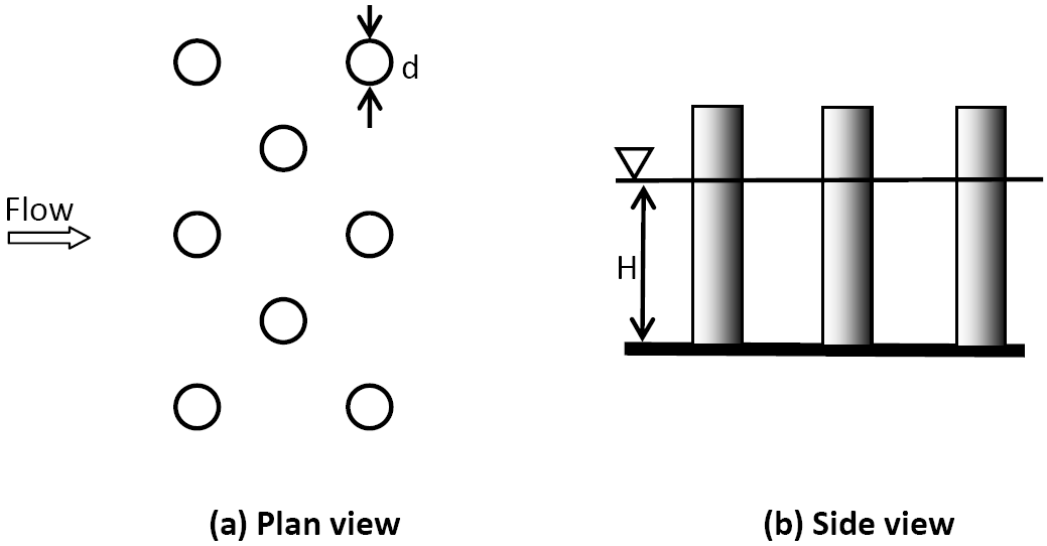

Fig. 4-4. Emergent vegetation simulated with circular cylindrical rods.

For open channel flows without vegetation, the hydraulic radius is associated only with the geometry of cross section, being taken as the ratio of the cross-section area to the wetted perimeter. For vegetated flows without sidewall and bed effects, we consider the volume of the vegetation zone that measures $B \times H \times L$, where L is the length of vegetation zone. Here, since the fraction of the

stem-occupied bed area is the same as λ, the number of cylinders per unit bed area is $N = BL\lambda/(\pi d^2/4)$. Similar to the regular hydraulic radius, we may define the hydraulic radius as the ratio of the volume occupied by water to the wetted surface area of all cylinders. Such approaches were applied previously to quantify flow resistance associated with porous media (Cheng 2003; Cheng et al. 2008). However, in terms of vegetation-induced form drag, it is not the total wetted surface area that should be taken into account. Instead, we only need to consider the frontal area of the stem, which is the area of the stem projected on a plane normal to the streamwise direction. This yields an effective wetted area equal to *NHd*, and then the vegetation-related hydraulic radius can be reasonably defined as

$$r_v = \frac{(1-\lambda)BHL}{NHd} = \frac{\pi}{4}\frac{1-\lambda}{\lambda}d \tag{4.3}$$

It it noted that r_v defined above is comparable to the concentration length proposed by James et al. (2008). In addition, r_v can be related to the overall hydraulic radius for a typical vegetated cross section, which is discussed in section 4.5.1.

With the vegetation-related hydraulic radius, the Colebrook-type resistance relation for open channel flows subject to emergent vegetation is proposed here,

$$f_v = f\left(\mathrm{Re}_v\right) \tag{4.4}$$

where f_v is the vegetation friction factor defined as

$$f_v = \frac{8gr_v S}{V_v^2} \tag{4.5}$$

and Re_v is the vegetation Reynolds number defined as

$$\mathrm{Re}_v = \frac{V_v r_v}{\nu} \tag{4.6}$$

In comparison with the previous studies (see Table 4-1), the use of r_v in the Reynolds number is novel. As shown subsequently, r_v performs much better than other length scales, such as H, d and s, for collapsing drag coefficient data from disparate sources.

In the above consideration, effects of the channel boundary have not been included. In natural situations and laboratory studies, vegetated flows are usually subject to boundary roughness, such as channel beds covered by sediment grains and even bed forms. Although some experimental observations have shown that vegetation-induced drag could be dominant in comparison to boundary shear, it is generally necessary to correct boundary effects so that vegetation-induced drag can be singled out. Such a procedure called sidewall and bed corrections is introduced later in this chapter for modifying r_v, and thus the resistance relation given in Eq. (4.4).

4.3.2 Drag coefficient

Similar to the friction factor, drag coefficient is also a useful parameter for quantifying vegetation-induced drag. For each cylindrical stem, the drag force

in the streamwise direction is defined as (e.g. Kothyari et al. 2009; Tanino and Nepf 2008)

$$F_D = C_{Dv}\rho H d\frac{V_v^2}{2} \tag{4.7}$$

where C_{Dv} is the drag coefficient, the product of H and d measures the size of the frontal area and V_v is the average pore velocity approaching the stem. The total drag per unit bed area is

$$\frac{4\lambda}{\pi d^2}F_D = \frac{4\lambda}{\pi d^2}C_{Dv}\rho H d\frac{V_v^2}{2} = C_{Dv}\frac{2\lambda\rho H V_v^2}{\pi d} \tag{4.8}$$

which is equivalent to the streamwise component of the gravitational force for the condition of uniform flows, i.e.

$$C_{Dv}\frac{2\lambda\rho H V_v^2}{\pi d} = (1-\lambda)\rho g H S \tag{4.9}$$

Here, the shear forces induced by sidewalls and bed are considered negligible. Otherwise, sidewall and bed corrections are applied in the way as described subsequently. From Eq. (4.9),

$$C_{Dv} = \frac{1-\lambda}{2\lambda V_v^2}gS\pi d = 2\frac{gr_v S}{V_v^2} \tag{4.10}$$

It is noted that the definition of the drag coefficient as given by Eq. (4.10) has also been proposed previously (James et al. 2008; Tanino and Nepf 2008). Furthermore, by comparing Eq. (4.10) with Eq. (4.5) one gets

$$C_{Dv} = \frac{1}{4} f_v \tag{4.11}$$

Therefore, from Eqs. (4.4) and (4.11), it follows that C_{Dv} would generally vary with Re_v.

Fig. 4-1 to Fig. 4-3 seem to show that the dependence of drag coefficient on Reynolds number always varies with the vegetation density. However, the same data, when presented in the form of C_{Dv} against Re_v as shown in Fig. 4-5 to Fig. 4-7, respectively, demonstrate that in general, C_{Dv} decreases monotonically with Re_v, and the deviation that may be associated with the variation in the vegetation density can be considered relatively minor. The monotonic decrease does not diminish even when the drag coefficient varies in a limited range for the data provided by Ishikawa et al. (2000) and Kothyari et al. (2009). As mentioned early, Kothyari et al. (2009)'s experiments were conducted with the short vegetation zone where the flow might be still developing, and the drag measured could be greater than those obtained in the developed flows. Being superposed with the trend of the data by Kothyari et al., Fig. 4-5 shows that C_{Dv} derived from Kothyari et al.'s data are greater by about 0.6-0.8 than those from Ishikawa et al. Plotted in Fig. 4-7 are the data collected by Tanino and Nepf (2008), which again demonstrate the monotonic decrease of C_{Dv} with increasing Re_v.

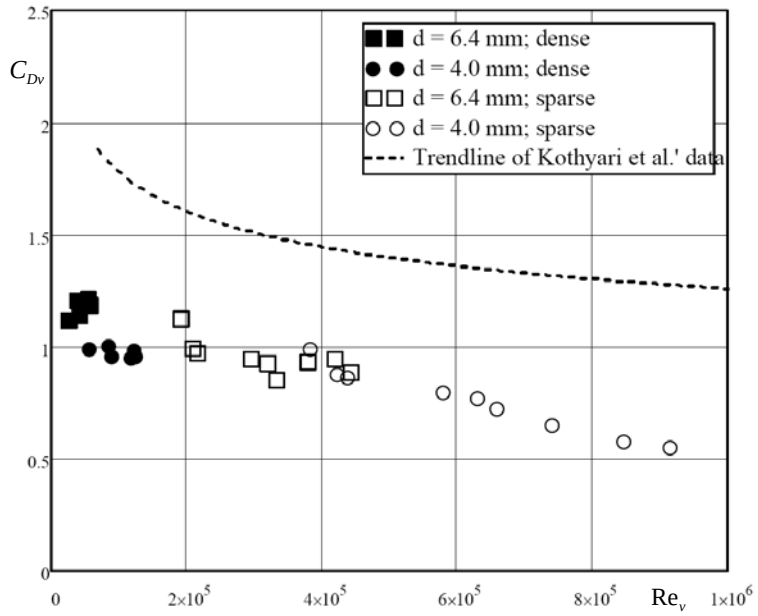

Fig. 4-5. Dependence of drag coefficient [$C_{Dv} = 2F_D/(\rho H d V_v^2)$] on Reynolds number ($Re_v = 4V_v r_v/v$). The data points are from Ishikawa et al. (2000), the same as those used in Fig. 4-1. The solid line represents the trend of the data from Kothyari et al. (2009), as shown in Fig. 4-6.

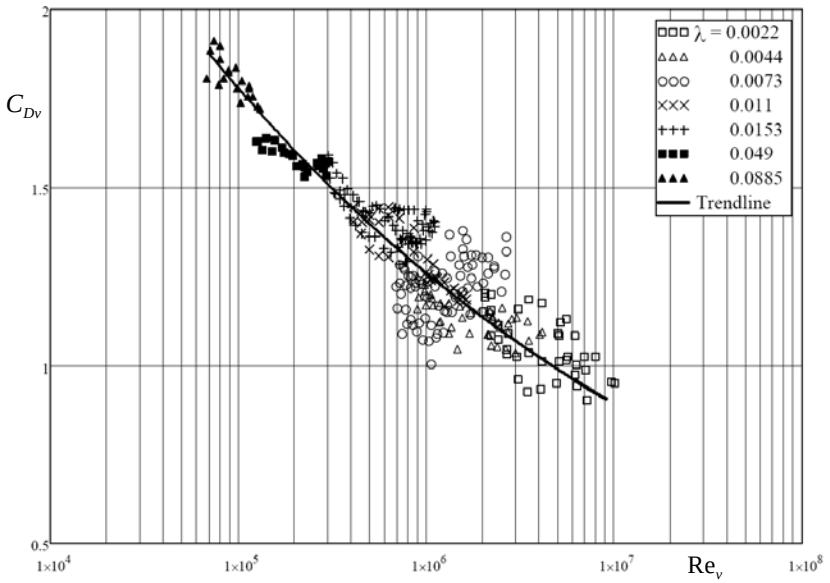

Fig. 4-6. Dependence of drag coefficient [$C_{Dv} = 2F_D/(\rho H d V_v^2)$] on Reynolds number ($Re_v = 4V_v r_v/v$). The data points are from Kothyari et al. (2009), the same as those used in Fig. 4-2.

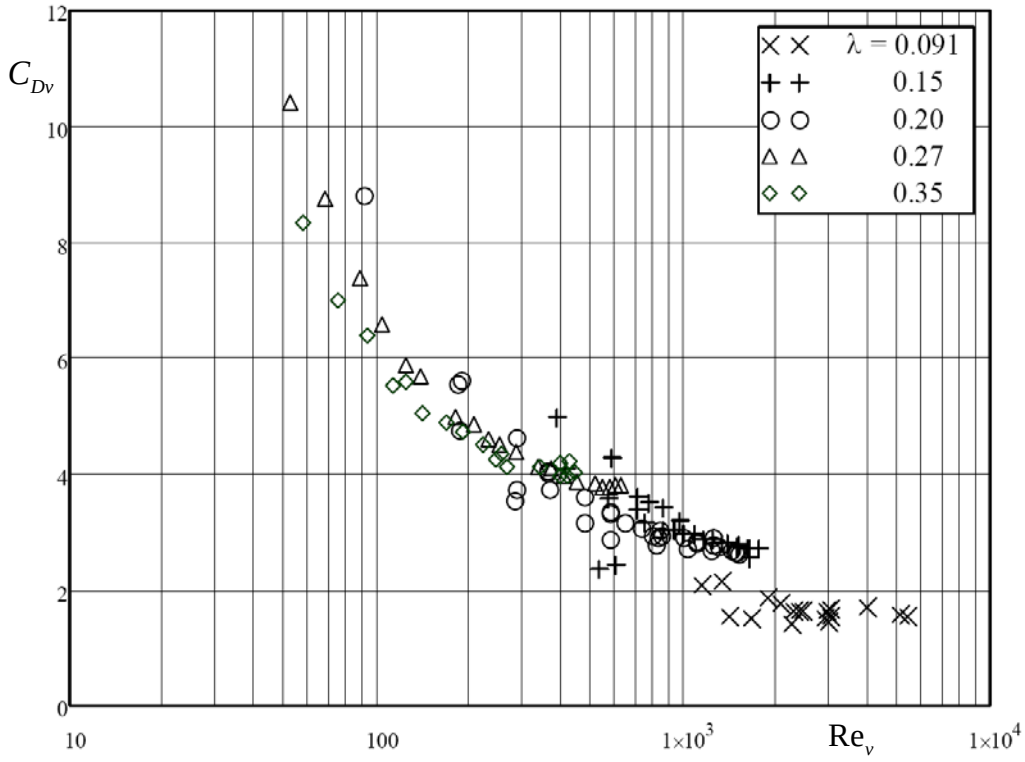

Fig. 4-7. Dependence of drag coefficient [$C_{Dv} = 2F_D/(\rho HdV_v^2)$] on Reynolds number ($Re_v = 4V_v r_v/v$). The data are from Tanino and Nepf (2008), the same as those used in Fig. 4-3.

To justify the suitability of C_{Dv} and Re_v for the description of resistance to vegetated open channel flows, laboratory experiments were conducted in this study to facilitate data analysis.

4.4 Laboratory experiments

As described on Chapter 3, totally 143 runs of experiments were conducted under emergent flow conditions which summarized in Table 3-2. The streamwise flow velocity among the rods in the centre of the vegetation zone was also measured at the midpoint between two adjacent rods (as shown in Fig. 3-8). Almost uniform velocity distributions in the vertical direction were

observed for all cases. As the depth-averaged velocity computed based on such measurements may not represent the average pore velocity, the values of V_v used for the following analysis were all calculated from the measured flow discharges, i.e. $V_v = Q/(BH)/(1-\lambda)$. An uncertainty analysis shows that the relative root mean square deviations of Re_v and C_{Dv} that were calculated from the collected data are 7.6% and 15.1%, respectively, whereas the maximum deviations are 15.2% and 30.2%, respectively, at the 95% confidence level.

4.5 Data analysis

The analysis is performed with two categories of experimental data. The first category is associated with randomly distributed cylindrical rods, as described by Tanino and Nepf (2008). The relevant data consist of those reported earlier by Tanino and Nepf (2008) and two additional sets of unpublished data for λ = 0.031 and 0.056 respectively (Tanino and Nepf 2010). The second category is related to stems arranged in staggered patterns. The data used for analysis are those collected in this study (Table 4-2) and also those published previously (e.g. Kothyari et al. 2009; Tanino and Nepf 2008) (see Table 4-2). In addition, two data points provided by Liu et al. (2008) for the case of stems arranged in a linear pattern are also included.

It is noticed that various flow and vegetation conditions have been employed by different investigators (see Table 4-2). For example, while smooth sidewalls were used in all studies, the channel bed involved was either smooth (e.g.

Kothyari et al. 2009; Tanino and Nepf 2008) or sand-covered (Ferreira et al. 2009; Ishikawa et al. 2000; James et al. 2004; Liu et al. 2008). Ishikawa et al. (2000) and Kothyari et al. (2009) used strain gauge to measure the drag force directly, while the others estimated the drag from the energy slope of uniform or non-uniform flows. All these variations in the experimental setup and measurement technique imply that the data collected should be treated with care. In the next section, it is shown that the data can be unified to a certain extent by correcting boundary effects that are associated with characteristics of sidewall and bed roughness. However, possible effects of other factors such as flow uniformity and vegetation configuration (regular or random) are not incorporated in the analysis.

4.5.1 Sidewall and bed corrections for vegetated open channel flows

By noting that a sand-covered bed is generally rougher than flume walls and thus subject to higher shear stress, Vanoni and Brooks (1957) developed a procedure for determining bed-related hydraulic radius and thus average bed shear stress from known values of V, S, r, etc. In this correction, the bed and sidewall-related hydraulic radius are defined without specifying individual average velocities and energy slopes. Despite some deficiencies, the side-wall correction procedure yields reliable estimates of the friction factor for flow over sand beds.

Table 4-2. Summary of data of resistance induced by emergent vegetation.

Investigator	Rectangular channel				Vegetation zone			Vegetation model			Drag measurement approach
	length (m)	**width (m)**	**bed slope**	**bed condition**	**length (m)**	**width (m)**	**density λ**	**shape of rod**	**pattern**	**stem diameter d (mm)**	
Ishikawa et al. (2000)	15	0.3	0.1-0.02 (nearly uniform flow)	covered with sand d_{50} = 1.8mm	15	0.3	0.00314-0.0126	cylindrical	staggered	4; 6.4	strain gauge
James et al. (2004)	3	0.1	0.002-0.01 (uniform flow)	covered with sand d_{50} = 2.4-4.8mm			0.0035-0.0314	cylindrical	staggered	5	energy slope
Liu et al. (2008)	4.3	0.3	0.003 (uniform flow)	smooth; glued with sand d_{50} = 0.7mm	3	0.3	0.0031-0.0160	cylindrical	staggered; linear	6.35	energy slope
Tanino and Nepf (2008)			0 (nonuniform flow)	smooth	2.84 6.7	0.4 0.203	0.15-0.35 0.091	cylindrical	random	6.4	water surface slope
Ferreira et al. (2009)	10	0.409	0 (nonuniform flow)	covered with sand d_{50} = 9mm	3.1	0.409	0.022-0.038	cylindrical	random	11	water surface slope
Kothyari et al. (2009)	16	0.5	0-0.02 (nonuniform flow)	smooth	1.8	0.5	0.0022-0.0885	cylindrical	staggered	10	strain gauge
Stoesser et al. (2010)							0.0157-0.2513	cylindrical	staggered		CFD (LES)
Present study	12	0.3	0.00095-0.00811 (uniform flow)	smooth	9.6	0.3	0.0043-0.119	cylindrical	staggered	3.2; 6.6; 8.3	energy slope

Here, the correction procedure is modified for determining the vegetation-related hydraulic radius in the presence of both sidewalls and channel bed. First, we consider the forces exerted on vegetated flow in the streamwise direction. The resistance forces are wall shear, bed shear and vegetation drag. With the same energy slope, the wall shear may be expressed as $\rho g S r_w p_w$, and the bed shear as $\rho g S r_b p_b$, where r_w and p_w are wall-related hydraulic radius and wetted-perimeter, respectively, and r_b and p_b are bed-related hydraulic radius and wetted-perimeter, respectively. Similarly, the vegetation drag can be taken as $\rho g S r_v p_v$, where r_v and p_v are vegetation-related hydraulic radius and wetted-perimeter, respectively. The sum of the three resistance forces is equivalent to $\rho g r S p$, which yields

$$pr = p_w r_w + p_b r_b + p_v r_v \tag{4.12}$$

where p (= $p_w + p_b + p_v$) is the total wetted-perimeter and r [= $BH(1-\lambda)/p$] is the total hydraulic radius. It is assumed that the velocity are same for each division of cross section. By defining that $f = 8grS/V_v^2$, $f_w = 8gr_wS/V_v^2$, $f_b = 8gr_bS/V_v^2$, and $f_v = 8gr_vS/V_v^2$, Eq. (4.12) is rewritten to be

$$pf = p_w f_w + p_b f_b + p_v f_v \tag{4.13}$$

The three wetted perimeters are evaluated as follows. First, we can take that $p_w = 2H$ and on average, $p_b = (1-\lambda)B$ by noting that the channel bed is partially occupied by the vegetation stems. To evaluate p_v, it is convenient to consider a channel reach, of which the width is B and the length is unity. The number of

stems in this unit reach is $B\lambda/(\pi d^2/4)$. Then, p_v is taken to be the total frontal area of the stems, which represents the effective area that the form drag exerts on, i.e. $p_v = BH\lambda/(\pi d/4)$. Note that p_v so obtained is an equivalent but not real wetted-perimeter. With p_b, p_w and p_v given above, we get

$$r = \left(\frac{1}{H} + \frac{1}{0.5B(1-\lambda)} + \frac{1}{r_v} \right)^{-1} \tag{4.14}$$

where $r_v = \pi d(1-\lambda)/(4\lambda)$. Without vegetation or when $\lambda = 0$, r reduces to

$$r = \left(\frac{1}{0.5B} + \frac{1}{H} \right)^{-1} = \frac{BH}{B+2H} \tag{4.15}$$

Furthermore, substituting the expressions of p_b, p_w and p_v into Eq. (4.13) and then dividing both sides by $(1-\lambda)$BH yields

$$f_v = r_v \left(\frac{f}{r} - \frac{f_w}{0.5B(1-\lambda)} - \frac{f_b}{H} \right) \tag{4.16}$$

In studying vegetated open channel flows, different investigators engaged different bed conditions. Most used smooth beds, while a few used rough and even mobile sediment beds (Ishikawa et al. 2000; James et al. 2004). Therefore, when comparing such results that are obtained for different bed conditions, it is necessary to first correct possible bed and sidewall effects. Once f_v is known, the vegetation hydraulic radius r_v is modified to r_{vm} in the way similar to that proposed by Vanoni and Brooks (1957),

$$r_{vm} = \frac{r}{f} f_v \tag{4.17}$$

Substituting Eq. (4.16) into Eq. (4.17),

$$r_{vm} = r_v \left[1 - \left(\frac{f_w}{0.5B(1-\lambda)} + \frac{f_b}{H} \right) \frac{r}{f} \right] \tag{4.18}$$

The evaluation of f_w and f_b can be made by applying the Colebrook equation, which generally requires iterations. Here, we propose an equivalent but explicit formula as follows,

$$f_w^{\alpha} = f_{wS}^{\alpha} + f_{wR}^{\alpha} \tag{4.19}$$

where

$$f_{wS} = 31 \left[\ln \left(1.3 \frac{\mathrm{Re}}{f} \right) \right]^{-2.7} \tag{4.20}$$

$$f_{wR} = 11.7 \left[\ln \left(7.6 \frac{4r}{f k_{sw}} \right) \right]^{-2.5} \tag{4.21}$$

$$\alpha = 2 \left(\frac{4r}{f k_{sw}} \right)^{0.1} \tag{4.22}$$

In Eqs. (4.19) to (4.22), the Reynolds number *Re* is defined as $4rV_v/\nu$, k_{sw} is the equivalent wall roughness height, and subscript *w* indicates that the equations are proposed for finding f_w. For known bed roughness height k_{sb}, f_b is evaluated using Eqs. (4.19) to (4.22) with subscript *b* in place of *w*.

With the above consideration, the calculation of r_{vm} proceeds as follows: (1) Obtain r using Eq. (4.14), f (= $8grS/V_v^2$) and Re (= $4rV_v/\nu$) from experimental data; (2) Calculate Re/f, $4r/(fk_{sw})$, and $4r/(fk_{sb})$; (3) Obtain f_w and f_b with Eqs. (4.19) to (4.22); and (4) Calculate r_{vm} using Eq. (4.18).

It is interesting to note that for vegetated open channel flows, the hydraulic radius r generally comprises three components, i.e. H, $0.5B(1-\lambda)$ and r_v, and it is equivalent to r_v when both sidewall and bed effects are negligible. Table 4-3 compares various hydraulic radius applied in different flows.

Table 4-3. Length scales for characterizing flow geometry.

Flow geometry	**Geometrical dimension**	**Hydraulic radius**
Circular pipe	pipe diameter, D	$\frac{D}{4}$
Rectangular open channel	channel width, B flow depth, H	$\left(\frac{1}{H}+\frac{1}{0.5B}\right)^{-1}=\frac{BH}{B+2H}$
Porous media comprising grains	grain size, d_{50} pore size	$\frac{1}{6}\frac{1-\lambda}{\lambda}d_{50}$
Vegetated channel without channel boundary effects	stem diameter, d stem spacing, s	$r_v=\frac{\pi}{4}\frac{1-\lambda}{\lambda}d$
Rectangular open channel with emergent vegetation	channel width, B flow depth, H stem diameter, d stem spacing, s	$\left(\frac{1}{H}+\frac{1}{0.5B(1-\lambda)}+\frac{1}{r_v}\right)^{-1}$
Notes: For porous media, the hydraulic radius is defined by considering the total wetted area (Cheng et al. 2008).		

The above correction can be implemented with known B, H, d, λ, S, Q, k_{sb}, k_{sw}, and ν, where k_{sb} is the bed roughness height and k_{sw} is the sidewall roughness height. To justify the correction, we here apply it to the experiments conducted

by Ishikawa et al. (2000), who measured both energy slope and vegetation-induced forces for flows bounded by smooth glass sidewalls and a rough channel bed covered with sand of diameter d_{50} = 1.8 mm. With the data provided by Ishikawa et al., the drag coefficient was first computed directly using the measured drag, i.e. $C_{Dv(exp)} = 2F_D/(\rho HdV_v^2)$ [see Eq. (4.7)]. Then, it was also estimated from the energy slope in two different methods, one being based on r_v, yielding that $C_{Dv(cal)} = 2gr_vS/V_v^2$ [see Eq.(4.10)] and the other based on r_{vm}, i.e. $C_{Dvm(cal)} = 2gr_{vm}S/V_v^2$.

In Fig. 4-8, both $C_{Dv(cal)}$ and $C_{Dvm(cal)}$ are compared with $C_{Dv(exp)}$. It can be observed that without any correction made, $C_{Dv(cal)}$ differs significantly from $C_{Dv(exp)}$; however using the corrected hydraulic radius r_{vm}, the calculated drag coefficient $C_{Dvm(cal)}$ appears close to the measurement. Here in making the correction, it is assumed that $k_{sb} = 2.5d_{50}$ (Qian and Wan 1999). Additional calculations performed show that the best agreement between the measured and calculated drag coefficients can be achieved by varying k_{sb} in the range of d_{50} to $6d_{50}$ for the four cases, which may imply the presence of bed forms.

Fig. 4-9 shows the ratio of r_{vm} to r_v computed with the data collected in this study and those given by Ishikawa et al. (2000) and James et al. (2004). It is noted that r_{vm} is slightly smaller than r_v for the experiments conducted in this study with smooth bed and sidewalls, while the difference becomes large for the experiments conducted using sand-covered beds (Ishikawa et al. 2000;

James et al. 2004). Moreover, the difference is expected to be generally negligible for vegetation of high density, e.g. $\lambda > 0.1$.

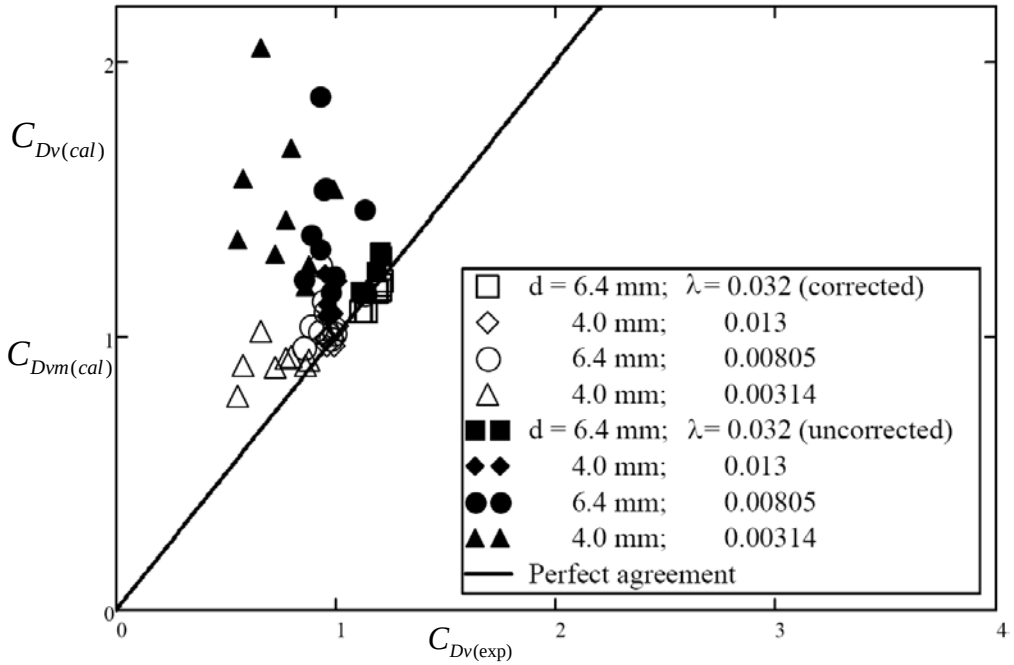

Fig. 4-8. Comparisons of drag coefficients $C_{Dv(cal)}$ (denoted by solid symbols) estimated using uncorrected hydraulic radius (r_v) and $C_{Dvm(cal)}$ (denoted by open symbols) using corrected hydraulic radius (r_{vm}) with measurements ($C_{Dv(exp)}$). The data are from Ishikawa et al. (2000).

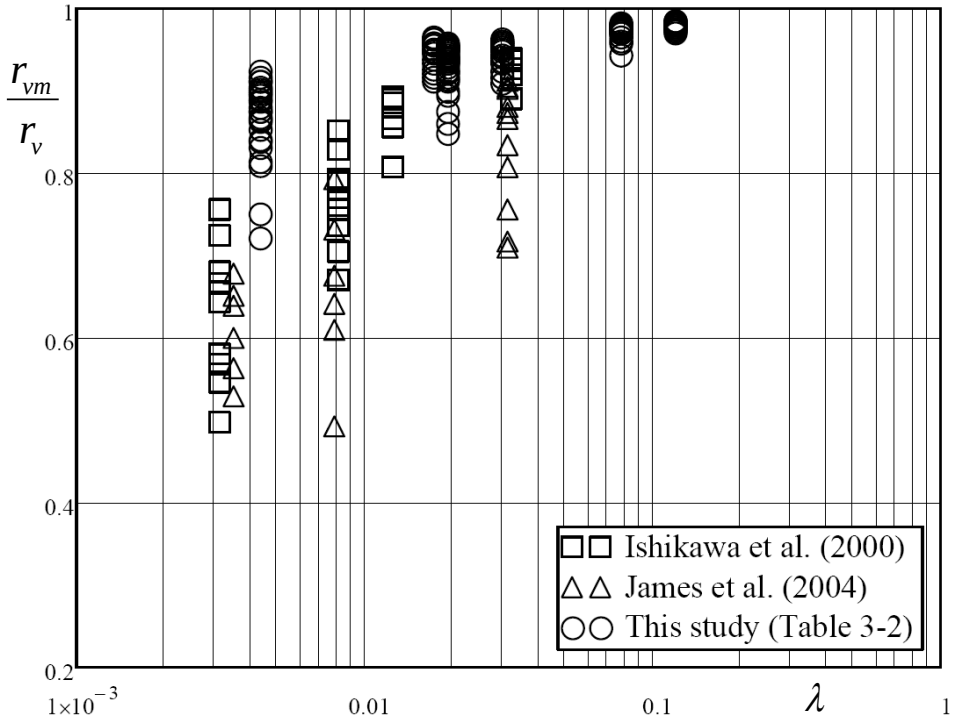

Fig. 4-9. Variation of ratio of corrected to uncorrected hydraulic radius with vegetation density.

4.5.2 Dependence of C_{Dv} on Re_v

As discussed earlier, the previous studies (Ishikawa et al. 2000; Kothyari et al. 2009; Tanino and Nepf 2008) seem to suggest that the dependence of drag coefficient on Reynolds number always varies with the vegetation density. However, the same data, when presented in the form of C_{Dv} against Re_v as shown in Fig. 4-10, demonstrate that C_{Dv} decreases monotonically with increasing Re_v. From Fig. 4-10, the following observations could be made. First, though scattered to some extent, all data points generally follow the same decreasing trend of C_{Dv} with increasing Re_v. Second, it seems that for the same

Re_v, there is no significant difference in the drag coefficient between the randomly distributed and staggered stems.

It should be mentioned that the sidewall and bed corrections were applied only for the data with the information available for the relevant variables, i.e. those from Ishikawa et al. (2000), James et al. (2004) and this study. The data by Kothyari et al. (2009) are not included in Fig. 4-10 by considering inconsistence related to the short vegetation zone. However, a separate analysis also shows that the use of Re_v results in similar collapsing of their data, in spite of the variation in the measured drag coefficient, i.e. $C_{Dv} = 0.9 – 1.9$.

For comparison purposes, we also made a companion to Fig. 4-10 by plotting C_{Dv} against the more commonly used Reynolds number $V_v d/\nu$. The result is shown in Fig. 4-11, indicating that the use of d rather than r_v yields significant data spread.

To empirically describe the relationship of C_{Dv} and Re_v, a best-fit function is proposed here for $Re_v = 52 – 5.6 \times 10^5$,

$$C_{Dv} = \frac{50}{\mathrm{Re}_v^{0.43}} + 0.7\left[1 - \exp\left(-\frac{\mathrm{Re}_v}{15000}\right)\right] \tag{4.23}$$

which is superimposed on Fig. 4-10. In addition, by noting that an iterative procedure is needed to solve for the average pore velocity using Eq. (4.23), we also express C_{Dv} in the form,

$$C_{Dv} = \frac{130}{r_{v*}^{0.85}} + 0.8\left[1 - \exp\left(-\frac{r_{v*}}{400}\right)\right] \tag{4.24}$$

for r_{v*} = 24 – 5000, where r_{v*} is the dimensionless vegetation-related hydraulic radius defined as,

$$r_{v*} = \left(\frac{gS}{\nu^2}\right)^{1/3} r_v \tag{4.25}$$

With C_{Dv} estimated from Eq. (4.24), the average pore velocity can be calculated as $V_v = \sqrt{2gr_vS/C_{Dv}}$ [see Eq. (4.10)]. When the sidewall and bed effects are significant, r_{vm} should be used in place of r_v for evaluating C_{Dv} and then V_v.

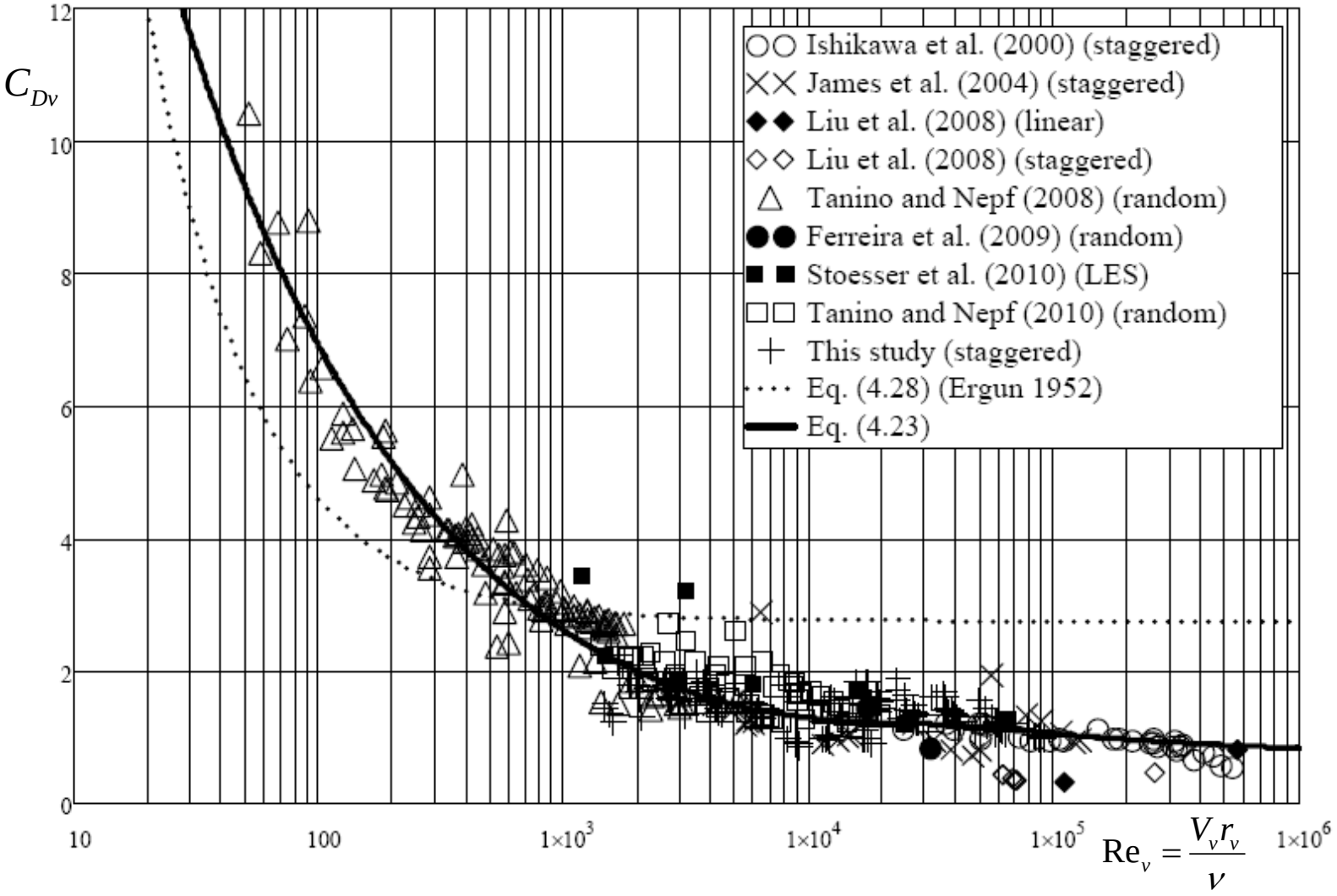

Fig. 4-10. Variation of C_{Dv} with Re_v.

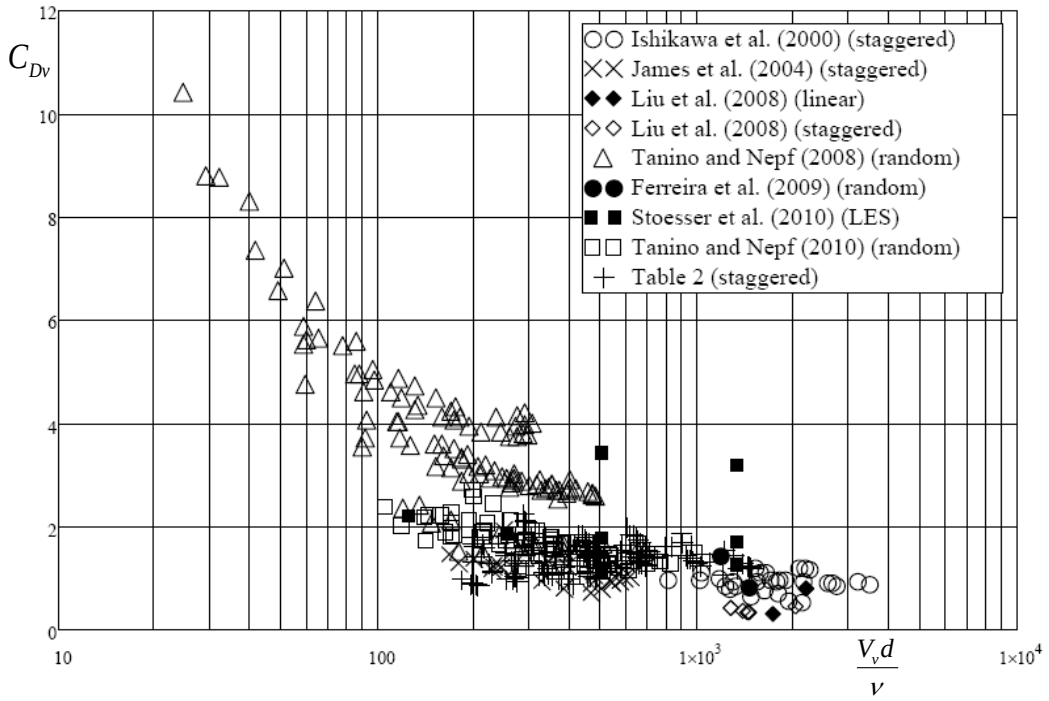

Fig. 4-11. C_{Dv} plotted against $V_v d/\nu$. The data are the same as those used in Fig. 4-10.

4.5.3 Comparison with Ergun equation

Some studies (e.g. Tanino and Nepf 2008; Zinke 2010) have attempted to explore probability of the description of vegetated flows using Ergun equation. Here we use C_{Dv} and Re_v to reformulate Ergun equation, the latter being expressed as (Ergun 1952),

$$\Delta p = 150\frac{\lambda^2}{(1-\lambda)^3}\frac{\rho\nu V}{d_{50}^2} + 1.75\frac{\lambda}{(1-\lambda)^3}\frac{\rho V^2}{d_{50}} \tag{4.26}$$

where Δp is the pressure drop (per unit length) through a column of packed grains, V is the superficial flow velocity (= flow discharge divided by the gross

cross-sectional area of the packed bed), d_{50} is the grain diameter, and λ is the volumetric fraction of grains. To apply Ergun equation to the vegetated channel flows, we replace d_{50} with d, V/ε with V_v, and also take that $S = \Delta p/(\rho g)$, $f_v = 8gr_vS/V_v^2$ and $Re_v = r_vV_v/\nu$. As a result, Eq. (4.26) is revised to be

$$f_{v(Ergun)} = \frac{75\pi^2}{\mathrm{Re}_v} + \frac{7\pi}{2} \tag{4.27}$$

and thus

$$C_{Dv(Ergun)} = \frac{f_{v(Ergun)}}{4} = \frac{75\pi^2}{4\,\mathrm{Re}_v} + \frac{7\pi}{8} \tag{4.28}$$

Eq. (4.28) is superimposed on Fig. 4-10, showing that Ergun equation, if applied to vegetated open channel flows, would underestimate C_{Dv} for low Reynolds numbers and overestimate C_{Dv} for high Reynolds numbers.

4.5.4 Manning coefficient

The Manning coefficient can be determined experimentally from the bulk flow velocity V [= $Q/(BH)$], regular open channel hydraulic radius $BH/(B+2H)$, and energy slope S, i.e.

$$n = \frac{\sqrt{S}}{V}\left(\frac{BH}{B+2H}\right)^{2/3} \tag{4.29}$$

Obviously, the n-values so obtained would generally depend on vegetation configuration for vegetated open channel flows. From Eq.(4.10),

$$\frac{\sqrt{S}}{V} = \sqrt{\frac{C_{Dv}}{2gr_v(1-\lambda)^2}} \tag{4.30}$$

Substituting Eq. (4.30) into (4.29), we get

$$n = \sqrt{\frac{C_{Dv}}{2gr_v(1-\lambda)^2}} \left(\frac{BH}{B+2H} \right)^{2/3} \tag{4.31}$$

Fig. 12 shows that the Manning coefficients predicted using Eq. (4.31), where C_{Dv} is estimated using Eq. (4.24), agree well with the measurements, i.e. those determined using Eq. (4.29) with the data provided by Ishikawa et al. (2000), and James et al. (2004), and also those by this study. Here, r_{vm} was used in place of r_v for estimating C_{Dv} with Eq. (4.24) and n using Eq. (4.31). The average relative errors are 3.6% and 10.2% for the data by Ishikawa et al. and James et al., respectively, and 9.1% for the data collected in this study. However, it should be mentioned that the good agreement shown in Fig. 4-12 is inherent in the method of calculating n, by noting that the same sets of experimental data were also used in the derivation of C_{Dv} included in Eq. (4.31). Therefore, further efforts are needed to verify Eq. (4.31).

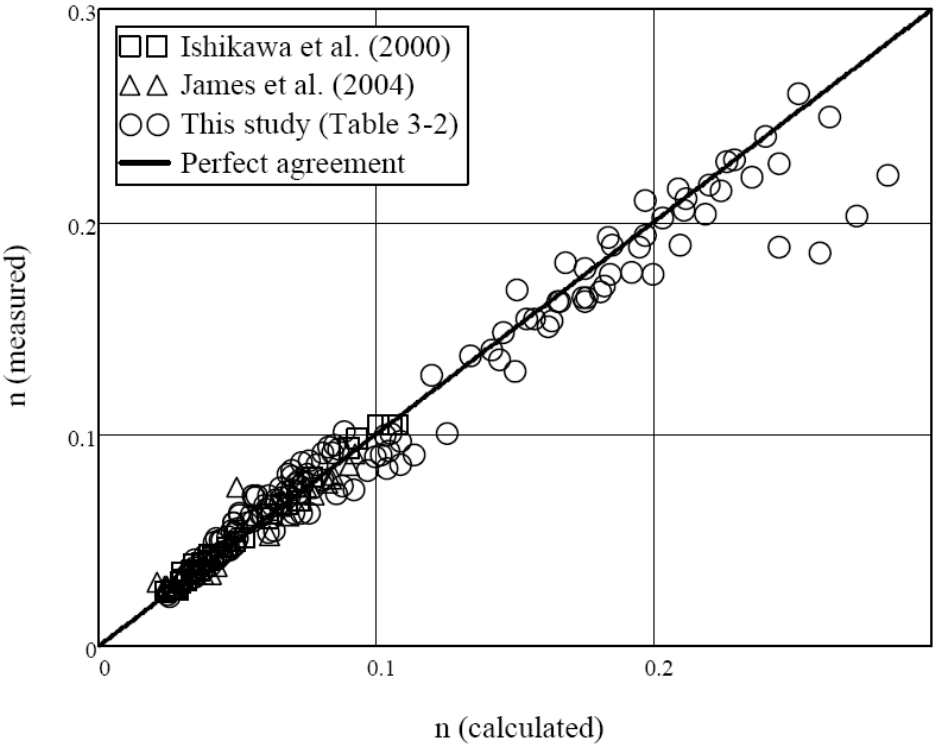

Fig. 4-12. Comparison of predicted and measured Manning coefficients.

4.6 Conclusions

This study demonstrates that the concept of hydraulic radius is useful to unify experimental data of resistance to vegetated open channel flows for various bed and vegetation configurations. The vegetation hydraulic radius is defined by taking into account effects of vegetation size and density, and channel geometry. It serves as an important length scale in the definition of drag coefficient, friction factor and Reynolds number for open channel flows subject to emergent vegetation. From the results of data analysis, it follows that the drag coefficient decreases monotonically with the Reynolds number, independent of vegetation density. This study also shows that Ergun equation, if applied to vegetated open channel flows, would underestimate drag

coefficients for low Reynolds numbers and overestimate for high Reynolds numbers. In addition, a procedure is proposed in this study for correcting sidewall and bed effects that may appear significant for both laboratory and field conditions.

CHAPTER 5

REPRESENTATIVE ROUGHNESS HEIGHT OF SUBMERGED VEGETATION

5.1 Introduction

Many studies have been conducted to analyze the effects of submerged vegetation on flow resistance and flow characteristics in open channel flows. However, it is still difficult to describe velocity profile and evaluate flow resistance in submerged flow condition. Therefore, in this study, we attempt to formulate representative roughness height of submerged vegetation in open channel flows.

For flows over immobile sediment beds, sediment size can be used to estimate roughness length. However, it seems more difficult to find the roughness length scales in vegetated open channel flows in which the roughness length scale could vary with vegetation configuration. Therefore, to find the appropriate roughness length scale, different parameters such as vegetation density or vegetation diameter need to be considered in the formulation. Different considerations have been presented in the literature. Kouwen et al. (1969)

proposed the vegetation height as the roughness length to evaluate the flow resistance induced by submerged vegetation. They reported that the flow velocity in submerge cases can be described in a logarithmic law

$$\frac{U}{u_*} = a_1 + a_2 \ln\left(\frac{H}{h_v}\right) \tag{5.1}$$

where U is the cross-sectional average velocity, u_* is the shear velocity, H is the flow depth, h_v is the vegetation height, and a_1 and a_2 are constants which varying with vegetation density and flexibility. Eq. (5.1) suggests that the vegetation height be considered as an equivalent roughness height.

Huthoff et al. (2007) scaled the average velocity in the surface layer in the power-law form using stem spacing as the length scale to estimate the equivalent roughness height,

$$\frac{U_s}{\sqrt{gh_sS}} \sim \left(\frac{h_s}{k}\right)^{1/6} \tag{5.2}$$

where U_s is the average flow velocity in the surface layer (see Fig. 5-1), h_s is the surface layer thickness, S is the energy slope, g is the gravitational acceleration and k is an equivalent roughness height that scales with other variables,

$$k \sim \frac{(C_D d)^3}{(s+d)^2} \tag{5.3}$$

where C_D is the stem drag coefficient, d is the stem diameter and s is the stem spacing. If the number of stems per unit bed area is N, and the vegetation

concentration is λ, then $(s+d)^2 \sim 1/N$, and $N = 4\lambda/(\pi d^2)$ for cylindrical stems. With these considerations, k can be further scaled as

$$k \sim \frac{4}{\pi} C_D^3 \lambda d \tag{5.4}$$

Eq. (5.4) shows that k varies in the order of λd if C_D can be approximated as a constant close to unity.

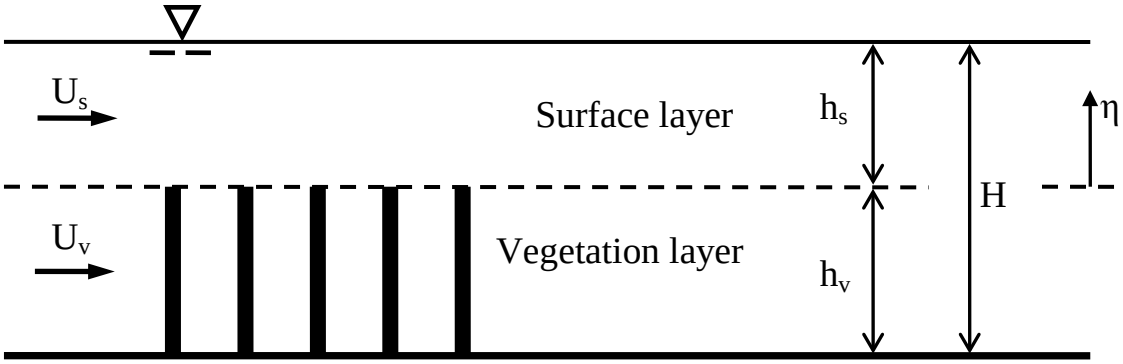

Fig. 5-1. Vegetated open channel flow comprising surface and vegetation layer. U_v is the average velocity of the flow through stems.

Other researchers such as Nepf and Vivoni (2000) and Baptist et al. (2007), also applied logarithmic distribution to depict the streamwise velocity profile distributed within the upper layer,

$$\frac{u}{\sqrt{gh_s S}} = \frac{1}{\kappa} \ln\left(\frac{\eta - \Delta\eta}{\eta_o}\right) \tag{5.5}$$

where η is measured upwards from the edge of vegetation, $\Delta\eta$ is the zero-plane displacement, κ is the von Karman constant and η_0 is the hydrodynamic roughness length. For example, Baptist et al. (2007) proposed that

$$\eta_o = L\left(1-\exp(-\frac{h_v}{L})\right)\exp\left(-\kappa\sqrt{\frac{40L}{h_s}(1+\frac{L}{h_s})}\right) \quad (5.6)$$

where $L = [\pi d h_s/(80\lambda)]^{0.5}$. If assuming that the power law and logarithmic function applied above are equivalent, as demonstrated in open channel hydraulics, one may expect that η_0 and k are comparable. This will be discussed further later in this chapter.

From the above-mentioned studies, it can be concluded that the vegetation height h_v should not be taken as a representative length scale to describe vegetation roughness height even though it is an important factor. Besides that, it could be more appropriate to define a single roughness length applicable to the entire bulk flow rather than using separate different length scales of the flow in the surface and vegetation layer (see Fig. 5-1).

This study aims to propose a representative roughness height for the surface layer, and then develop an approach to evaluation of bulk flow velocity and thus resistance coefficients (e.g. Manning and Chezy coefficient). Only simulated vegetation stems are considered, including rigid cylindrical rods and flexible film strips.

5.2 Conceptual consideration

The idea to quantify vegetation-induced roughness is developed by the concept of vegetation hydraulic radius, i.e. r_v, in which r_v is the dimension of the unblocked flow volume per unit frontal area that blocks the flow. In an opposite

manner, the roughness height is the length scale defined as the dimension of the blocked flow volume per unit frontal area that does not block the flow. In Chapter 4, the vegetation hydraulic radius with vegetation simulated by rigid, cylindrical stems is defined as

$$r_v = \frac{\Phi_f}{A_v} = \frac{(1-\lambda)h_v}{4\lambda h_v/(\pi d)} = \frac{\pi}{4}\frac{1-\lambda}{\lambda}d \tag{5.7}$$

where Φ_f [= (1-λ)h_v] is fluid-occupied volume and A_v is the total wetted surface area of all stems.

Using the same way to define the vegetation hydraulic radius to quantify how rough the stems are, the roughness height is defined as

$$k_v = \frac{\Phi_v}{A_f} = \frac{\lambda h_v}{4(1-\lambda)h_v/(\pi d)} = \frac{\pi}{4}\frac{\lambda}{1-\lambda}d \tag{5.8}$$

where Φ_v (= λh_v) is vegetation-occupied volume and A_f = 4(1-λ)h_v/(πd) is the frontal area for the fluid-occupied volume. However, it should be mentioned that A_f is not the actual frontal area, and it is evaluated by imagining that Φ_f be filled up with stems as in Φ_v. Both r_v and k_v provide length scales in the sense of hydrodynamics. Like the hydraulic radius defined for other flows, r_v given in Eq. (5.7) signifies how spacious the flow domain is in the presence of boundary resistance (i.e. vegetation stems) for vegetated channel flows. In contrast, k_v given in Eq. (5.8) denotes the dimension of the vegetation-induced blockage is with respect to the flow.

Therefore, as a reasonable measure, k_v could be taken as the representative length scale to describe the size of stem-induced roughness. Eq. (5.8) shows that k_v is proportional to the vegetation concentration and stem diameter. If λ is constant, k_v would be in the order of d, which resembles the sediment size, i.e. roughness length scale for rough flows over a sediment bed. In Section 5-4, it is shown that this roughness height, when normalized with the flow depth in the surface layer, performs well in collapsing resistance data collected with a wide range of vegetation configurations.

5.3 Data collection

5.3.1 Experiments and other data sources

In this study, altogether 24 runs of experiments under submerged flow conditions were conducted as described in Chapter 3. The flow velocity profile was measured at the centreline of the flume using a laser Doppler velocimetry. The flow discharges were measured with a standard deviation of 0.1-7.5%. The data collected are listed in Table 3-3.

Data from previous studies are also collected which consist of 10 data sources fo rigid vegetation (277 sets of data) and 6 the case of flexible vegetation (103 sets of data). The relevant information is summarized in Table 5-1. The collected data simulated different type of vegetation configurations, i.e. cylindrical rods, strips and actual plants, in staggered pattern, linear pattern, and random pattern.

Table 5-1. Summary of experiments conducted by previous investigators.

Investigator	**Vegetation zone**		**Vegetation configuration**					**Flow condition**	**No. of runs**
	Width (m)	**Length (m)**	**Stem diameter d (mm)**	**Stem height h_v (m)**	**Concen-tration λ (%)**	**Stem shape**	**pattern**		
Rigid vegetation									
Shimizu et al (1991)	0.5	6	1	0.041	0.44-0.79	cylindrical	linear	uniform	20
	0.4	6	1.5	0.046					8
Dunn et al (1996)	0.91	2.44	6.35	0.118	0.14-1.23	cylindrical	staggered	uniform	12
Meijer (1998) (see Baptist 2005)	3	20.5	8	0.45-1.5	0.32-1.29	cylindrical		non-uniform	48
Stone and Shen (2002)	0.45	11	3.18-12.7	0.124	0.55-6.10	cylindrical	staggered	uniform	128
Poggi et al (2004)	0.9	9	4	0.12	0.08-1.35	cylindrical	linear	non-uniform	5
Murphy et al (2007)	0.38		6.4	0.07; 0.14	1.18-3.77	cylindrical	random	non-uniform	24
Liu et al (2008)	0.3	3	6.35	0.076	0.31-1.57	cylindrical	linear; staggered	uniform	9
Nezu and Sanjou (2008)	0.4	9	8	0.05		flat strip	linear	uniform	9
Yan (2008)	0.42	8	6	0.06	1.41-5.66	cylindrical	linear	uniform	12
Yang (2008)	0.45	6	2	0.035	0.44	cylindrical	staggered	uniform	2
Present study	0.3	9.6	3.2-8.3	0.1	0.43-11.90	cylindrical	staggered	uniform	23
Flexible vegetation									
Kouwen et al (1969)	0.61		5	0.05-0.1	9.82	flat strip	staggered	uniform	27
Dunn et al (1996)	0.91		6.35	0.097-0.161	0.14-1.23	cylindrical	staggered	uniform	6
Jarvela (2003)	1.1	6	2.8-3	0.155-0.295	0.36-7.39	(wheat; sedge)		non-uniform	12
Yang (2008)	0.45	6	2	0.023-0.034	0.44	flat strip	staggered	uniform	5
Kubrak et al (2008)	0.58	3	0.7; 0.95	0.131-0.164	0.13-0.54	cylindrical	linear	uniform	25
Okamoto and Nezu (2010)	0.40	10	8	0.03-0.1	4.78	flat strip	linear	uniform	28

Notes: (1) For flat strips, d is taken as stem width. (2) For flexible vegetation, h_v is taken as deflected height, and λ is calculated as $\pi Nd^2/4$, where N is the number of stems per unit bed area.

Equivalent concentration of vegetation simulated by film strips

For the case of film strips, the strip width is taken as an equivalent stem diameter, which yields the same projected area in the flow direction. Then, the equivalent concentration is computed as $\pi d^2 N/4$, where d is the strip width and N is the number of stems per unit bed area.

5.4 Analyses and comparisons

5.4.1 Variations of friction factor with relative roughness height

With the pre-processed data for the case of rigid vegetation, some possible friction factor relationships are examined here. First, the friction factor is defined simply using cross-sectional flow parameters, i.e.

$$f = \frac{8grS}{U^2} \tag{5.9}$$

where U [= $Q/(BH)$] is the average flow velocity, r [= $BH/(B+2H)$] is the hydraulic radius, Q is the flow discharge, and B is the channel width. Correspondingly, the relative roughness height is defined as h_v/r. Fig. 5-2 shows that the relationship of f and h_v/r is unclear. This may imply that it is improper to use h_v as an equivalent roughness height in the description of vegetation effects.

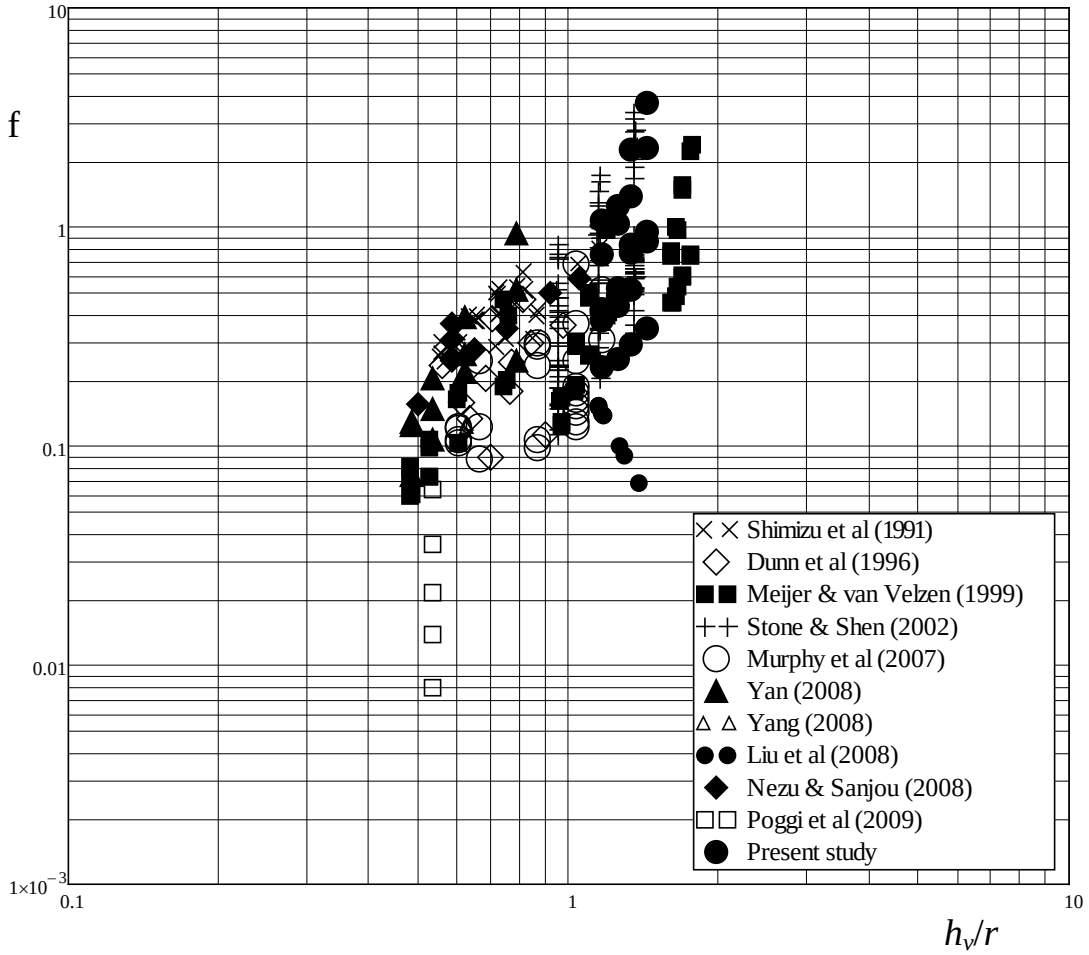

Fig. 5-2. Relationship of f [= $8grS/U^2$] and h_v/r.

Second, we only consider the upper surface layer by noting distinct characteristics of the two layers. Using the surface layer thickness h_s in place of r and the average surface layer velocity U_s in place of U, the friction factor is expressed as

$$f_s = \frac{8gh_sS}{U_s^2} \tag{5.10}$$

where subscript *s* denotes the surface layer. Similarly, the relative roughness height is taken as h_v/h_s. Fig. 5-3 shows that the relationship between f_s and h_v/h_s is again indistinct.

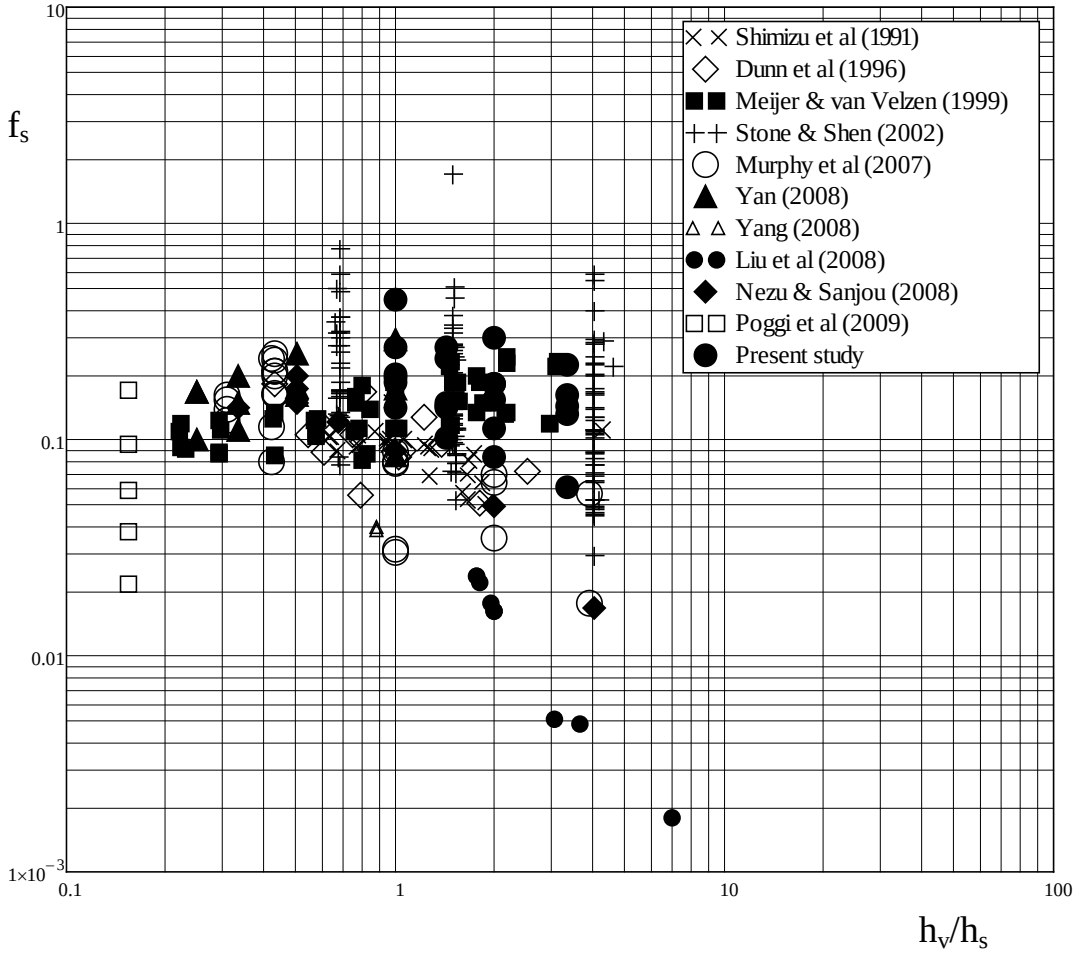

Fig. 5-3. Relationship of f_s [= $8gh_sS/U_s^2$] and h_v/h_s.

Next, the proposed roughness height k_v (i.e. Eq. (5.8)) is used to revise the relative roughness height as k_v/h_s. The relationship of f_s and k_v/h_s is plotted with the same data in Fig. 5-4. It shows that this relationship becomes much clearer than those plotted in Fig. 5-2 and Fig. 5-3, in spite of a few deviating data points that include those reported by Liu et al. (2008), and also those with small

values of h_s from Murphy et al. (2007) and Nezu and Sanjou (2008). The deviation could be explained because the slope in those studies were estimated from Reynolds shear stresses which would require that the flow depth of the surface layer is large enough so that the linear distribution of the Reynolds shear stress is clearly observed. This further suggests that it is the use of k_v that is helpful to clarify the friction factor relationship. As an approximation, the general data trend displayed in Fig. 5-4 is fitted using the following function,

$$f_s = \alpha \left(\frac{k_v}{h_s} \right)^{\beta} \tag{5.11}$$

where $\alpha \approx 0.40$ and $\beta \approx 1/8$. The goodness of fit by Eq. (5.11) can be assessed by quantifying the scatter of the data points with respect to the straight line plotted in the logarithmic scales, as shown in Fig. 5-4. To this end, the relative fluctuation for each data point was computed as $|\log(f_s^{measured}) - \log(f_s^{predicted})|/\log(f_s^{predicted})$. Statistics of the computed results show that on average, the relative fluctuation is 27.6%, which implies that Eq. (5.11) generally represents most of the data points. Substituting Eqs. (5.8) and into Eq. (5.11) and manipulating, we get the average flow velocity in the surface layer,

$$U_s = \psi \left(\frac{1-\lambda}{\lambda} \frac{h_s}{d} \right)^{1/16} \sqrt{g h_s S} \tag{5.12}$$

where $\psi \approx 4.54$.

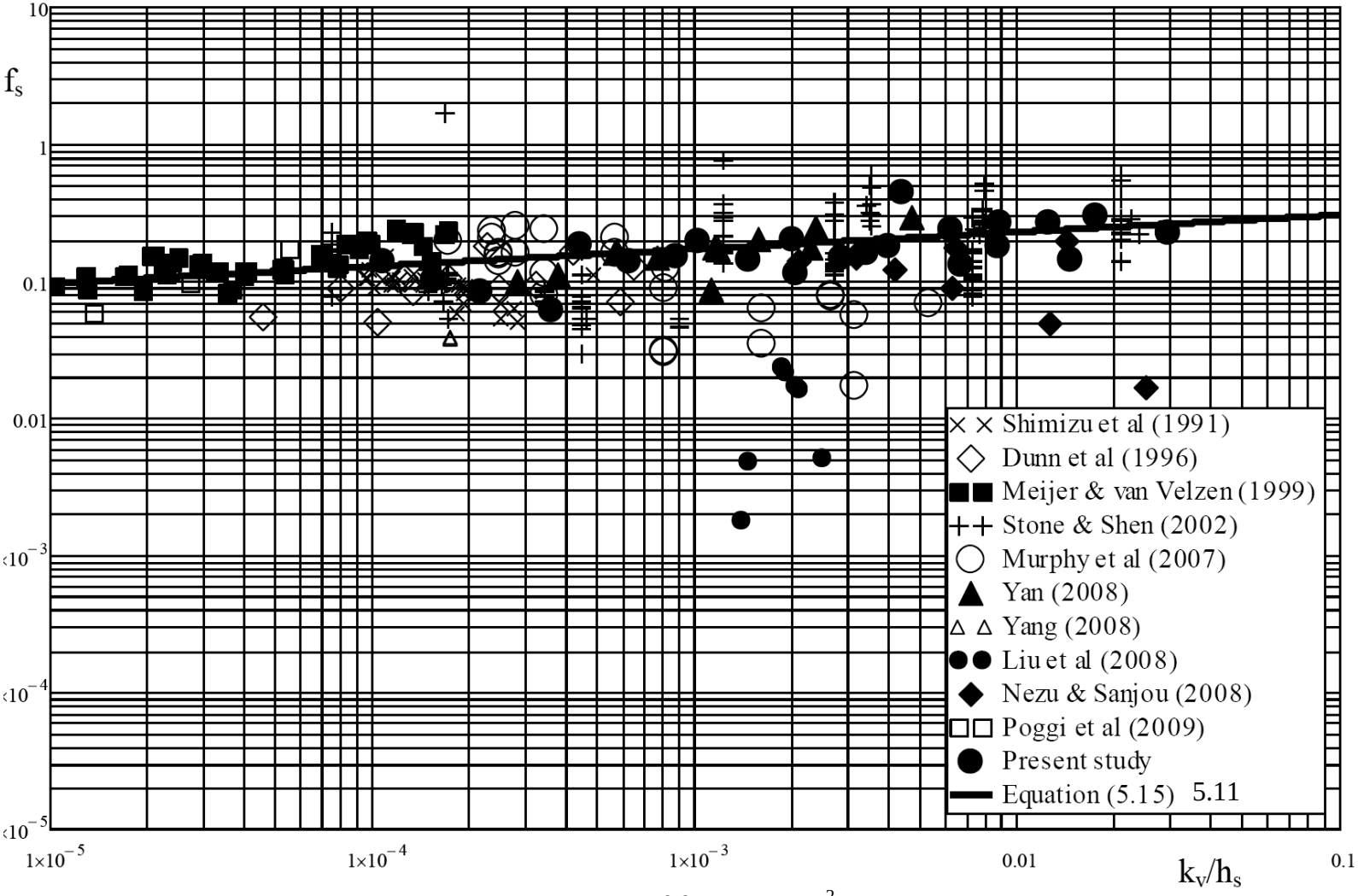

Fig. 5-4. Relationship of f_s [= $8gh_sS/U_s^2$] and k_v/h_s.

5.4.2 Calculation of average velocity and resistance coefficients

The average flow velocity through the cross-section can be computed by using the average velocity of flow in vegetation layer U_v and the average velocity of flow in upper layer U_s as presented by (Huthoff et al., 2007; Yang and Choi, 2010) (see Fig. 5-1). the average velocity of flow in vegetation layer

$$U = \frac{U_s h_s + U_v h_v (1-\lambda)}{H} \tag{5.13}$$

Moreover, the average velocity through the vegetation layer is comparable to that observed for the case of emergent vegetation for the same energy slope and vegetation configuration (Stone and Shen, 2002). Therefore, the average velocity of flow in vegetation layer U_v can be estimated using the drag coefficient C_D proposed in Chapter 4 [i.e. Eq. (4.24)] for the emergent case,

$$U_v = \sqrt{\frac{2gr_v S}{C_D}} \tag{5.14}$$

where

$$C_D = \frac{130}{r_{v*}^{0.85}} + 0.8\left[1 - \exp\left(-\frac{r_{v*}}{400}\right)\right] \tag{5.15}$$

with $r_{v*} = (gS/\nu^2)^{1/3} r_v$, $r_v = \pi(1\text{-}\lambda)d/(4\lambda)$ and ν is the kinematic viscosity of fluid. Since the measured data for U_v are usually not available in the previous studies, Eq. (5.14) is applied to all the data for estimating U_v in the subsequent analyses.

Substituting Eqs. (5.12) and (5.14) into Eq. (5.13), we get,

$$U = \left[\sqrt{\frac{\pi(1-\lambda)^3}{2C_D\lambda}\frac{d}{h_v}}\left(\frac{h_v}{H}\right)^{3/2} + 4.54\left(\frac{h_s}{d}\frac{1-\lambda}{\lambda}\right)^{1/16}\left(\frac{h_s}{H}\right)^{3/2} \right]\sqrt{gHS} \tag{5.16}$$

Using Eq. (5.16), the Chezy coefficient, i.e. $C = U/(HS)^{0.5}$, is expressed as,

$$C = \sqrt{\frac{\pi g}{2C_D}\frac{(1-\lambda)^3}{\lambda}\frac{d}{h_v}}\left(\frac{h_v}{H}\right)^{3/2} + 4.54\sqrt{g}\left(\frac{h_s}{d}\frac{1-\lambda}{\lambda}\right)^{1/16}\left(\frac{h_s}{H}\right)^{3/2} \tag{5.17}$$

Similarly, the expression for the Manning coefficient can also be obtained by noting that $n = H^{1/6}/C$.

5.4.3 Comparisons with previous formulas

First, the values of the roughness height computed using the proposed formula, i.e. Eq. (5.8), are compared with other two formulas, i.e. Eq. (5.4) (Huthoff et al. 2007) and Eq. (5.6) (Baptist et al. 2007). Fig. 5-5 shows that Eq. (5.8) is comparable only to Eq. (5.4) with C_D computed using Eq. (5.15). In comparison, the results of η_o computed using Eq. (5.6) appear completely unrelated to k_v given by Eq. (5.8). This is understandable by noting that both Eq. (5.4) and (5.8) are proportional to the product of λd. However, in Huthoff et al. (2007), the choosing of characteristic length scale for the surface layer as the stem spacing is somewhat arbitrary. In comparison, the framework presented in this study for defining the roughness length has a better physical basis.

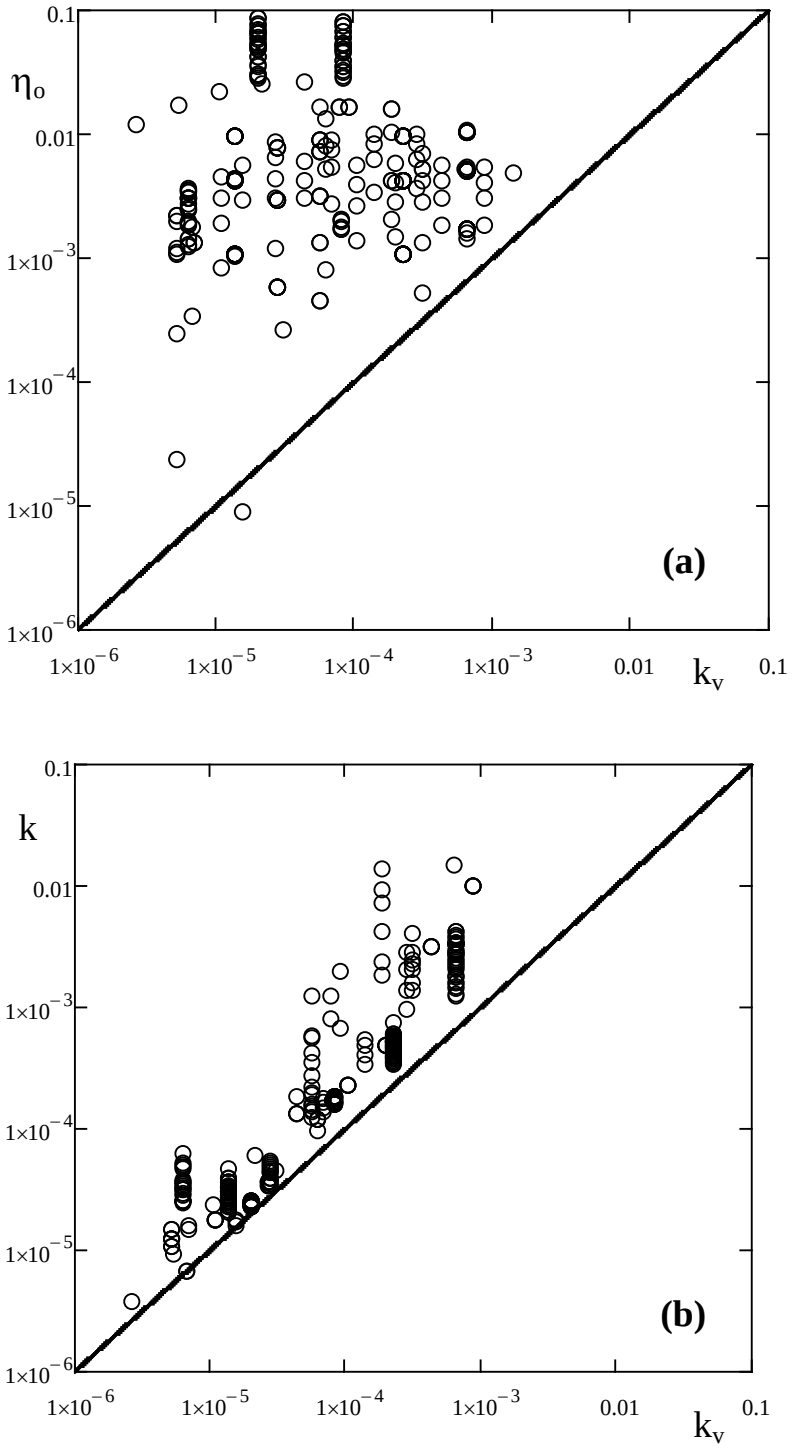

Fig. 5-5. Comparisons of estimated roughness heights. They are computed using Baptist et al.'s formula (η_o given by Eq. (5.6)), Huthoff et al.'s formula (k by Eq. (5.4)) and the present formula (k_v by Eq. (5.8)). The unit is m.

Second, the average velocities predicted using Eq. (5.16) are compared with four previous formulas as follows:

(1) Stone and Shen's (2002) formula

$$U = 1.385\left(\frac{H}{h_v}\sqrt{\frac{\pi}{4\lambda}} - 1\right)\sqrt{gdS} \tag{5.18}$$

where S is the vegetation-related energy slope, and close to the total energy slope if the bed friction is negligible.

(2) Baptist et al.'s (2007) formula By applying genetic programming (GP), Baptist et al. obtained

$$U = \left[\sqrt{\frac{1}{g/C_b^2 + 2C_D\lambda h_v/(\pi d)}} + 2.5\ln\left(\frac{H}{h_v}\right)\right]\sqrt{gHS} \tag{5.19}$$

where C_b is the bed-related Chezy coefficient (≈ 60 $m^{0.5}/s$ for smooth bed), and C_D could be taken to be 1.0.

(3) Huthoff et al.'s (2007) formula A analytical solution for the depth-averaged velocity for flow in presence of submerged vegetation is developed as,

$$U = \left[\frac{h_s}{H}\left(\frac{h_s}{\left(\sqrt{\pi/(4\lambda)} - 1\right)d}\right)^{\frac{2}{3}\left[1-\left(\frac{h_v}{H}\right)^5\right]} + \sqrt{\frac{h_v}{H}}\right]\sqrt{\frac{\pi gdS}{2C_D\lambda}} \tag{5.20}$$

where C_D was assumed almost constant with a value of nearly 1.0.

For model calibration, Huthoff et al. also used experimental data from Meijer and van Velzen (1999).

(4) Yang and Choi's (2010) formula By applying the logarithmic distribution of velocity profile to the surface layer, Yang and Choi proposed following relationship to calculate the depth-averaged velocity

$$U = \sqrt{\frac{\pi g d H S}{2 C_D h_v \lambda}} + \frac{C_u \sqrt{g h_s S}}{0.41}\left(\ln \frac{H}{h_v} - \frac{h_s}{H} \right) \tag{5.21}$$

where C_D = 1.13, and C_u = 1 for $4\lambda/(\pi d) \le 5$ and 2 for $4\lambda/(\pi d) > 5$.

Table 5-2 summarizes the prediction errors associated with Eqs. (5.16), (5.18), (5.19), (5.20) and (5.21). Here, the errors were computed as |prediction – measurement|/measurement. For comparison, 24 datasets were collected experimentally by this study (Table 3.3) and 277 datasets were collected from previous study. It can be seen that the prediction error of varies with the predicted average flow velocity, and Manning and Chezy coefficients for each formula applied. In addition, it can be observed that the formulas proposed in this study and Huthoff et al perform better than Baptist, Stone and Shen, and Yang and Choi's formulas.

Since the variation of flow rate is much wider than other variables, the predictions of flow rate by individual formula are plotted against the measurements in Fig. 5-6 for comparison. Fig. 5-6 (a) and Fig. 5-6 (d) show that both Stone and Shen's and Yang and Choi's formulas generally underestimate the flow rates, in particular for high flow rates. Baptist et al.'s

formula works well for high flow rates but yields over prediction for low flow rates (see Fig. 5-6(b)). Huthoff et al.'s formula gives the best prediction for high flow rates, but underestimates low flow rates, as shown in Fig. 5-6(c). This could be resulted by their calibration process mainly using the high flow rate data conducted by Meijer and van Velzen (1999) (see Table 5-1).

Table 5-2. Prediction errors for different formulas.

Investigator	**Equation**	**Absolute error (%)**			
		Rigid vegetation		**Flexible vegetation**	
		Flow rate or average velocity or Chezy coefficient	Manning coefficient	Flow rate or average velocity or Chezy coefficient	Manning coefficient
Stone and Shen (2002)	(5.18)	18.9	26.1	27.0	60.0
Baptist et al. (2007)	(5.19)	24.2	18.6	27.1	20.6
Huthoff et al. (2007)	(5.20)	14.0	18.0	15.3	18.7
Yang and Choi (2010)	(5.21)	20.9	30.8	15.7	21.9
Present study	(5.16)	14.3	16.8	16.6	15.2

In comparison, being calibrated with the larger database, the formula proposed in this study applies equally well, as expected, for both high and low flow rates, as shown in Fig. 5-6(e).

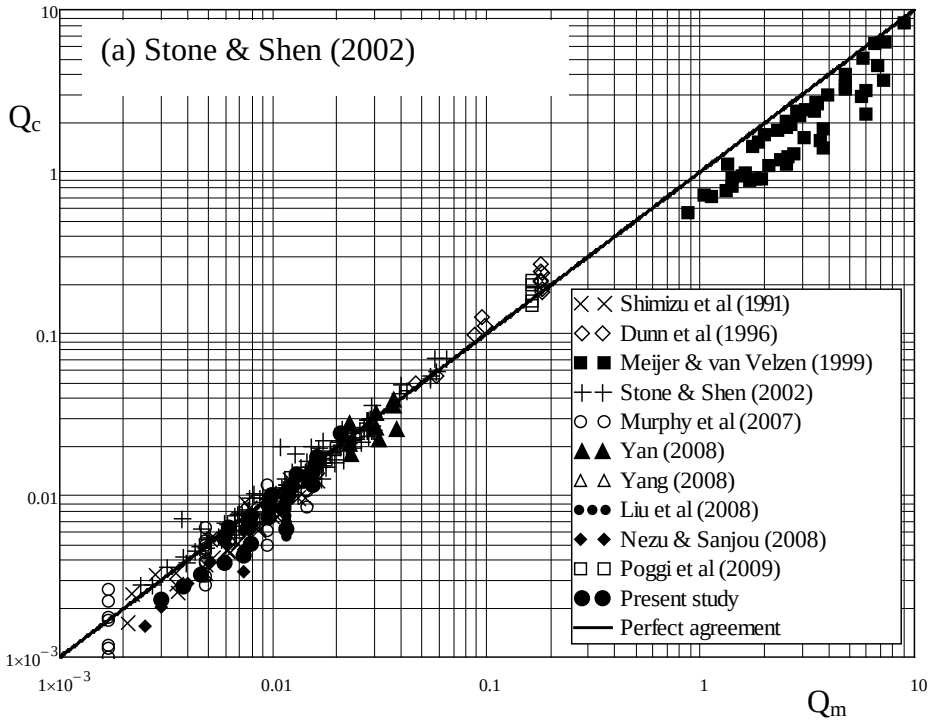
(a) Stone & Shen (2002)
Q_c
Q_m
10
1
0.1
0.01
1×10^{-3}
1×10^{-3}
0.01
0.1
1
10
Shimizu et al (1991)
Dunn et al (1996)
Meijer & van Velzen (1999)
Stone & Shen (2002)
Murphy et al (2007)
Yan (2008)
Yang (2008)
Liu et al (2008)
Nezu & Sanjou (2008)
Poggi et al (2009)
Present study
Perfect agreement

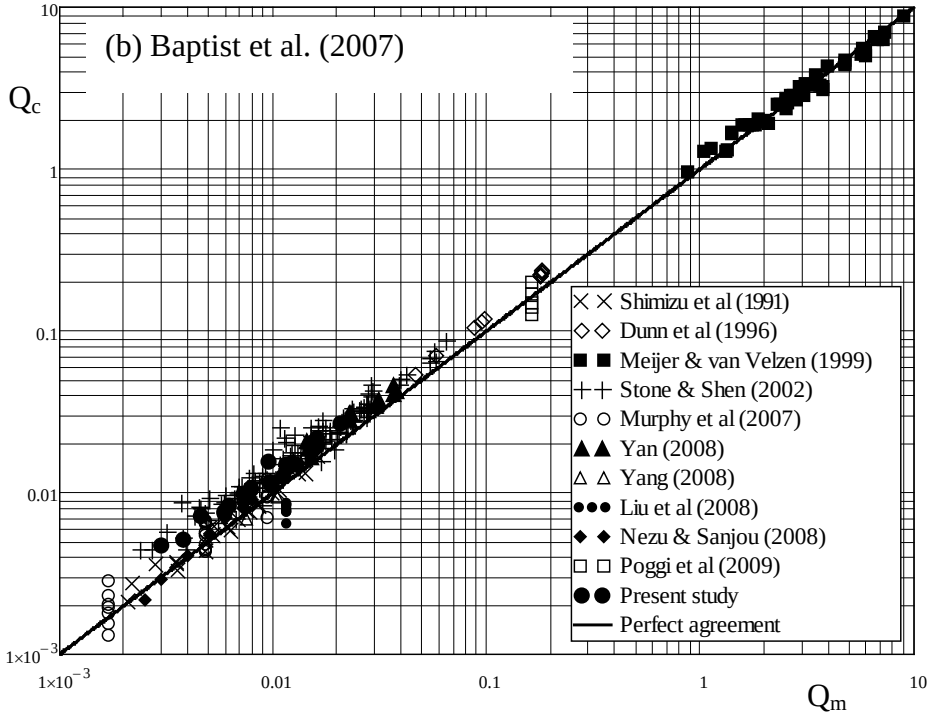
(b) Baptist et al. (2007)
Q_c
Q_m
10
1
0.1
0.01
1×10^{-3}
1×10^{-3}
0.01
0.1
1
10
Shimizu et al (1991)
Dunn et al (1996)
Meijer & van Velzen (1999)
Stone & Shen (2002)
Murphy et al (2007)
Yan (2008)
Yang (2008)
Liu et al (2008)
Nezu & Sanjou (2008)
Poggi et al (2009)
Present study
Perfect agreement

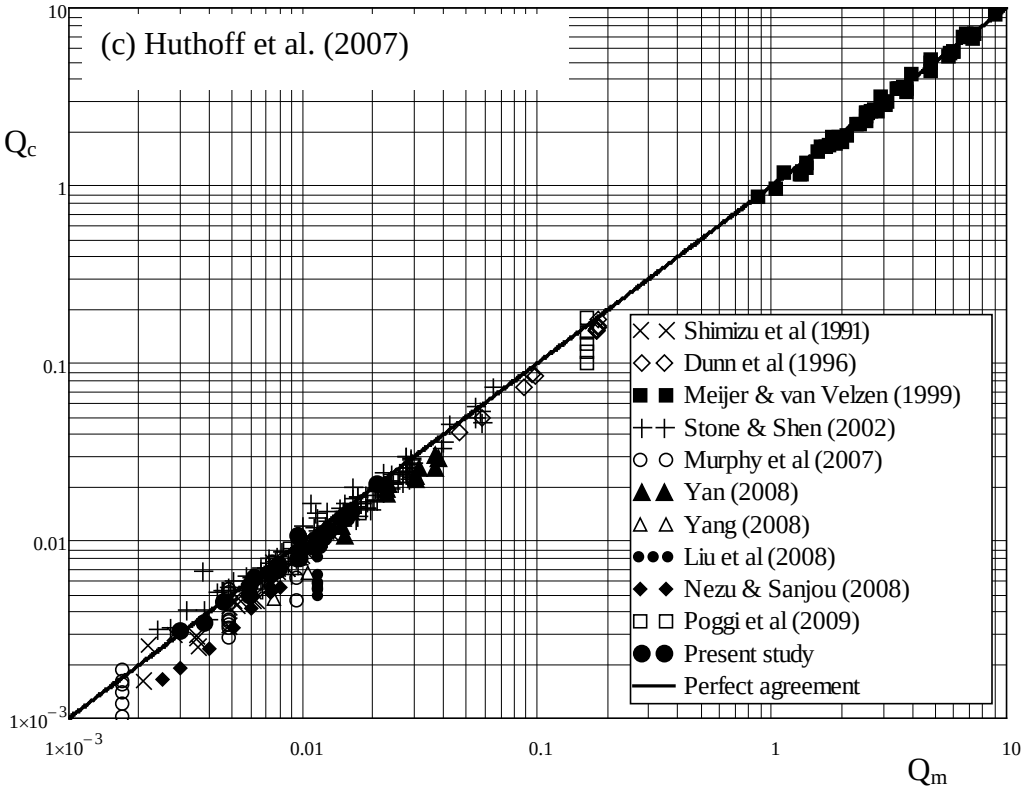
(c) Huthoff et al. (2007)
Q_c
Q_m
10
1
0.1
0.01
1×10^{-3}
1×10^{-3}
0.01
0.1
1
10
Shimizu et al (1991)
Dunn et al (1996)
Meijer & van Velzen (1999)
Stone & Shen (2002)
Murphy et al (2007)
Yan (2008)
Yang (2008)
Liu et al (2008)
Nezu & Sanjou (2008)
Poggi et al (2009)
Present study
Perfect agreement

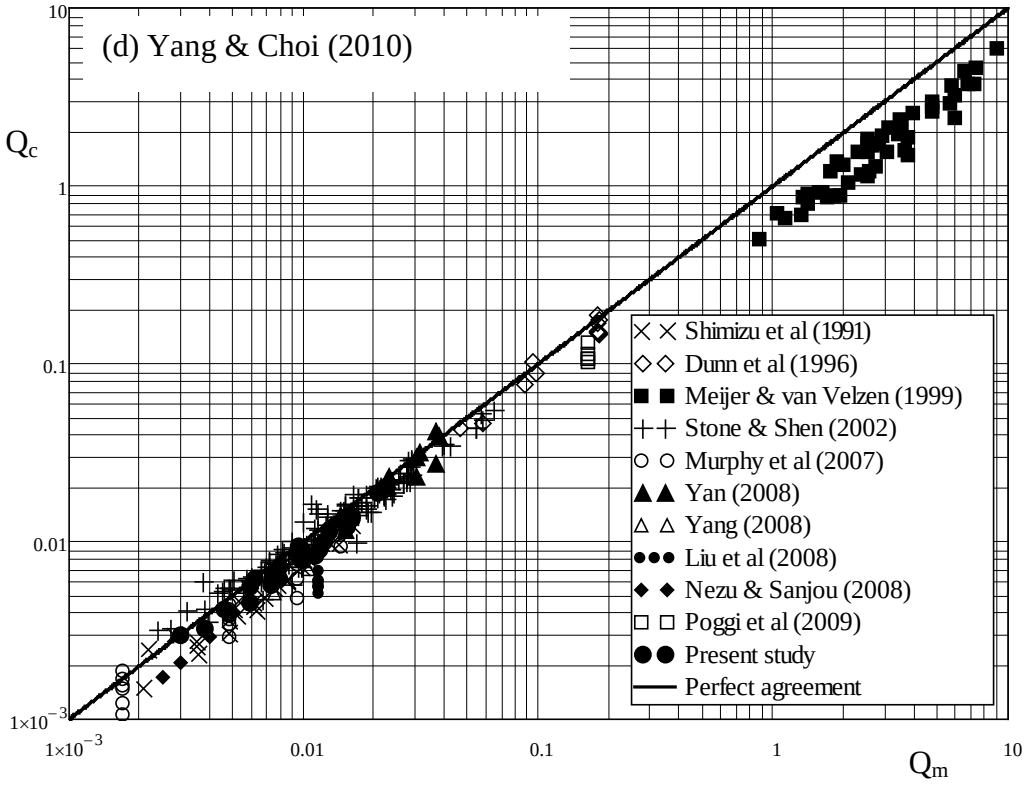
(d) Yang & Choi (2010)
Q_c
Q_m
10
1
0.1
0.01
1×10^{-3}
1×10^{-3}
0.01
0.1
1
10
Shimizu et al (1991)
Dunn et al (1996)
Meijer & van Velzen (1999)
Stone & Shen (2002)
Murphy et al (2007)
Yan (2008)
Yang (2008)
Liu et al (2008)
Nezu & Sanjou (2008)
Poggi et al (2009)
Present study
Perfect agreement

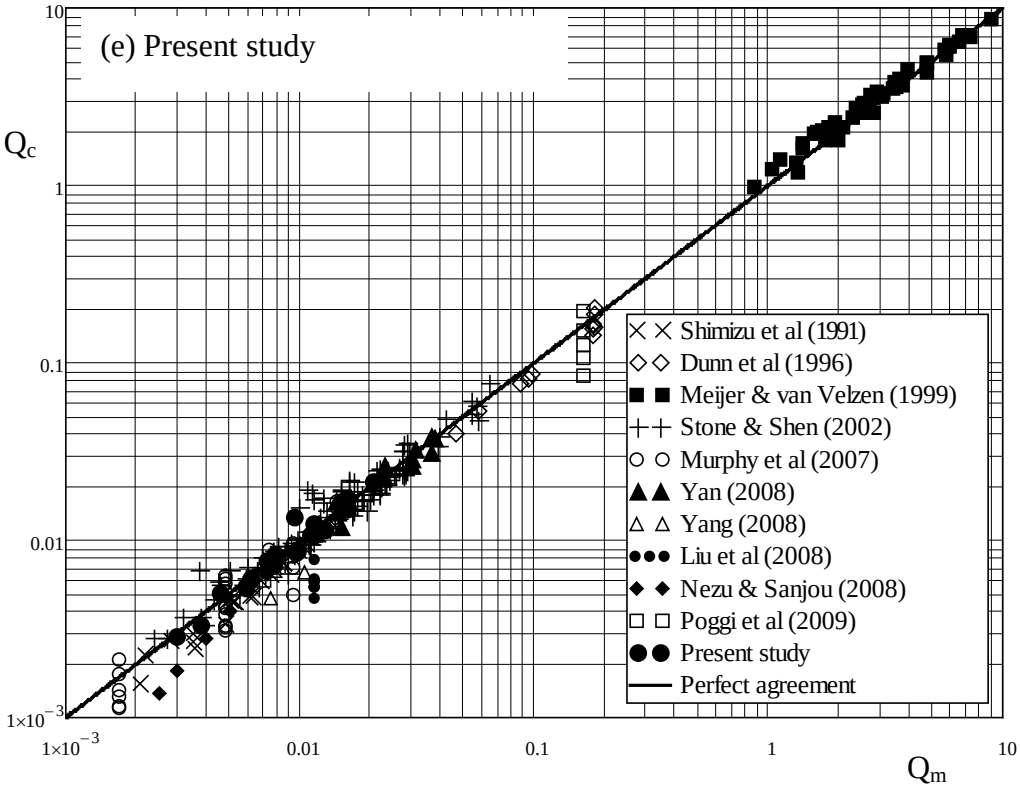

Fig. 5-6. Comparisons of calculated flow rates (Q_c) with measurements (Q_m) (in m^3/s) for the case of submerged rigid vegetation.

5.5 Discussion

5.5.1 Simplification of formulas

Although the mentioned four formulas and the one proposed by this study have been derived with different considerations and resulted in different forms, they can be simplified and expressed similarly. Such an attempt is given as follows.

First, consider the case of emergent vegetation, for which $h_s = 0$ and $H = h_v$. Then, Eq. (5.16) reduces to

$$U_v = 1.25\sqrt{\frac{(1-\lambda)^3 dgS}{C_D \lambda}} \tag{5.22}$$

Furthermore, if assuming that $\lambda << 1$ and $C_D \approx 1$, Eq. (5.22) can be rewritten as

$$U_v = 1.25\sqrt{\frac{dgS}{\lambda}} \tag{5.23}$$

It can be shown that Eq. (5.23) can also be obtained by simplifying Eqs. (5.18) to (5.20) for the same condition.

Next, with the assumptions of $\lambda << 1$ and $C_D \approx 1$ and Eq. (5.23), we can rewrite all velocity formulas, i.e. Eqs. (5.16), (5.18), (5.19), (5.20) and (5.21) in the following general form,

$$\frac{U}{U_v} = \left(\frac{h_v}{H}\right)^{c_1} + c_2 \lambda^{c_3} \left(\frac{H}{d}\right)^{c_4} \left(1 - \frac{h_v}{H}\right)^{c_5} \tag{5.24}$$

where constants c_1 to c_5 are given in Table 5-3 for each formula. To simplify Eq. (5.16), we note that $[(h_s/d)(1-\lambda)/\lambda]^{1/16}$ varies in a limited range, and could be replaced with a constant of 1.6 that was estimated using the data collected. In addition, we also replace $\ln(H/h_v)$ in Eq. (5.19) using $2(1 - h_v/H)^{1.5}$ with an accuracy of 4.8% for H/h_v = 1.5 - 4. Similarly, to rewrite Eq. (5.21), we use $0.56(1- h_v/H)^{2.5}$ to approximate $[\ln(H/h_v)-(1-h_v/H)][\ h_v/H\ (1-h_v/H)]^{0.5}$ with an accuracy of 3.8% for H/h_v = 1.5 – 4. From the constants summarized in Table 5-3, it follows that although derived from the different considerations, the five formulas except for Eq. (5.18) appear similar by noting that each of constants c_3 to c_5 has close values for the different formulas.

Table 5-3. Values of the five constants included in Eq. (5.24).

Investigator	**Equation**	c_1	c_2	c_3	c_4	c_5
Stone and Shen (2002)	(5.18)	-1	-1.1	0.5	0	0
Baptist et al. (2007)	(5.19)	-0.5	4	0.5	0.5	1.5
Huthoff et al. (2007)	(5.20)	0.5	1.1	0.33	0.67	1.67
Yang and Choi (2010)	(5.21)	-0.5	1.1 – 2.2	0.5	0.5	2.5
Present study	(5.16)	1	5.1	0.5	0.5	1.5

With Eq. (5.28) together with each set of constants given in Table 5-3, we also performed additional computations using the data summarised in Table 5-1. As can be seen from Table 5-4, the results predicted using the simplified formula differ to some extent from those using the complete version. For the formulas proposed by Stone and Shen (2002) and Baptist et al. (2007), the simplified versions reduced the prediction error by 0.1-1.3% as compared to the complete versions. For other three formulas including the present formula, the simplification resulted in the increasing of prediction errors by 1.4-5.7%. In comparison, the simplified version of the formula proposed in this study causes the largest error difference of 4.0% - 5.7%.

5.5.2 Application to submerged flexible vegetation

In the following, Eq. (5.16) is applied to predict the average flow velocity in the presence of submerged flexible vegetation. Altogether 103 sets of data from Dunn et al. (1996), Jarvela (2003), Kouwen et al. (1969), Kubrak et al. (2008), Okamoto and Nezu (2010), and Yang (2008) were collected as in Table 5-1. In

collected datasets, flexible vegetation was simulated by film strips (Kouwen et al., 1969; Okamoto and Nezu, 2010; Yang, 2008), cylindrical stems ([Dunn et al., 1996; Kubrak et al., 2008) and real plants (Jarvela, 2003). In applying equation (5.16), h_v is taken as the average value of deflected height, which partially reflects the effect of flexibility. For film strips, the equivalent concentration λ is computed as $\pi Nd^2/4$, where d is the strip width, and N is the number of strips per unit area. As shown in Fig. 5-7, the agreement between the measured and calculated flow rates is generally acceptable. The average of absolute errors of the prediction is 16.6%.

Table 5-4. Error differences of predictions with formulas in complete and simplified versions.

Investigator	**Difference of absolute errors (%)**			
	Rigid vegetation		**Flexible vegetation**	
	Flow rate or average velocity or Chezy coefficient	Manning coefficient	Flow rate or average velocity or Chezy coefficient	Manning coefficient
Stone and Shen (2002)	-0.3	-1.3	-0.3	-2.4
Baptist et al. (2007)	-0.5	-0.1	-2.0	-1.2
Huthoff et al. (2007)	1.4	2.6	6.8	10.1
Yang and Choi (2010)	1.4	2.7	11.6	28.2
Present study	4.0	5.7	2.3	3.2
Note: The error difference was computed as [absolute error (%) of prediction using a formula in the complete version – absolute error (%) of prediction using the formula in the simplified version].				

When applying the simplified versions of Stone and Shen's and Baptist et al.'s formulas to flexible vegetation, the absolute error reduces by 0.3% to 2.4% (see

Table 5-4) compared to the cases of rigid vegetation. However, the absolute errors increase when applying the simplified versions to other three formulas. The prediction error increases by 11.6%-28.2% for Yang and Choi's formula, and 6.8%-10.1% for Huthoff et al.'s formula. The increase in the error for the formula proposed in this study is relatively small, i.e. from 2.3% to 3.2%.

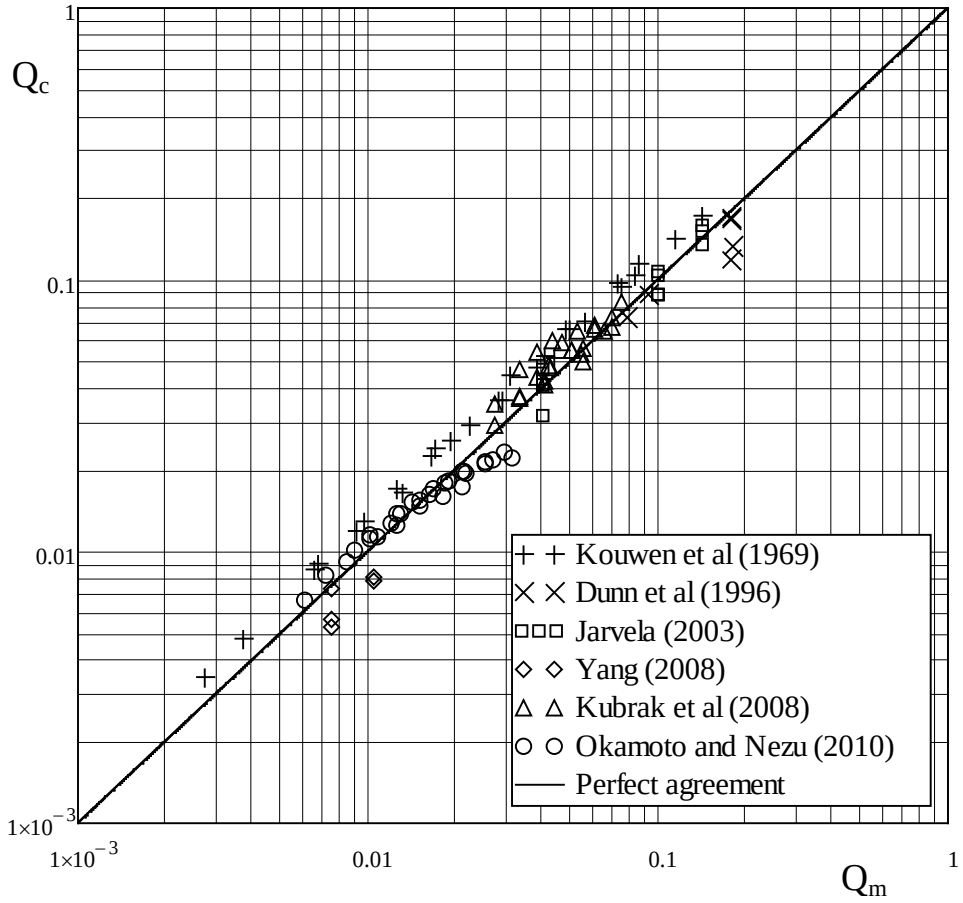

Fig. 5-7. Comparison of calculated flow rates (Q_c) with measurements (Q_m) (in m^3/s) for the case of submerged flexible vegetation.

5.6 Summary

In this Chapter, a representative roughness height is proposed by considering the relative blockage caused by submerged vegetation which is related to stem

diameter and vegetation density. The analysis shows that the friction factor defined for the surface layer above the vegetation slightly increases with increasing relative roughness height. The resistance relationship can be approximated using a power-law function. Comparing to previous formulas, the formula proposed by this study results in more accurate flow rate predictions, especially for the case of low flow rates. In addition, even though all formulas were derived with different considerations, they still can be simplified to a general form for some simple conditions. The analysis also showed that the proposed formula can be applied for the case of flexible vegetation with acceptable results although the effects of vegetation flexibility have not been fully incorporated.

CHAPTER 6

SCALING OF VELOCITY PROFILES FOR DEPTH-LIMITED OPEN CHANNEL FLOWS OVER RIGID VEGETATION

6.1 Introduction

In open channel flows, the large scale roughness could be represented by gravels, dunes or submerged vegetations. Flows over such a rough bed may differ significantly from those over smooth boundaries, in particular, for depth-limited conditions. If the channel bed is smooth and impermeable, the no-slip flow condition applies and the shear turbulence is diffusive in nature, which can be well described using the boundary layer theory. In contrast, the presence of submerged vegetation obstructs the lower portion of the channel flow, functioning as a porous medium to reduce flow velocity (Cheng and Chiew 1998; Cheng et al. 2008). This results in a flow with two parallel streams of different velocities, one above the vegetation (referred to as free-surface or surface layer) and the other through the vegetation (referred to as vegetation layer). The two streams interact, in a manner that is very similar to the plane mixing layer rather than the boundary layer (Nepf and Vivoni 2000; Raupach et al. 1996).

Unlike the flow over a smooth impermeable boundary, the vegetated flow invalidates the ‘no-slip’ velocity at the edge of vegetation and a point of inflection appears in the velocity profile, approximately at the interface of the two streams as sketched in Fig. 6-1. Inherent in such inflectional velocity profiles is the Kevin-Helmholtz instability as observed in the plane mixing layer (Kundu et al. 2004) and has been illustrated by Raupach et al. (1996) using high-order turbulence statistics for atmospheric canopy flows. Ghisalberti (2009) further demonstrated that shear flows characterised by the inflectional velocity profile, though on different scales, could be considered to be hydrodynamically similar.

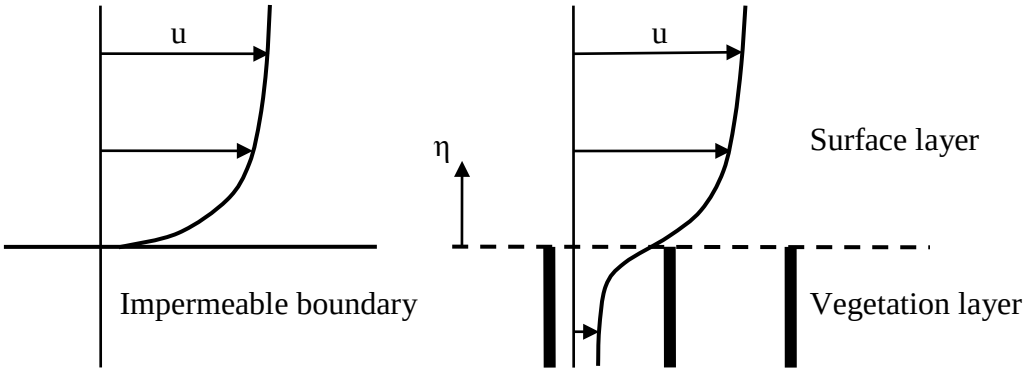

Fig. 6-1. Inflectional velocity profile in vegetated open channel flow.

Although important for characterizing vegetated open channel flows, the effect of interfacial mixing and turbulence transfer has not been fully taken into account for scaling velocity profiles. Empirically, the logarithmic law developed for impermeable boundaries has been employed in many studies for scaling velocity profiles observed in vegetated open channel flows. By

engaging zero-plane displacement Δy and hydrodynamic roughness length y_o, the logarithmic law is expressed as

$$\frac{u}{u_*} = \frac{1}{\kappa} \ln \frac{\eta + \Delta\eta}{\eta_o} \tag{6.1}$$

where η is measured upwards from the edge of vegetation, u_* is the shear velocity derived from the shear stress evaluated at η = 0 and κ is a constant close to 0.4. It is known that for rough flows over gravel beds, both $\Delta\eta$ and η_o are proportional to gravel size. However, for vegetated open channel flows, it is still unclear how $\Delta\eta$ and η_o can be correctly evaluated. As a result, a variety of empirical formulations have been presented in the literature, as reported by Stephan and Gutknecht (2002). Each empirical formula applied to some flow and vegetation configurations but appeared to be inconsistent with the others.

It is also noted that the logarithmic law is theoretically applicable to the inertial sublayer although it can be extended to the outer region with a wake function correction. However, if the flow depth is reduced, roughness elements may significantly affect the flow up to the free surface. Then, the major portion of the flow above vegetation may be characterised more appropriately as a roughness sublayer (RSL) than an inertial sublayer where the logarithmic law applies. This scenario is sketched in Fig. 6-2, with explanations given as follows.

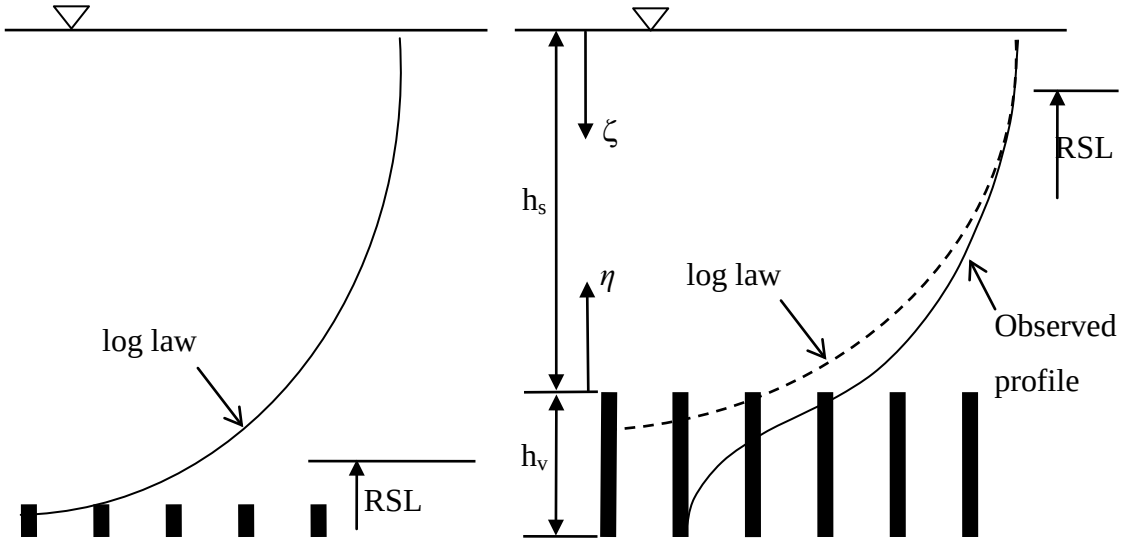

Fig. 6-2. Deviation of velocity profile from the logarithmic law in the presence of roughness sublayer (RSL).

For scaling purposes, an open channel flow can be divided vertically into two major regions, a near-bed inner region and an outer region above, both overlapping in part. In the presence of a fully rough boundary, the inner region is further divided into a near-bed roughness sublayer and an inertial sublayer above. As its name implies, the roughness sublayer is influenced predominantly by roughness elements. If the surface layer above vegetation is thick, the logarithmic law not only applies for the inertial sublayer but may also provide an acceptable approximation for the entire flow. If the surface flow becomes very shallow, the roughness sublayer may extend up to the free surface, and thus the logarithmic layer would become thinner and might even be squeezed out (Brunet et al. 1994). Nezu and Sanjou (2008) reported that the surface layer should be at least 0.5-1 times as thick as the vegetation layer for the logarithmic layer to appear. Studies of atmospheric canopy flows show that the thickness of

the roughness sublayer is about 1-4 times the vegetation height (Cheng and Castro 2002; Harman and Finnigan 2007). In other words, the scaling that underlies the logarithmic law would not be applicable for depth-limited, vegetated open channel flows.

In this study, we attempt to investigate how the velocity profile in vegetated open channel flows could be properly scaled for depth-limited conditions. First, laboratory experiments were conducted with vegetation simulated using rigid, cylindrical rods and flow depth varied from one to two times vegetation height. Altogether 24 tests were completed by varying vegetation density, stem diameter, flow depth and flow rate (see Table 6-1). Then, to scale the measured velocity profiles, a length scale is proposed by drawing an analogy between the roughness sublayer and the plane mixing layer, following the concept developed by Raupach et al. (1996). In comparison with others, the new scaling methodology yields a better collapsing of the velocity profiles measured with various flow and vegetation configurations. Finally, the result is further compared with other experimental data and also explained using a simple viscosity model.

6.2 Experiments

The detail of experiments was described in Chapter 3 and summarized in Table 6-1. Totally 24 flow velocity profiles for H/h_v = 1.3 – 2.0 were measured under uniform flow conditions with a two-component laser Doppler anemometer (LDA). The measuring location of velocity profile was chosen at the centerline

of the flume to minimize sidewall effects. The location for velocity measurement is shown in Fig. 3-8. This location was selected for two reasons. First, to facilitate the measurement, it should be accessible by laser beams from a sidewall. Second, the velocity profile measured at the location was assumed to be typical and a good representation of the average velocity distribution. It is noted that in the vegetation layer, the velocity measured at the selected location may deviate to some extent from the space-averaged value. However, such deviations would not be important as only the flow velocity above the vegetation is of concern here.

Table 6-1. Summary of experimental data collected in the present study for submerged conditions.

No.	Average surface layer velocity U_s (m/s)	Average vegetation layer velocity U_v (m/s)	Surface layer thickness h_s (m)	Stem diameter d (mm)	Vegetation concentration λ (%)	Maximum flow velocity u_{max} (m/s)	Half-thickness $\zeta_{1/2}$ (m)	β
1	0.264	0.140	0.03	3.15	1.73	0.298	0.029	1.80
2	0.289	0.140	0.05	3.15	1.73	0.345	0.042	1.80
3	0.307	0.141	0.07	3.15	1.73	0.386	0.052	1.70
4	0.328	0.138	0.10	3.15	1.73	0.443	0.064	1.40
5	0.356	0.244	0.03	3.15	0.43	0.394	0.026	1.60
6	0.365	0.234	0.05	3.15	0.43	0.419	0.040	1.50
7	0.390	0.232	0.07	3.15	0.43	0.457	0.055	1.50
8	0.424	0.235	0.10	3.15	0.43	0.500	0.083	1.60
9	0.252	0.097	0.03	6.64	7.69	0.294	0.029	2.00
10	0.268	0.096	0.05	6.64	7.69	0.326	0.044	1.80
11	0.272	0.086	0.07	6.64	7.69	0.346	0.055	1.80
12	0.262	0.078	0.10	6.64	7.69	0.343	0.074	2.00
13	0.294	0.171	0.03	6.64	1.92	0.339	0.026	1.80
14	0.310	0.172	0.05	6.64	1.92	0.373	0.038	1.75
15	0.305	0.162	0.07	6.64	1.92	0.390	0.044	1.50
16	0.332	0.168	0.10	6.64	1.92	0.424	0.066	1.65
17	0.203	0.048	0.03	8.26	11.90	0.251	0.028	1.65
18	0.217	0.046	0.05	8.26	11.90	0.276	0.044	1.65
19	0.251	0.066	0.07	8.26	11.90	0.333	0.055	1.50
20	0.315	0.070	0.10	8.26	11.90	0.386	0.097	1.67
21	0.277	0.143	0.03	8.26	2.98	0.331	0.025	1.50
22	0.289	0.143	0.05	8.26	2.98	0.348	0.039	1.70
23	0.290	0.142	0.07	8.26	2.98	0.376	0.045	1.65
24	0.312	0.136	0.10	8.26	2.98	0.416	0.065	1.40

6.3 Scaling analyses

6.3.1 Applying of the power-law, logarithmic -law, and velocity-defect law

In this section, we first consider some possible scaling arguments that have been used in the studies of conventional boundary layers and open channel flows. For example, the velocity scale could be represented by the maximum

velocity u_{max}, occurred almost at the free surface, or the shear velocity u_*, computed as $(gh_sS)^{1/2}$ where g is the gravitational acceleration, h_s is the surface layer thickness and S is the energy slope. On the other hand, the length scale may be represented by h_s or representative roughness height k_s for fully rough turbulent flows.

In applying the power-law scaling to the surface layer, we may scale the velocity profile with u_{max} and h_s. Fig. 6-3 shows the plot of η/h_s against u/u_{max} with the data collected for the six different vegetation concentrations. It is known that the power law in the form of $u/u_{max} = (\eta/h_s)^{1/m}$, with m varying from 6 to 7, may approximate to a large extent the velocity profiles observed in regular open channel flows (Chen 1991; Cheng 2007). However, the scattering of data points plotted in Fig. 6-3 does not support the power law with m-values given in a narrow range. The data are roughly confined by the two power laws with m = 2.5 and 9. The high degree of scattering and the wide range of m-values imply that either or both of the selected velocity and length scales are inappropriate.

Then, we replace h_s with k_s and u_{max} with u_* to check if there exists a functional relationship similar to the logarithmic law for rough boundary conditions. Here, we assume that the vegetated flows are fully rough, with a representative roughness height denoted by k_s. In the literature, k_s has been taken to be the vegetation height, stem spacing or other lengths (Baptist et al. 2007; Huthoff et al. 2007; Kouwen et al. 1969). By transforming the concept of hydraulic radius, the representative roughness height was proposed in Chapter 5 for cylindrical vegetation stems, $k_s = (\pi/4)(\lambda d)/(1-\lambda)$. This definition of k_s is characterised by

its proportionality to both stem diameter and vegetation concentration and has been found to perform better than other length scales when tested with more than 400 sets of resistance data, which were collected from 17 sources under a wide range of vegetation conditions.

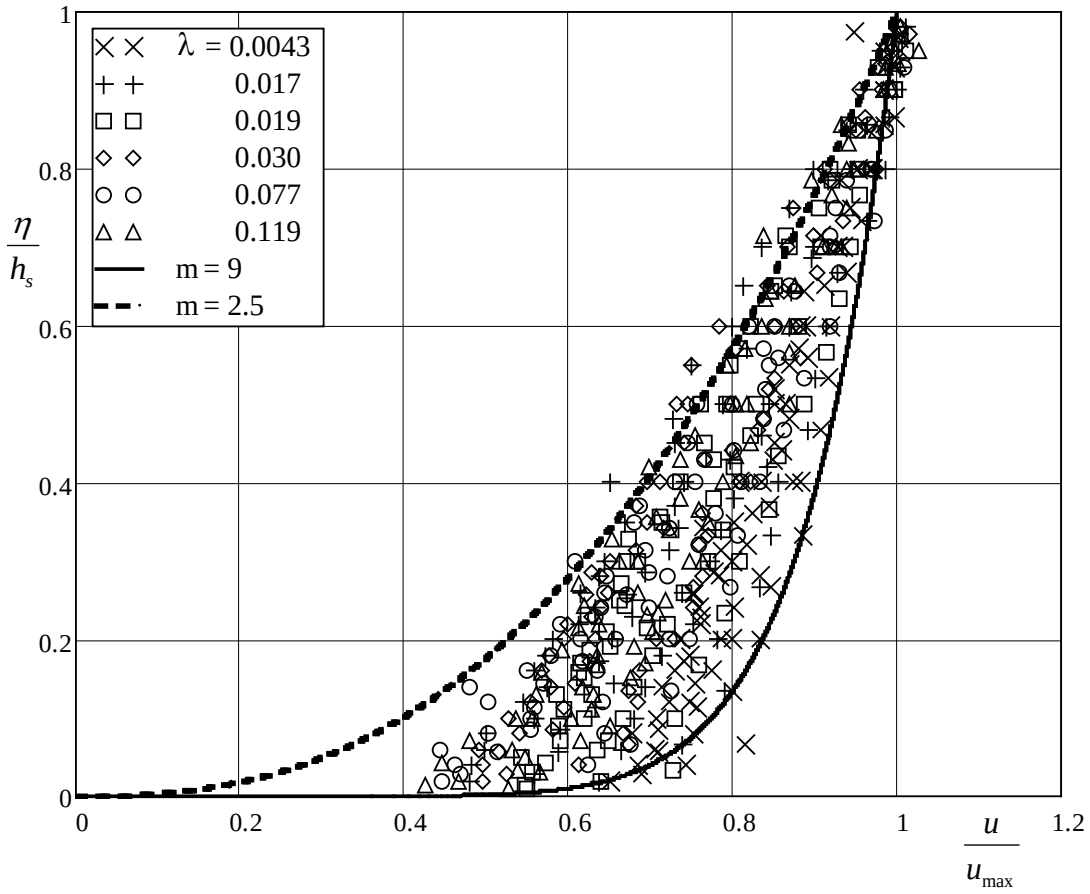

Fig. 6-3. Velocity profiles plotted as η/h_s against u/u_{max} using the power law.

In Fig. 6-4, u/u_* is plotted against η/k_s. It should be mentioned that the zero-plane displacement is not considered here. Fig. 6-5 shows that the relation of u/u_* and η/k_s is not unique, varying with the vegetation concentration and flow depth. We also observed similar degrees of data scattering when using other approaches to evaluate k_s. On the other hand, each velocity profile could be fitted individually to the logarithmic function, i.e. Eq. (6.1), by adjusting both

$\Delta\eta$ and η_o. However, as discussed in the subsequent section, the application of the logarithmic law to the surface layer under consideration is actually unsuitable as the inertial sublayer becomes very thin or even disappears for the depth-limited condition.

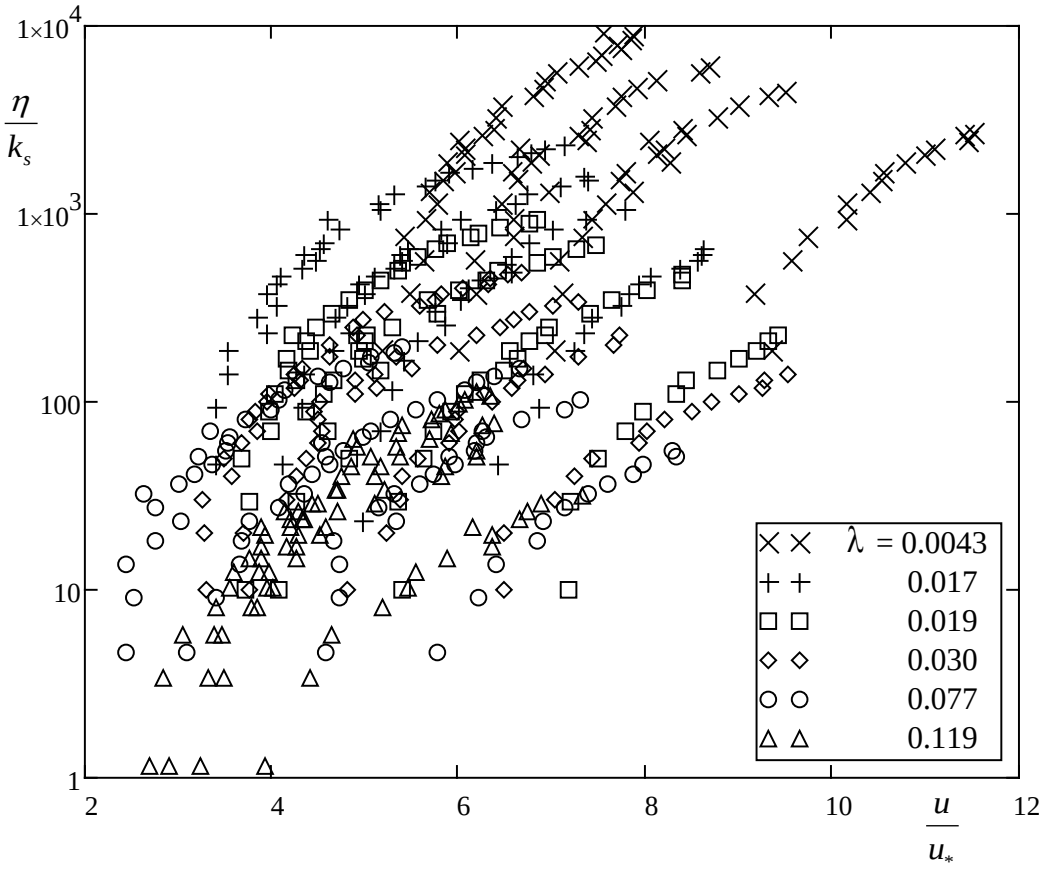

Fig. 6-4. Scaling of velocity profiles using shear velocity u_* and representative roughness height k_s.

Next, we consider if it is possible to apply the velocity-defect law to relate $(u_{max}-u)/u_*$ to η/h_s. This possibility is explored in Fig. 6-5, showing that the relationship is better than that presented in Fig. 6-4, but the spreading of the data points is still wide.

The above analyses show that the existing scaling arguments fail to realistically describe the mean flows under the depth-limited conditions; an alternative approach is thus explored in the following to correctly normalize the velocity profiles.

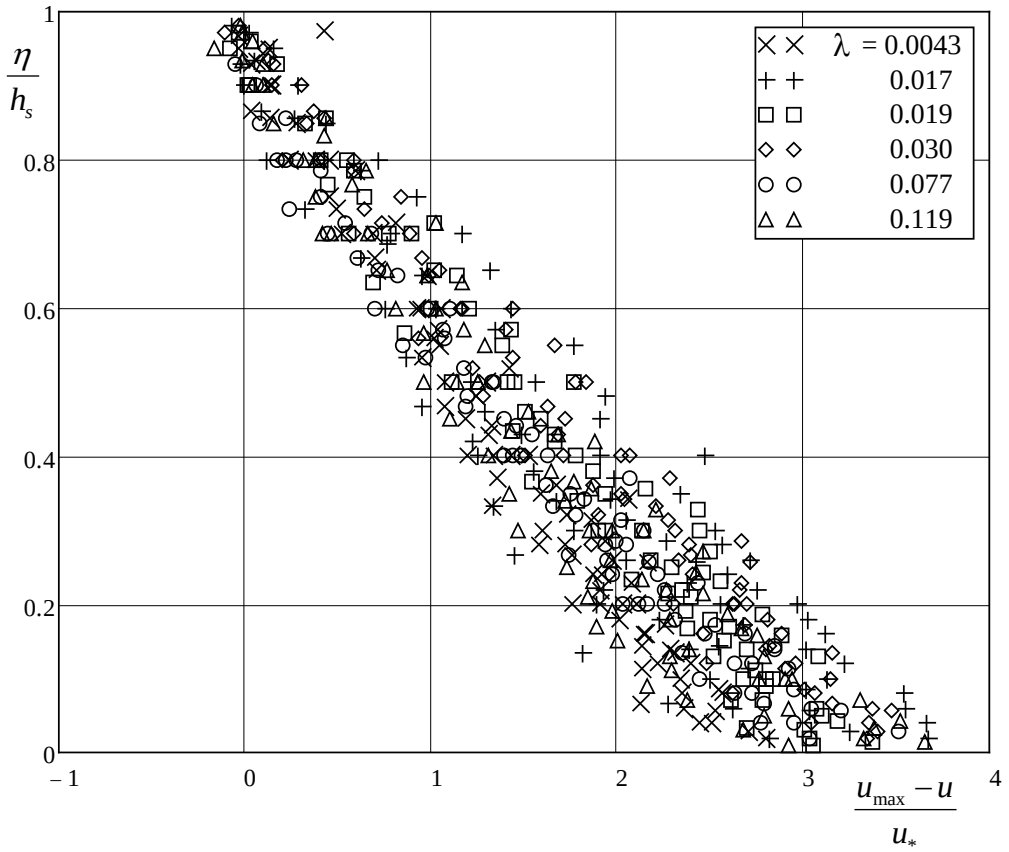

Fig. 6-5. Scaling of velocity-defect profiles using shear velocity u_* and surface layer thickness h_s.

6.3.2 Length scale proposed in this study

In this study, we are concerned only with the low submergence condition, in which the total flow depth H (= $h_s + h_v$) is not greater than twice the vegetation height h_v, i.e. $H \leq 2h_v$. For this shallow flow condition, it is reasonable to assume that the velocity profiles observed in the surface layer may be

normalised with the scales that characterise the roughness sublayer rather than the inertial sublayer where the logarithmic law applies. This assumption is consistent with the previous observation that the logarithmic law only fits the velocity profiles measured for $\eta > (0.5 - 4)h_v$ (Cheng and Castro 2002; Ghisalberti and Nepf 2009; Harman and Finnigan 2007; Nezu and Sanjou 2008; Poggi et al. 2004).

Following the idea developed by Raupach et al. (1996) for canopy flows, we further draw an analogy between the roughness sublayer and the plane mixing layer, both sharing similar turbulence features. A plane mixing layer is the turbulent flow that forms between two uniform, parallel streams of different velocities, for example when a plane jet enters into quiescent surroundings. Experimental results show that the plane mixing layer is self-similar, with the existence of a point of inflection in the mean velocity profile (Pope 2000).

and show clearly the existance of the vortices in depth-limited flow condition of rigid vegetation. The blue dyes were injected at different levels to illustrate the develoment of vortices inside and above the vegetation layer. It can be seen that when the dye moves downstream, the vortices penetrate a distance into the vegetation layer. The vortices grow continually in the downstream direction, and then stabilize. Besides that, the inflectional velocity profile which causes the Kelvin–Helmholtz instability has been observed. As a result, the assuming analogy between the roughness sublayer and the plane mixing layer could be accepted.

Like in the plane mixing layer, turbulence in the roughness sublayer is far from random, with major contributions arising from coherent eddies, which has been justified by high-order turbulence statistics (Raupach et al. 1996). The local balance of turbulence dissipation and production, as observed in the inertial sublayer, does not exist in the roughness sublayer (Nepf and Vivoni 2000; Raupach et al. 1996). Therefore, it would not be appropriate to use the logarithmic law to scale the velocity profile and to use diffusion-based theory to describe the vertical turbulent transfer in the roughness sublayer.

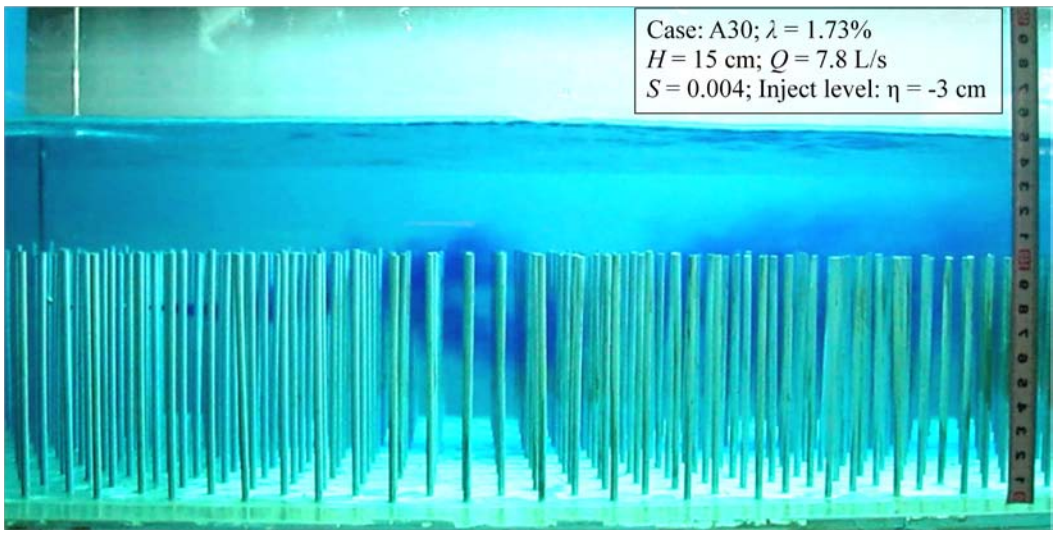
Case: A30; λ = 1.73%
H = 15 cm; Q = 7.8 L/s
S = 0.004; Inject level: η = -3 cm

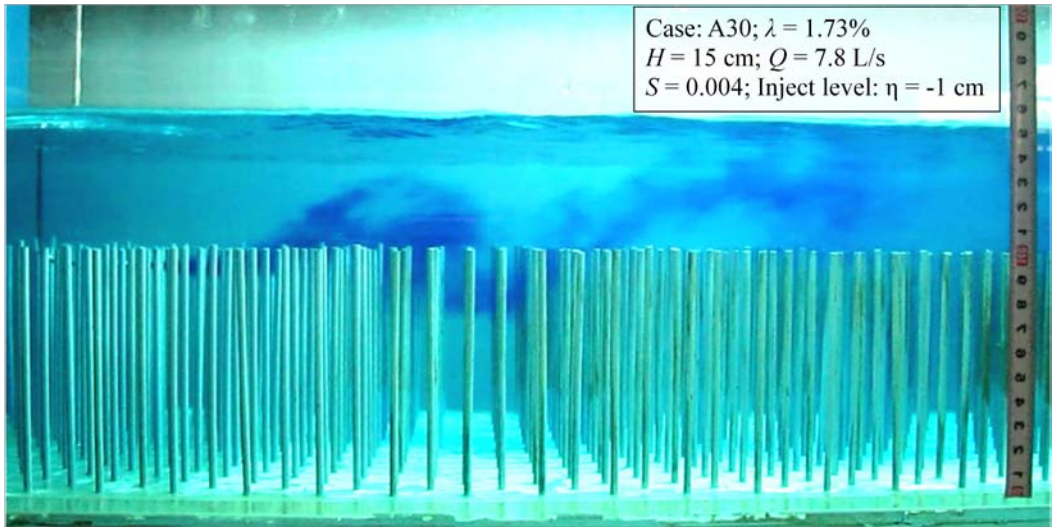
Case: A30; λ = 1.73%
H = 15 cm; Q = 7.8 L/s
S = 0.004; Inject level: η = -1 cm

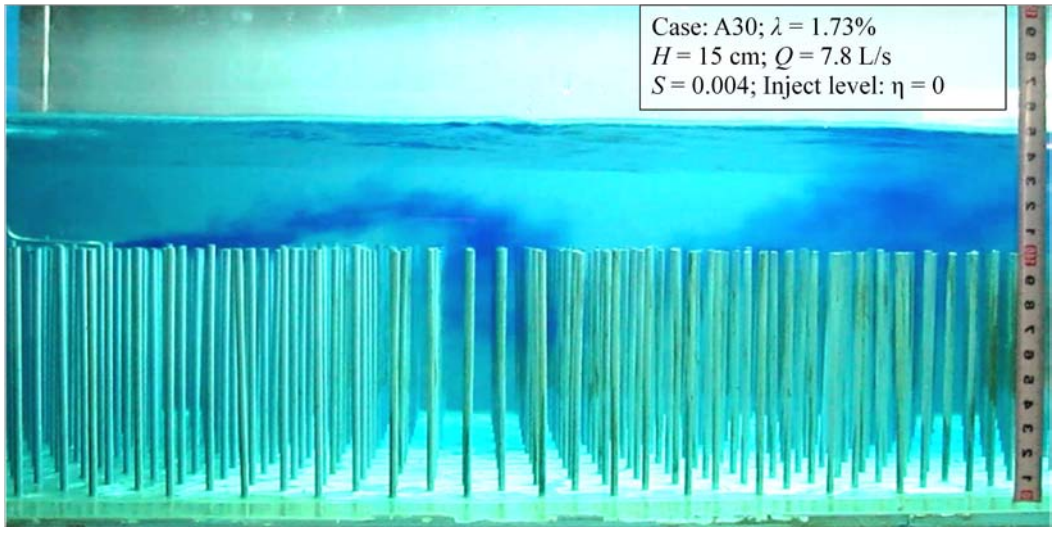
Case: A30; λ = 1.73%
H = 15 cm; Q = 7.8 L/s
S = 0.004; Inject level: η = 0

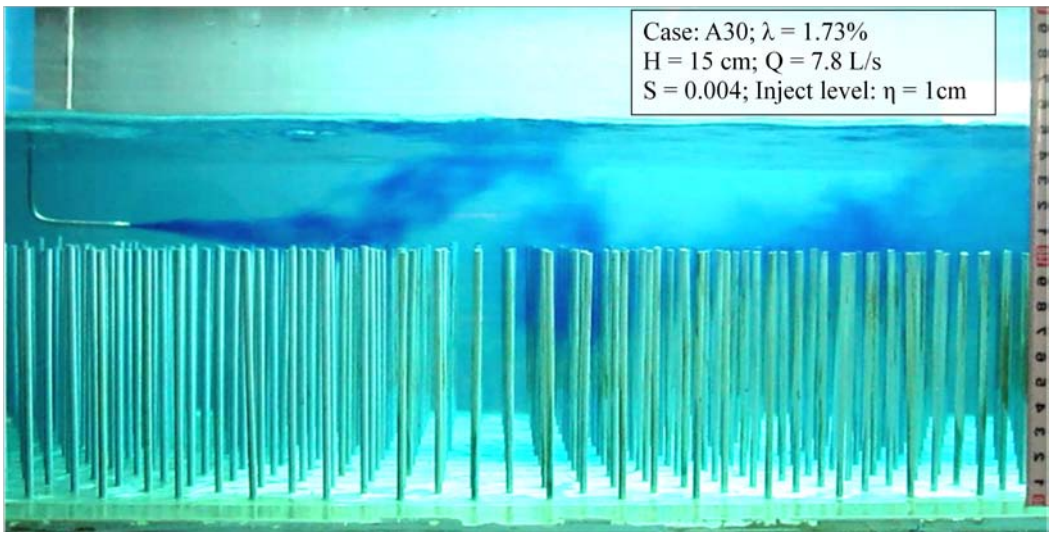
Case: A30; λ = 1.73%
H = 15 cm; Q = 7.8 L/s
S = 0.004; Inject level: η = 1cm

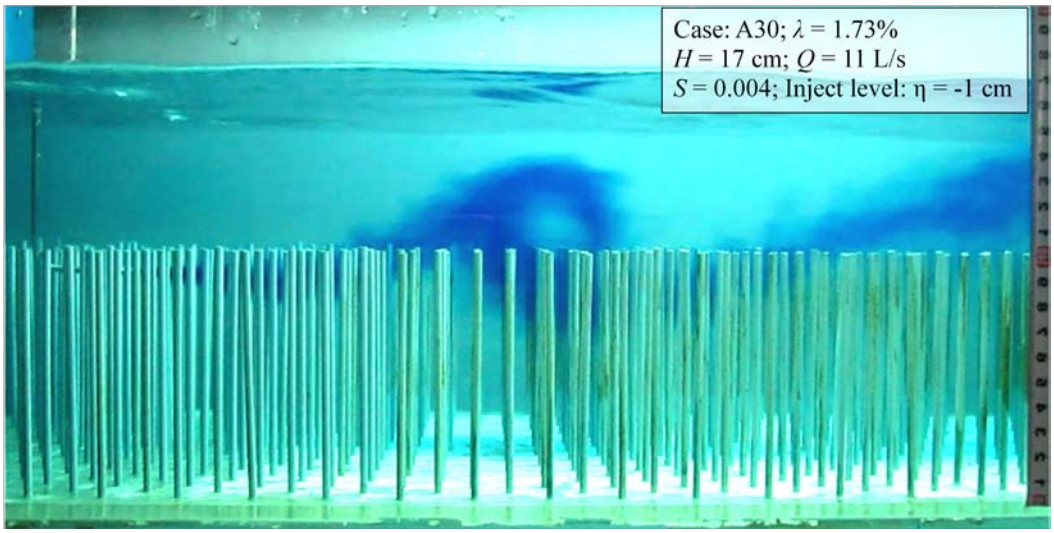
Case: A30; λ = 1.73%
H = 17 cm; Q = 11 L/s
S = 0.004; Inject level: η = -1 cm

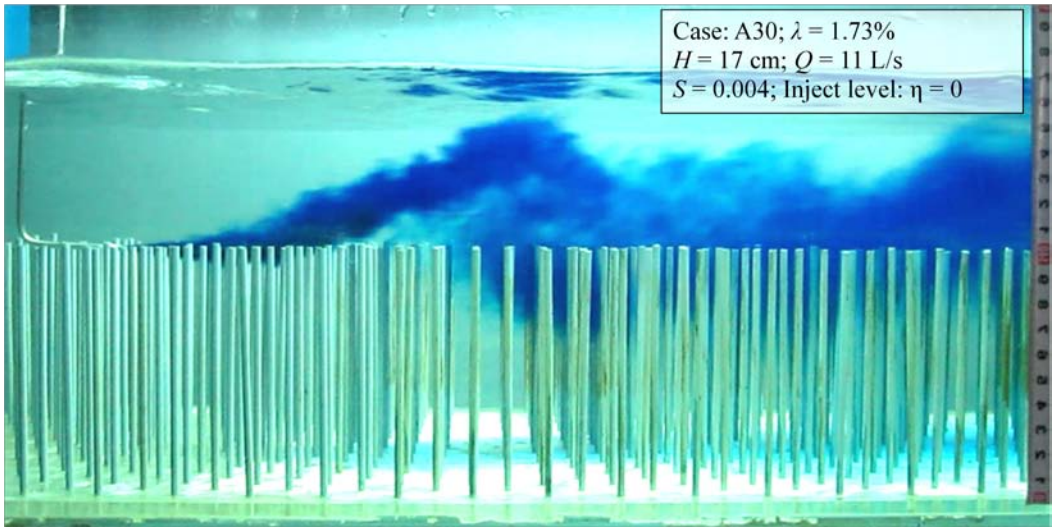
Case: A30; λ = 1.73%
H = 17 cm; Q = 11 L/s
S = 0.004; Inject level: η = 0

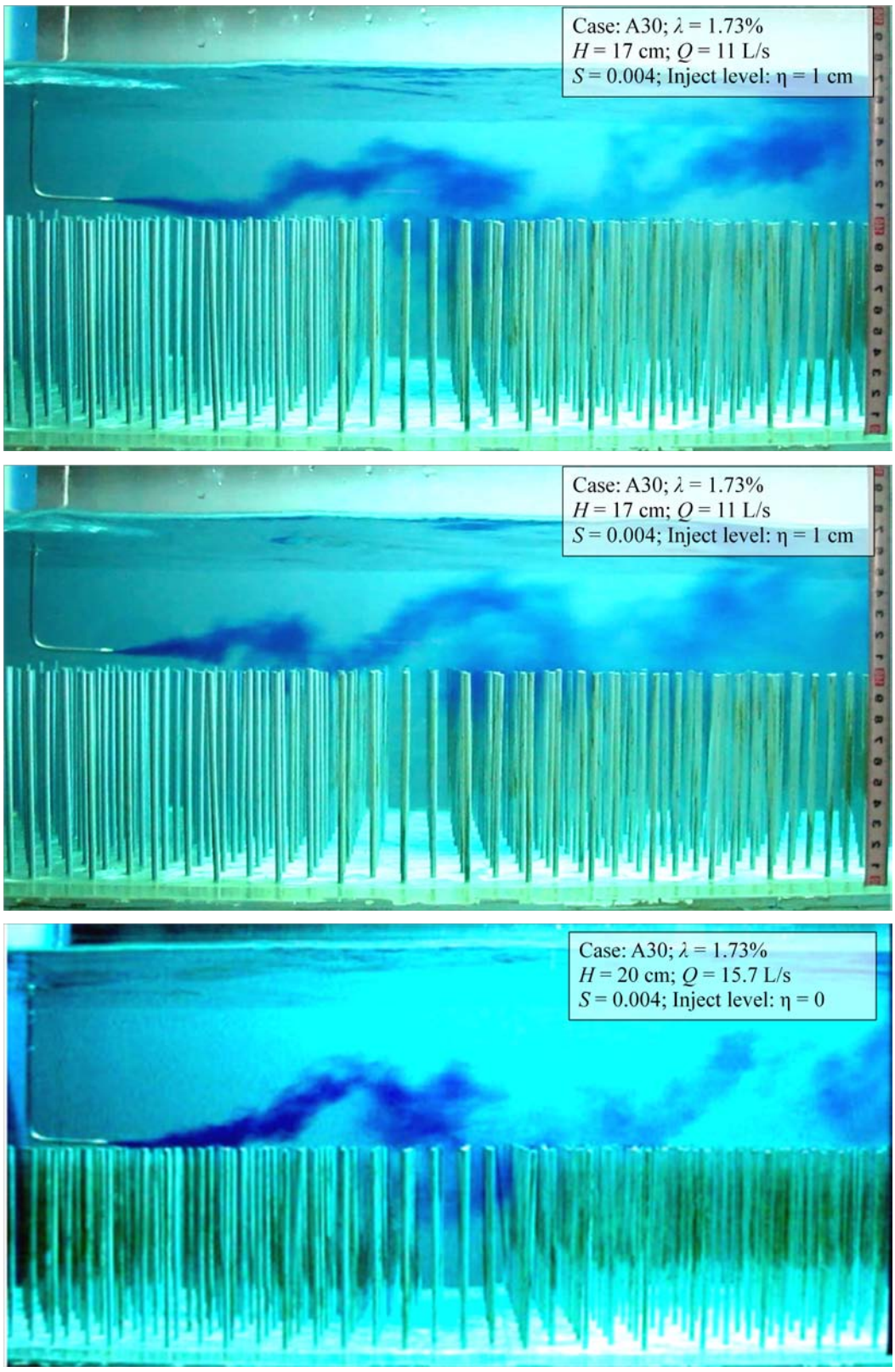

Fig. 6-6. The existence of Kelvin–Helmholtz vortex in submerged rigid vegetation. Experiments of case A30. The flow is from left to right.

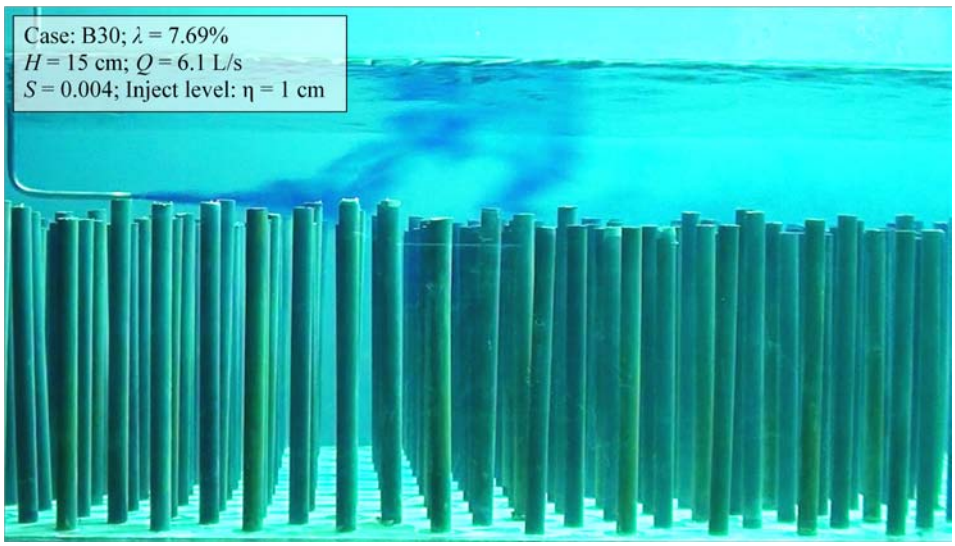
Case: B30; λ = 7.69%
H = 15 cm; Q = 6.1 L/s
S = 0.004; Inject level: η = 1 cm

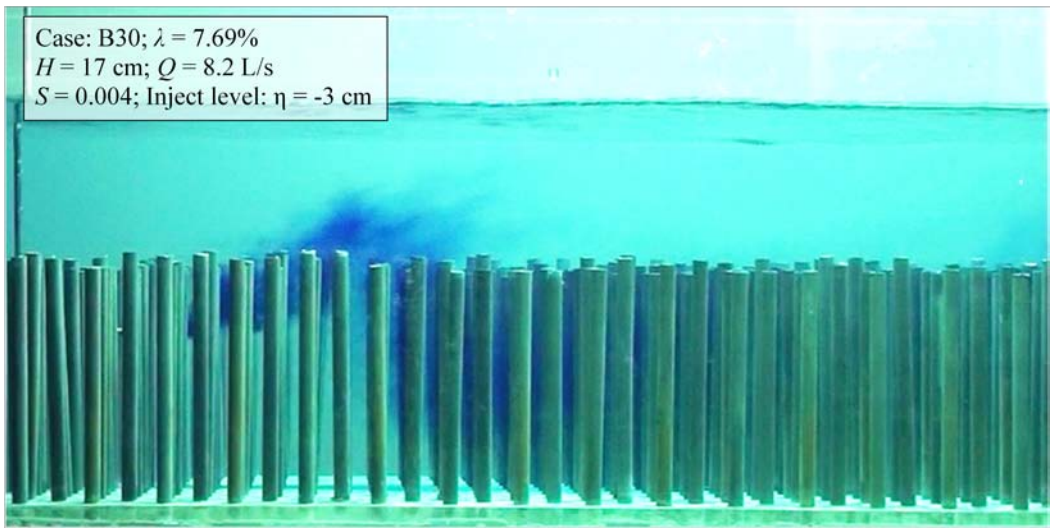
Case: B30; λ = 7.69%
H = 17 cm; Q = 8.2 L/s
S = 0.004; Inject level: η = -3 cm

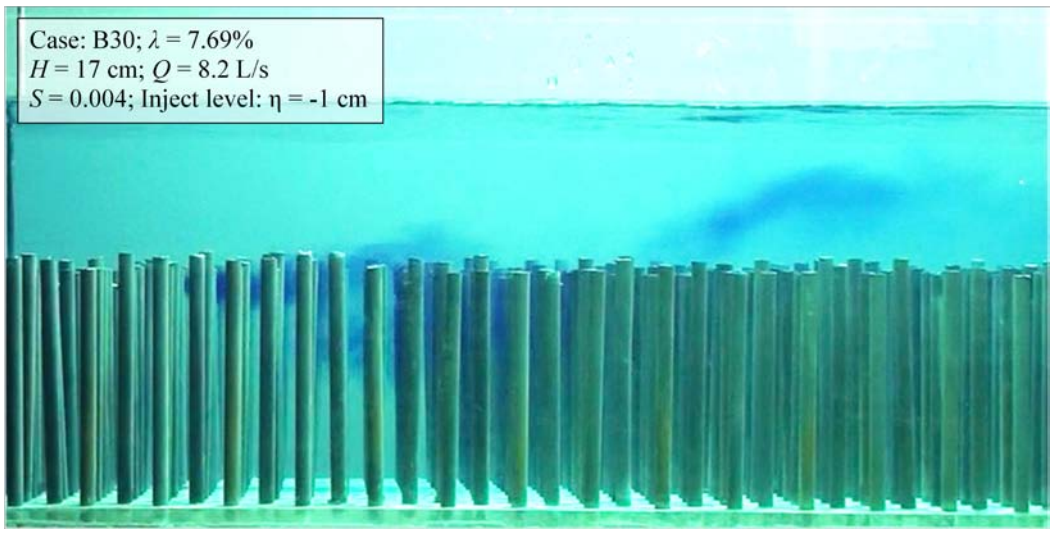
Case: B30; λ = 7.69%
H = 17 cm; Q = 8.2 L/s
S = 0.004; Inject level: η = -1 cm

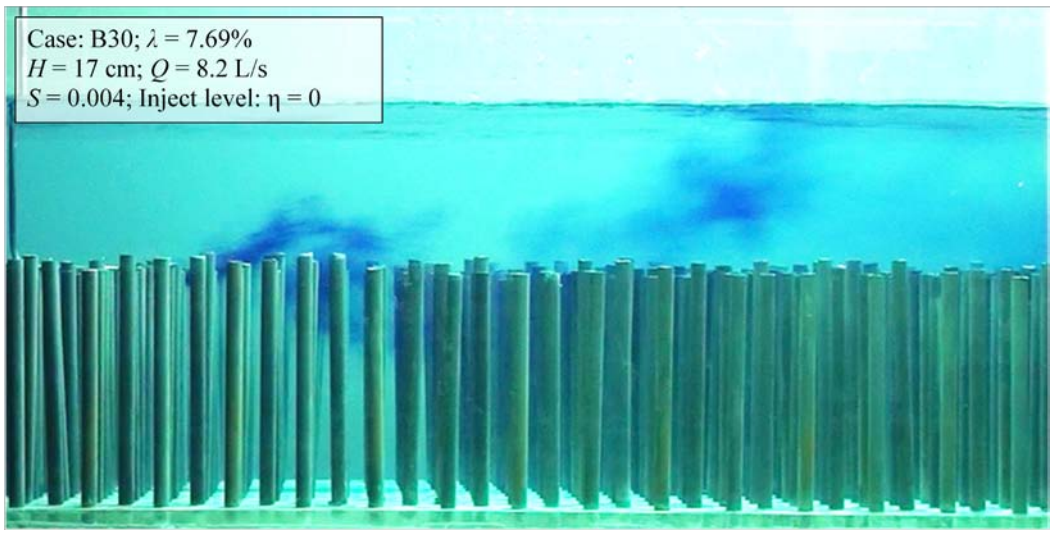
Case: B30; λ = 7.69%
H = 17 cm; Q = 8.2 L/s
S = 0.004; Inject level: η = 0

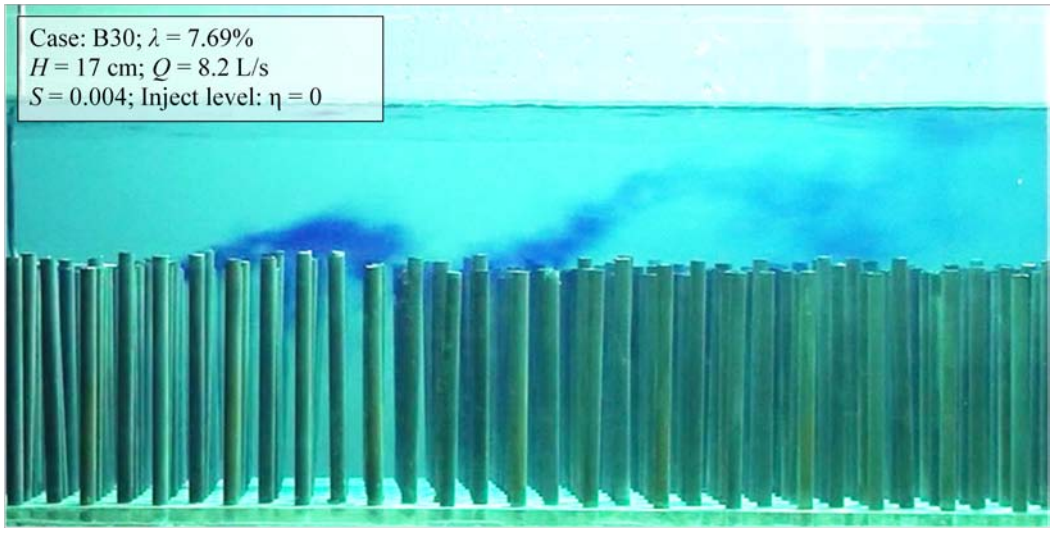
Case: B30; λ = 7.69%
H = 17 cm; Q = 8.2 L/s
S = 0.004; Inject level: η = 0

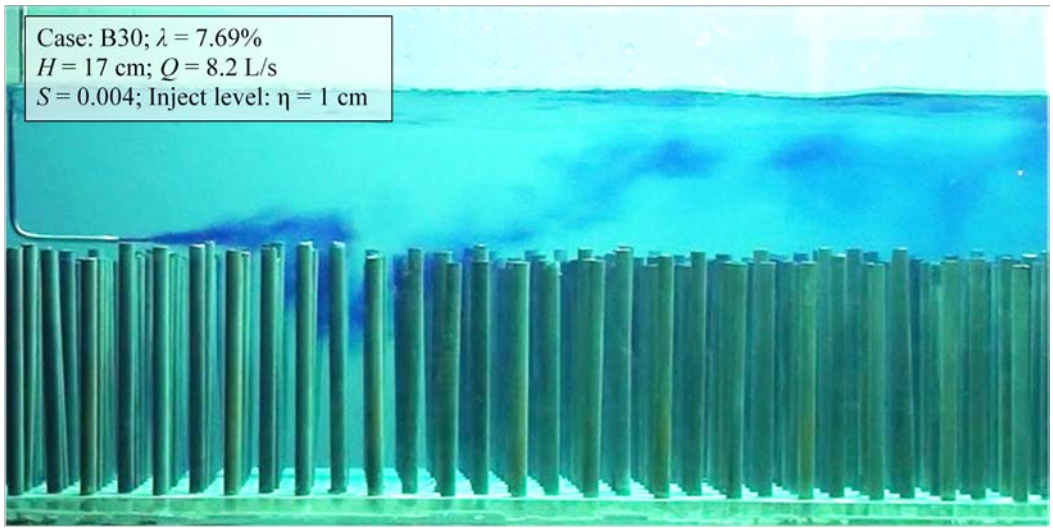
Case: B30; λ = 7.69%
H = 17 cm; Q = 8.2 L/s
S = 0.004; Inject level: η = 1 cm

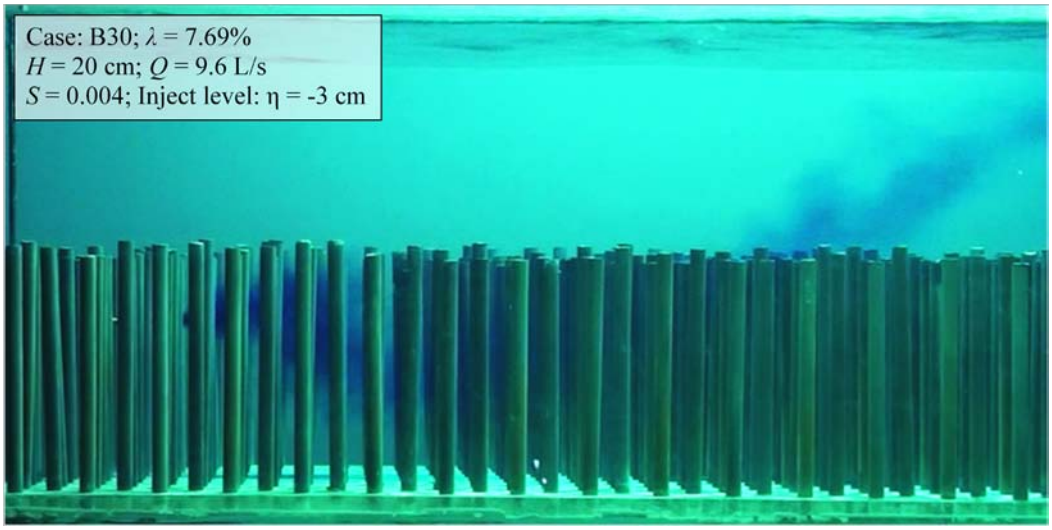
Case: B30; λ = 7.69%
H = 20 cm; Q = 9.6 L/s
S = 0.004; Inject level: η = -3 cm

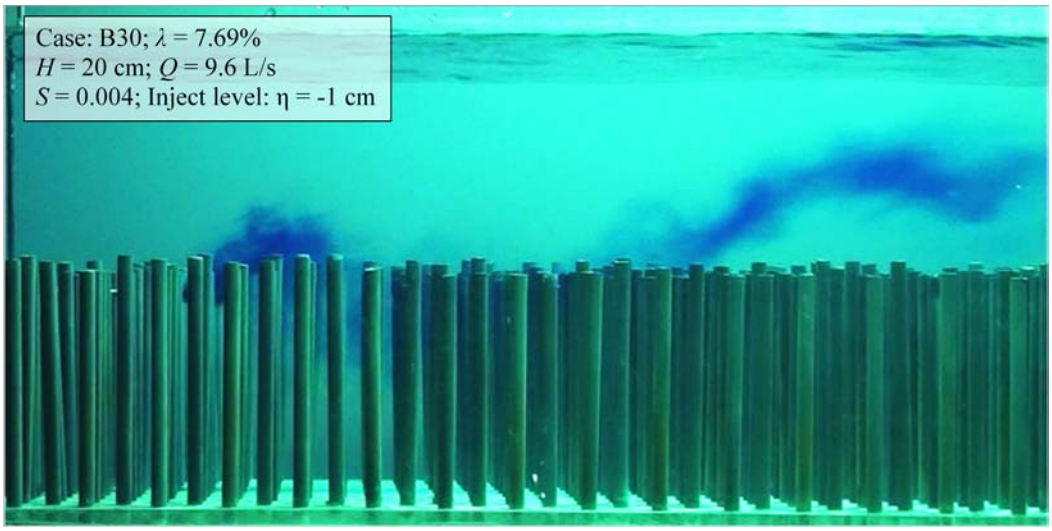
Case: B30; λ = 7.69%
H = 20 cm; Q = 9.6 L/s
S = 0.004; Inject level: η = -1 cm

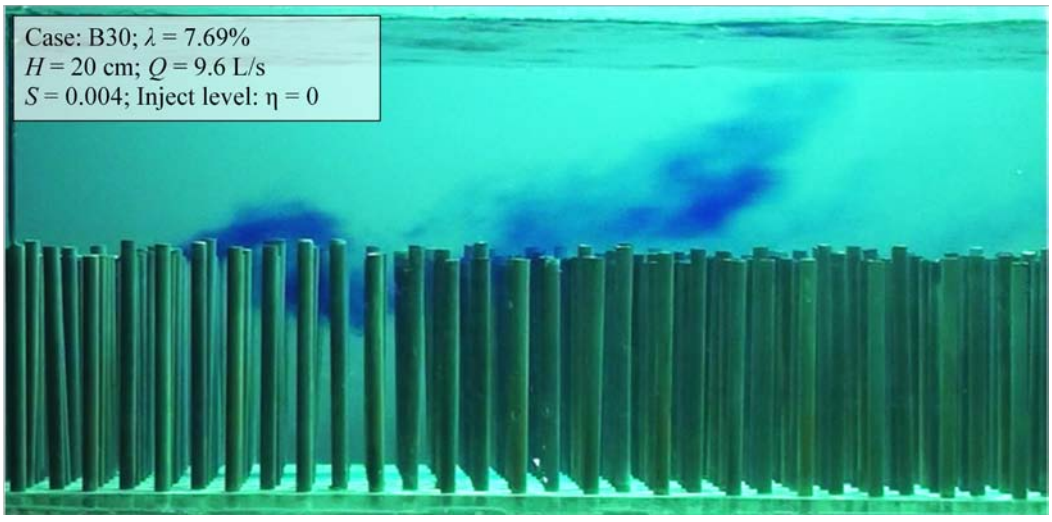
Case: B30; λ = 7.69%
H = 20 cm; Q = 9.6 L/s
S = 0.004; Inject level: η = 0

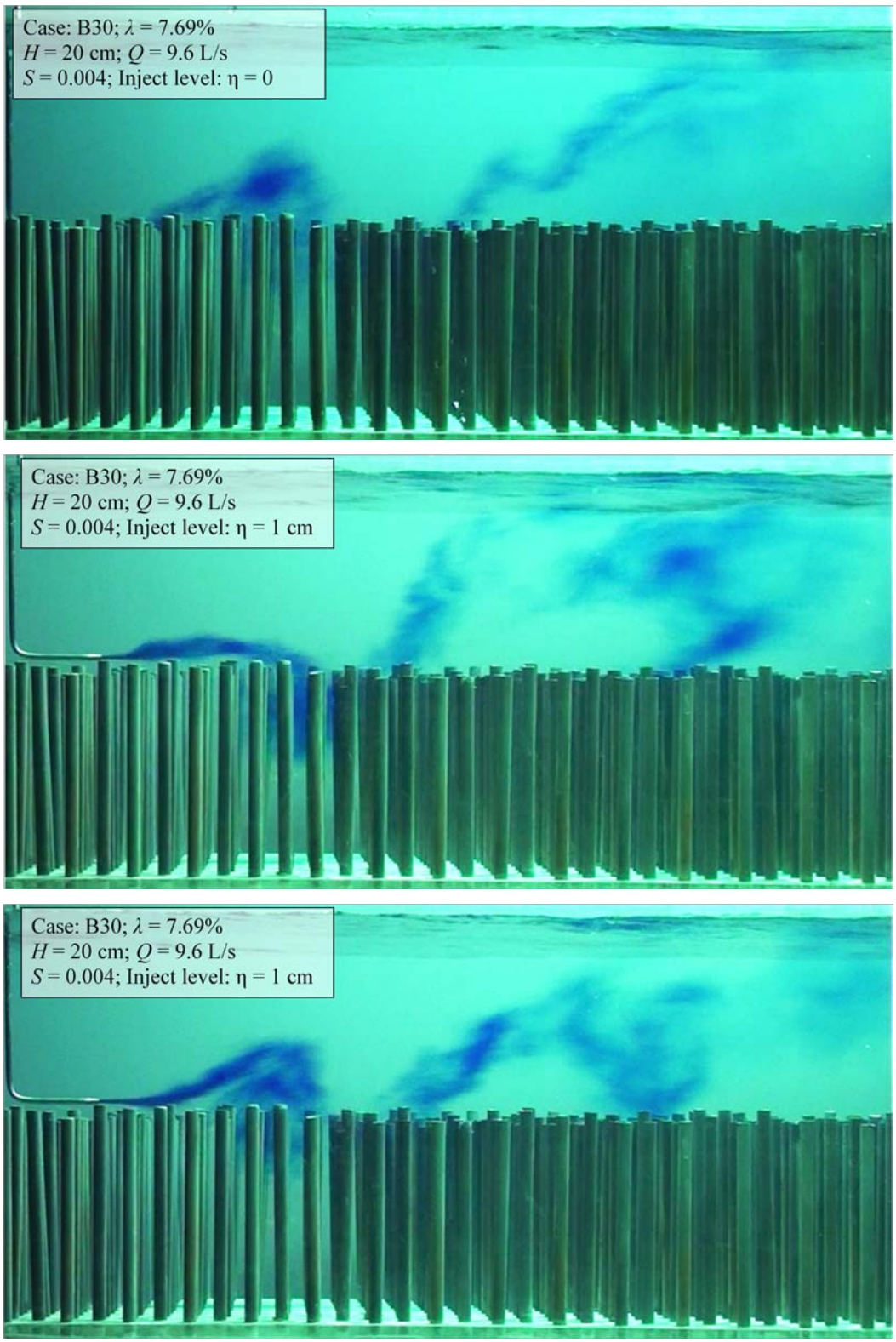

Fig. 6-7. The existence of Kelvin–Helmholtz vortex in submerged rigid vegetation. Experiments of case B30. The flow is from left to right.

In the presence of large-scale roughness elements, the roughness sublayer predominates and its effect could extend throughout the entire surface layer. However, the thickness of the roughness sublayer cannot be simply taken to be the same as the surface layer thickness even for the depth-limited condition. This can be explained using the mixing layer analogy. The development of the mixing layer in the vegetated open channel flow is restricted by the free surface but coherent eddies generated may penetrate downwards into the vegetation layer. Therefore, the spreading width of the mixing layer is not necessarily equal to (or proportional to) the surface layer thickness. In other words, even if the surface layer thickness is fixed, the mixing layer width may vary, depending on the strength of the flow. Therefore, as a possible measurement of the roughness sublayer thickness, the penetration depth that accounts for vegetation-induced momentum absorption could be employed in addition to the surface layer thickness (Harman and Finnigan 2007). However, the evaluation of the penetration depth requires the knowledge of Reynolds shear stresses (Brunet et al. 1994), and moreover, its dependence on other factors is not clear at present.

On the other hand, we note that in the similarity analysis of free shear flows such as jets, the half-width, which measures the spreading width at the location with the velocity equal to one half of the maximum velocity, renders an empirical but almost perfect length scale in collapsing velocity profiles. Here, by assuming that the maximum flow velocity u_{max} occurs at the free surface, we

may define a similar length scale as half-thickness $\zeta_{1/2}$. As sketched in Fig. 6-8, the half-thickness measures the vertical distance from the free surface to the location of the velocity difference (u-U_v), where U_v is the average flow velocity through the vegetation layer, reduced to one half of the maximum velocity defect (u_{max}-U_v). Similar to the half-width used for jets, $\zeta_{1/2}$ could be useful to quantify the spreading width of the mixing layer that forms at the edge of the vegetation for the depth-limited flow condition.

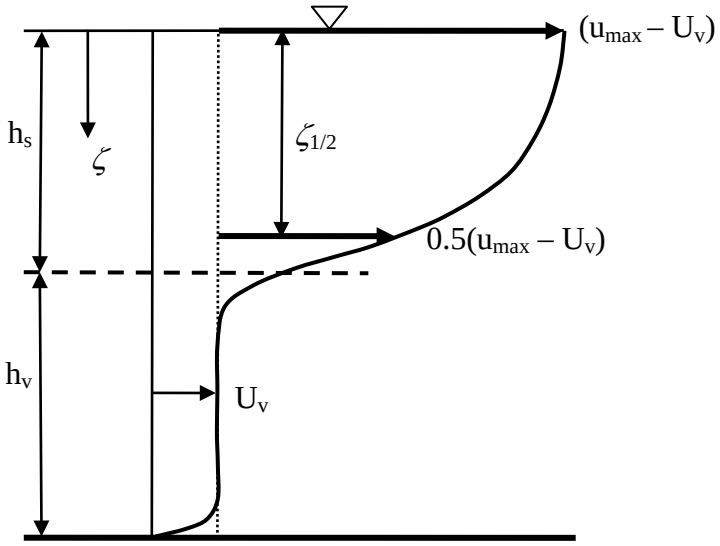

Fig. 6-8. Definition of half-thickness $\zeta_{1/2}$.

Using u_{max} and $\zeta_{1/2}$, we scale the measured streamwise velocity as (u-U_v)/(u_{max}-U_v) and the distance measured downwards from the free surface as $\zeta/\zeta_{1/2}$. Here, we normalize the velocity difference (u-U_v) rather than u, as for the plane mixing layer (Pope 2000). The value of U_v is taken as the constant flow velocity measured in the vegetation layer, away from the vegetation edge and channel bed. Alternatively, it can be estimated using the drag coefficient formula

proposed for the case of emergent vegetation as described in Chapter 4. The value of U_v can be calculated by Eq. (4.10) with the drag coefficient estimated by Eq. (4.24).

Applying new length scale

(a) to (d) show the data plotted in the form of $(u\text{-}U_v)/(u_{max}\text{-}U_v)$ against $\zeta/\zeta_{1/2}$ for the four different flow depths (i.e. h_s = 3 cm, 5 cm, 7 cm and 10 cm). It is noted that all the data presented in the figures are those measured above the edge of the vegetation, i.e. for $\zeta < h_s$. For each flow depth, six velocity profiles were measured for the different vegetation concentrations (λ = 0.43% - 11.9%). From (a) to (d), it can be seen that the large variation in the vegetation concentration has almost no effect on the relationship of $(u\text{-}U_v)/(u_{max}\text{-}U_v)$ to $\zeta/\zeta_{1/2}$.

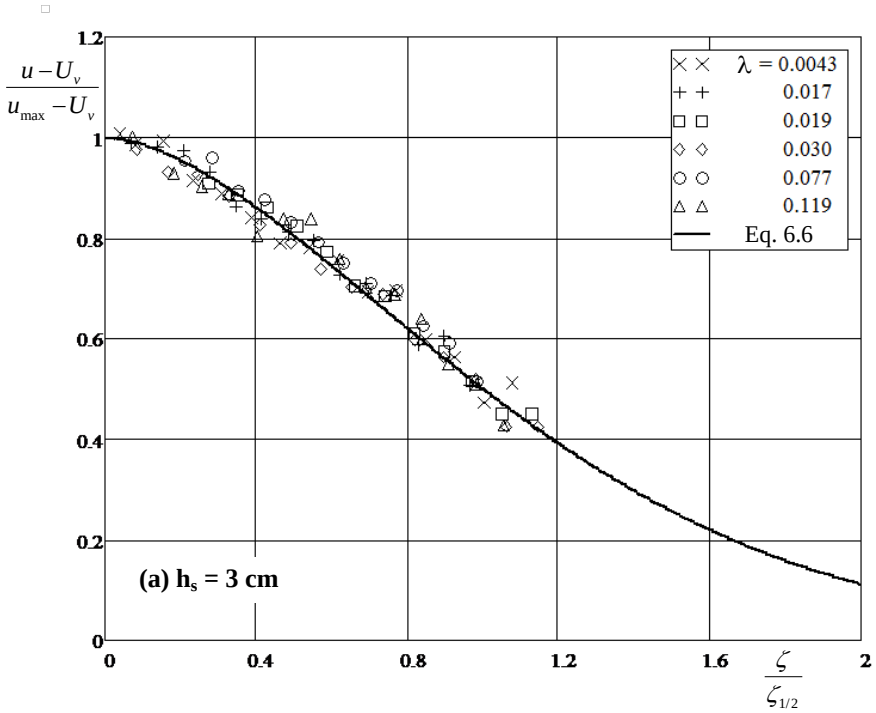

Fig. 6-9. Velocity profiles plotted as $(u\text{-}U_v)/(u_{max}\text{-}U_v)$ against $\zeta/\zeta_{1/2}$. (a) h_s = 3cm; (b) h_s = 5cm; (c) h_s = 7cm; and (d) h_s =10cm.

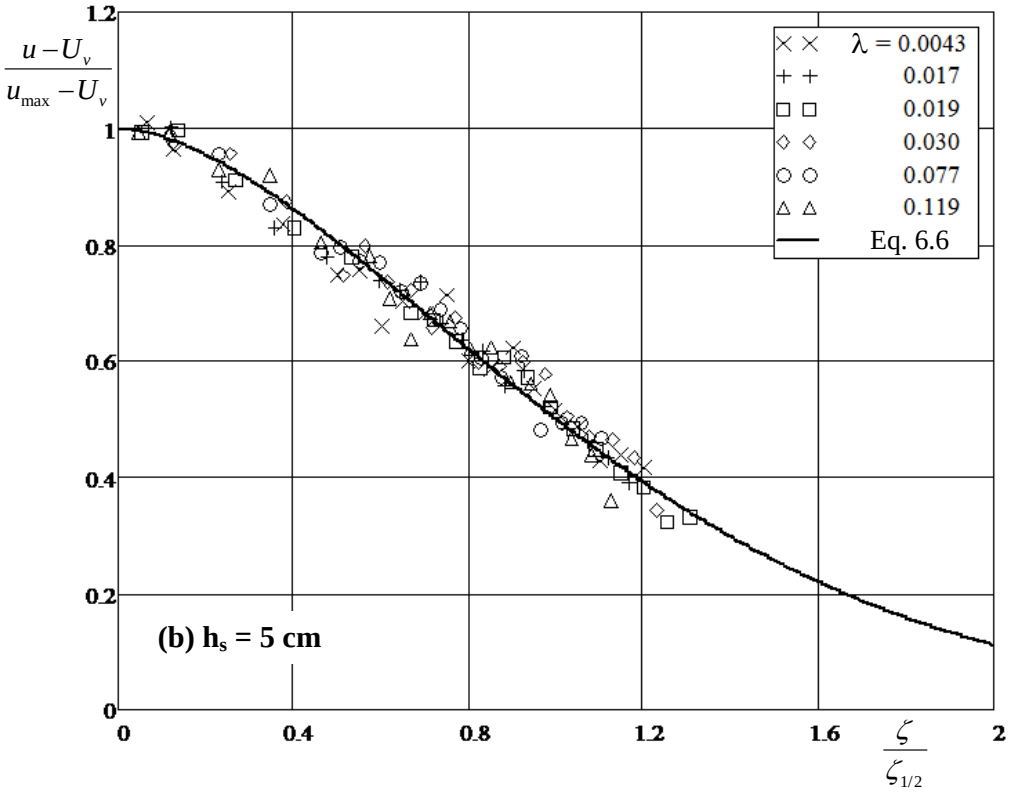
$\frac{u-U_v}{u_{max}-U_v}$
1.2
1
0.8
0.6
0.4
0.2
0
0
0.4
0.8
1.2
1.6
2
$\frac{\zeta}{\zeta_{1/2}}$
λ = 0.0043
0.017
0.019
0.030
0.077
0.119
Eq. 6.6
(b) h_s = 5 cm

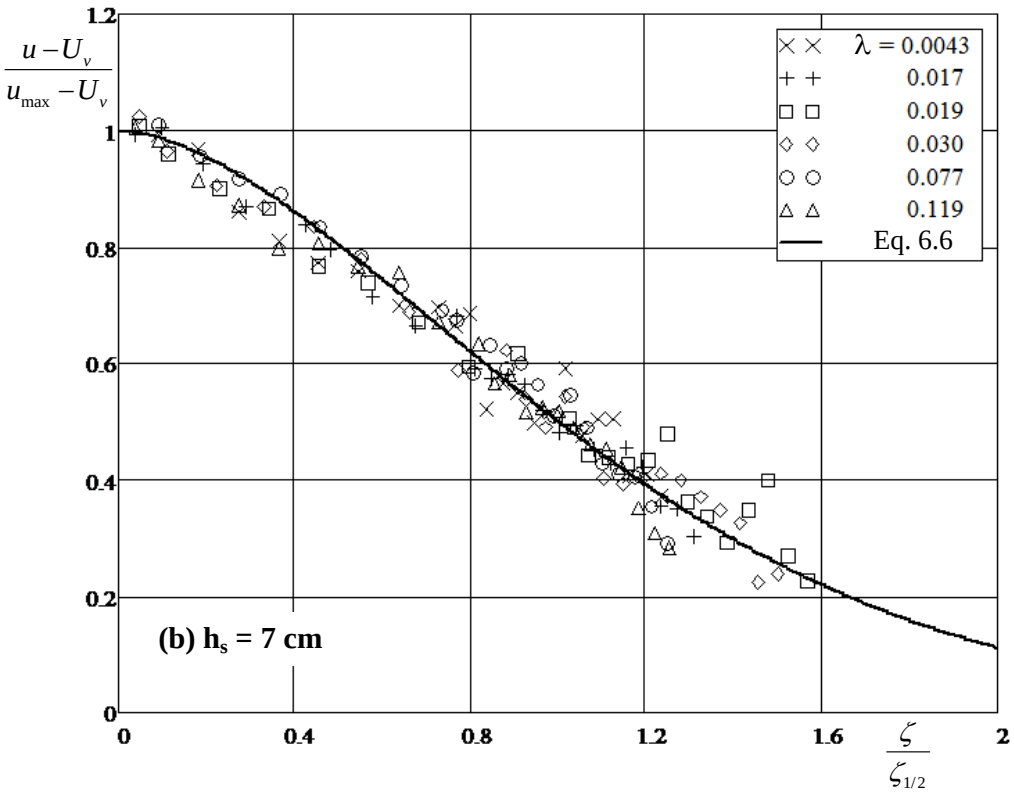
$\frac{u-U_v}{u_{max}-U_v}$
1.2
1
0.8
0.6
0.4
0.2
0
0
0.4
0.8
1.2
1.6
2
$\frac{\zeta}{\zeta_{1/2}}$
λ = 0.0043
0.017
0.019
0.030
0.077
0.119
Eq. 6.6
(b) h_s = 7 cm

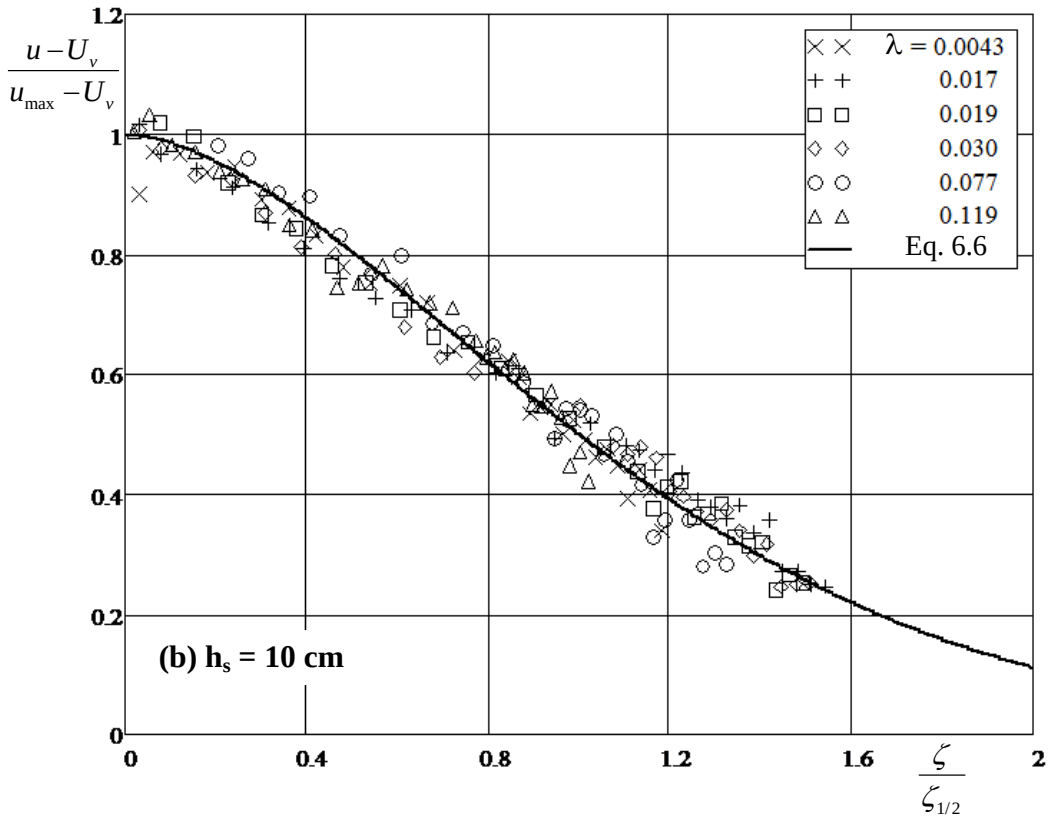

In Fig. 6-10, all the data for the 24 cases are plotted together, but identified as four series, each with a constant flow depth. It shows that the normalized profiles are similar to one another, independent of both the flow depths and vegetation concentrations. By comparing Fig. 6-10 with Fig. 6-3 to Fig. 6-5, we note that the scaling based on u_{max} and $\zeta_{1/2}$ yields significant improvement in collapsing the measured velocity profiles to a single curve. In the following section, we attempt to explain the scaling philosophy and describe the curve using a simple viscosity model.

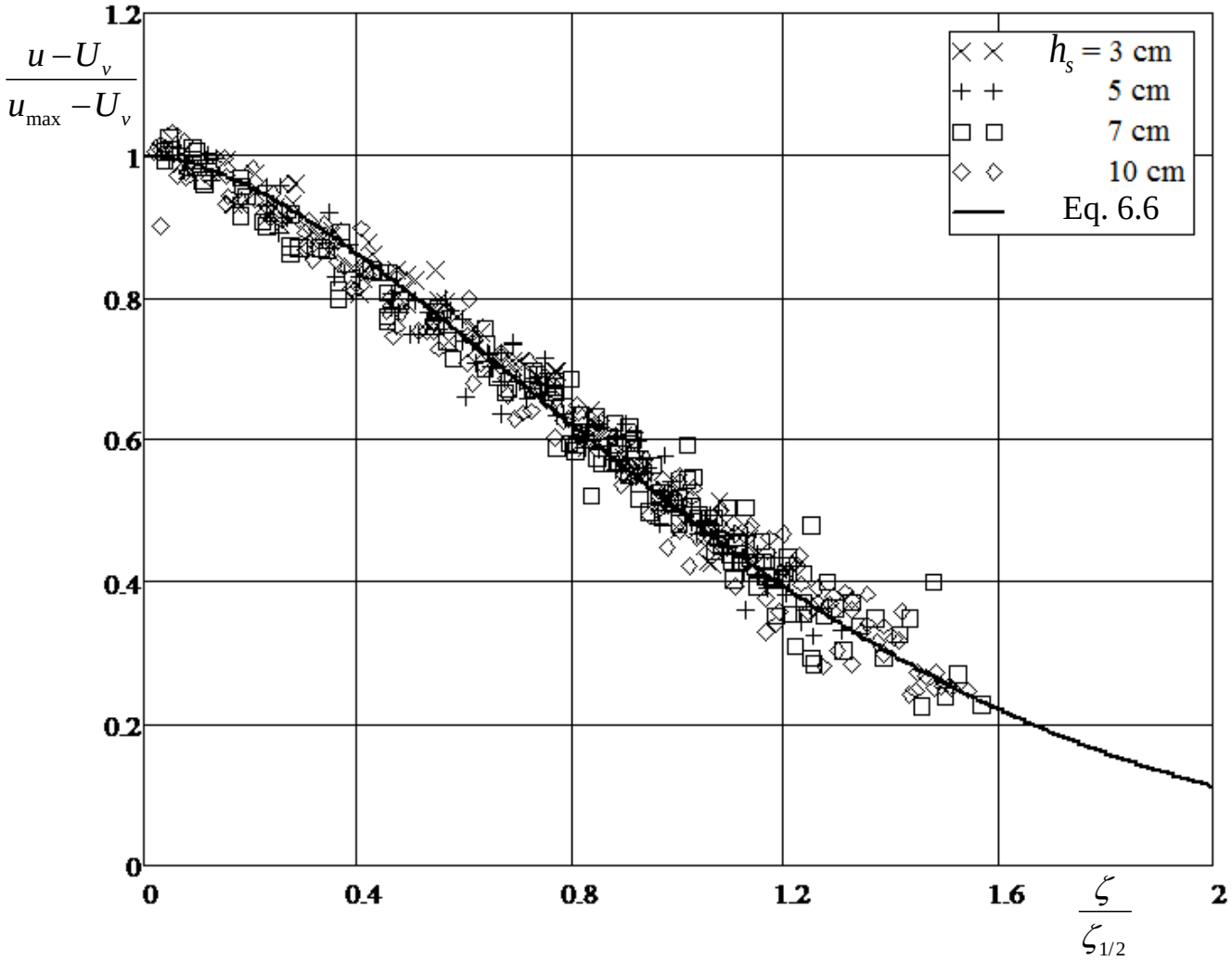

Fig. 6-10. Collapsing of the 24 velocity profiles measured for four difference flow depths and six different vegetation concentrations.

6.4 A viscosity model for velocity distribution

Consider a control volume, as shown in Fig. 6-11, of which the width is unity in the direction perpendicular to the main flow. As the flow is uniform and incompressible, the pressure difference, P_1-P_2, is zero. Thus, the x-components of the forces exerting on the control volume comprise only (1) the shear force, $\tau\Delta x$, where τ is the shear stress, and (2) the streamwise component of the gravity, $WS = \rho g \zeta S \Delta x$, where W is the weight of the control volume, S is the water surface slope, and ρ is the fluid density.

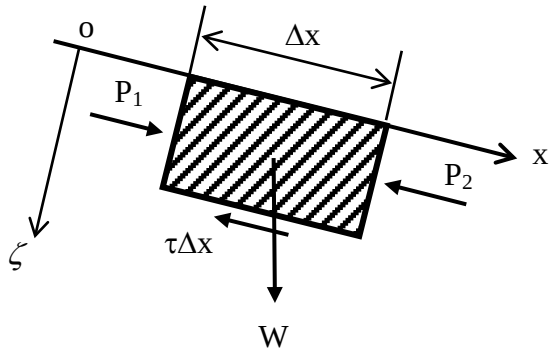

Fig. 6-11. Control volume with unity width perpendicular to flow direction.

We express the shear stress as

$$\tau = -\rho\varepsilon \frac{du}{d\zeta} \tag{6.2}$$

where ε is the apparent turbulence viscosity. By taking $\tau\Delta x = \rho g \zeta \Delta x S$ and substituting it to Eq. (6.2),

$$\frac{du}{d\zeta} = -\frac{g\zeta S}{\varepsilon} \tag{6.3}$$

Integration of Eq. (6.3) yields the velocity distribution if the variation in ε is known. To this end, some assumptions need to be made. For example, if ε is assumed to be proportional to ζ, then a linear velocity distribution is obtained. By analyzing the measured velocity profiles, we find that ε reduces with increasing (u - U_v). As a first approximation, we may assume that $\varepsilon(u - U_v)$ is weakly ζ-dependent in a power-law form, i.e. $\varepsilon(u - U_v) \sim \zeta^n$, where n is an exponent less than unity. This form will not invalidate the observation that (a) ε increases and reaches a maximum while (u - U_v) decreases to the 'slip' velocity at the flow-vegetation interface, and (b) ε approaches zero at the free surface while u reaches its maximum.

The kinematic viscosity has a dimension of the product of velocity and length. With $\zeta_{1/2}$ as the characteristic length, the combination of $\rho g \zeta_{1/2} S$ signifies the characteristic shear force per unit area at $\zeta = \zeta_{1/2}$. Moreover, $(g\zeta_{1/2}S)^{1/2}$ defines a shear velocity at $\zeta = \zeta_{1/2}$. Next, we may normalize ε with $(g\zeta_{1/2}S)^{1/2}\zeta_{1/2}$ and $\varepsilon(u-U_v)$ with $gS(\zeta_{1/2})^2$. Therefore, Eq. (6.3) may be rewritten as

$$\frac{du^+}{d\zeta^+} = -\frac{\zeta^+}{\varepsilon^+} \tag{6.4}$$

where $u^+ = (u\text{-}U_v)/(g\zeta_{1/2}S)^{1/2}$, $\zeta^+ = \zeta/\zeta_{1/2}$, and $\varepsilon^+ = \varepsilon/[(gS)^{1/2}(\zeta_{1/2})^{3/2}]$. We further assume that $\varepsilon^+u^+ = \alpha(\zeta^+)^n$, where α is a coefficient. Then, integrating Eq. (6.4) yields

$$u^+ = B\exp\left[-\frac{1}{\alpha\beta}\left(\zeta^+\right)^\beta\right] \tag{6.5}$$

where B is a coefficient and $\beta = 2\text{-}n$. The value of β is close to 2 if n is very small. By noting that $u = u_{max}$ at $\zeta = 0$, and $u - U_v = 0.5(u_{max} - U_v)$ at $\zeta = \zeta_{1/2}$, we get $B = (u_{max} - U_v)/(g\zeta_{1/2}S)^{1/2}$ and $\alpha\beta = 1/\ln(2)$, and thus Eq. (6.5) is rewritten as

$$\frac{u-U_v}{u_{\max}-U_v} = \exp\left[-\ln(2)\left(\frac{\zeta}{\zeta_{1/2}}\right)^\beta\right] \tag{6.6}$$

In Eq. (6.6), the dimensionless velocity difference and distance are the same as those used for normalizing the velocity profiles in and Fig. 6-10.

To scale measured velocity profiles in the form of Eq. (6.6), three parameters, U_v, $\zeta_{1/2}$ and β, must be known. First, as stated previously, U_v is taken as the average flow velocity measured in the vegetation layer, which is not affected by the surface layer and channel bed, or can be estimated using the drag coefficient developed for the emergent case. Second, by fitting Eq. (6.6) to the data plotted

in , we obtained $\beta \approx 1.66$, which is approximately the average of the β-values obtained by fitting Eq. (6.6) to individual velocity profiles (see Table 6-1). With the average β-value, Eq. (6.6) are superimposed in and Fig. 6-10, showing that the measurements can be described reasonably well using the viscosity model. Next, $\zeta_{1/2}$ can be evaluated using other known parameters, as explained as follows.

By integrating Eq. (6.6) from $\zeta = 0$ to $\zeta = h_s$, a relationship can be established between $\zeta_{1/2}$ and the other parameters including u_{max} and U_s, where U_s is the average velocity of the surface layer. In the explicit form, the relationship can be further approximated as

$$\frac{\zeta_{1/2}}{h_s} = 0.89 \frac{U_s - U_v}{u_{\max} - U_v} \exp\left[\left(\frac{U_s - U_v}{u_{\max} - U_v} \right)^{4.4} \right] \tag{6.7}$$

Fig. 6-12 shows that Eq. (6.7) compares well with the relation (denoted by circles) calculated using the values of U_s, $\zeta_{1/2}$ and u_{max}, which are estimated from the measured velocity profiles. Three sets of data are plotted in Fig. 6-12, the first set due to the present study and the other two derived from the previous studies as detailed in the following section.

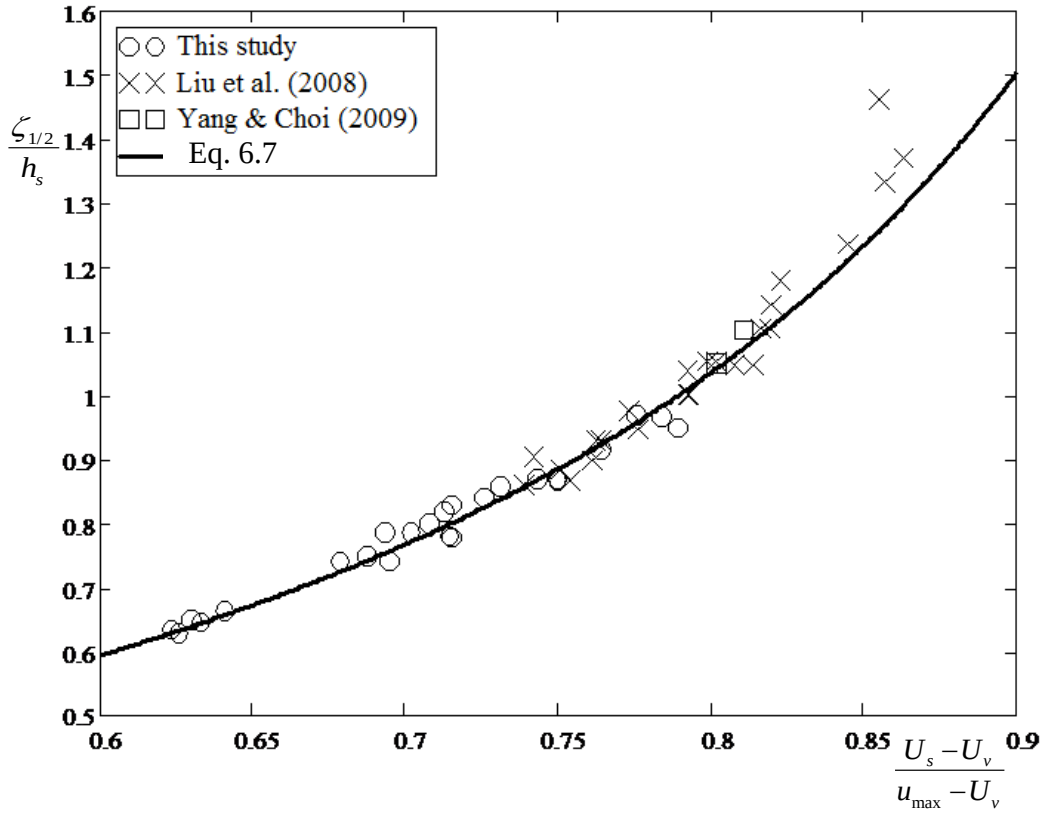

Fig. 6-12. Variation of $\zeta_{1/2}/h_s$ with $(U_s - U_v)/(u_{max}-U_v)$.

6.5 Further validation with other data

To further verify the proposed scaling, we also digitized 30 velocity profiles published in the literature, of which 24 were provided by Liu et al. (2008), 2 were conducted by Yang and Choi (2009), and the rest by Ghisalberti and Nepf (2009). Liu et al. (2008) conducted their experiments under various conditions of bed and rod roughness. They measured 24 flow velocity profiles for H/h_v = 1.50 – 1.57 at six different locations using a one-dimensional laser Doppler velocimeter. Yang and Choi (2009) sampled two velocity profiles using a two-dimensional laser Doppler velocimeter for H/h_v = 2.14. Additional data from

Ghisalberti and Nepf (2009) are included by considering the applicable of the proposed scaling to the high submerged flow conditions. The vegetation model was simulated with rigid rods, and the values of H/h_v were ranging from 3.36-3.38. The proposed scaling was first applied for the vegetation profiles from Liu et al. (2008) and Yang and Choi (2009). Fig. 6-13 shows good agreement between Eq. (6.6) with β = 1.66 and these measurements. In addition, the dependence of the normalised half-thickness, $\zeta_{1/2}/h_s$, was also worked out, and the result is superimposed on Fig. 6-12, showing its consistence with the present study. Fig. 6-14 shows the application of Eq. (6.6) to scale the velocity profiles with high ratio H/h_v of Ghisalberti and Nepf (2004). The scaling (6.6) was applied only for the shear layer. Ghisalberti and Nepf (2004) defined the limits of the shear layer as an average of the estimated location of zero shear and of zero Reynolds stress. The value of u_{max} was taken as the velocity at the upper limit of the shear layer. The results showed that the scaling could fit the velocity profiles in the shear layer to a single curve as in shallow flow conditions. It could be understandable because the shear layer contains an inflection point in which the mixing layer analogy could be applied.

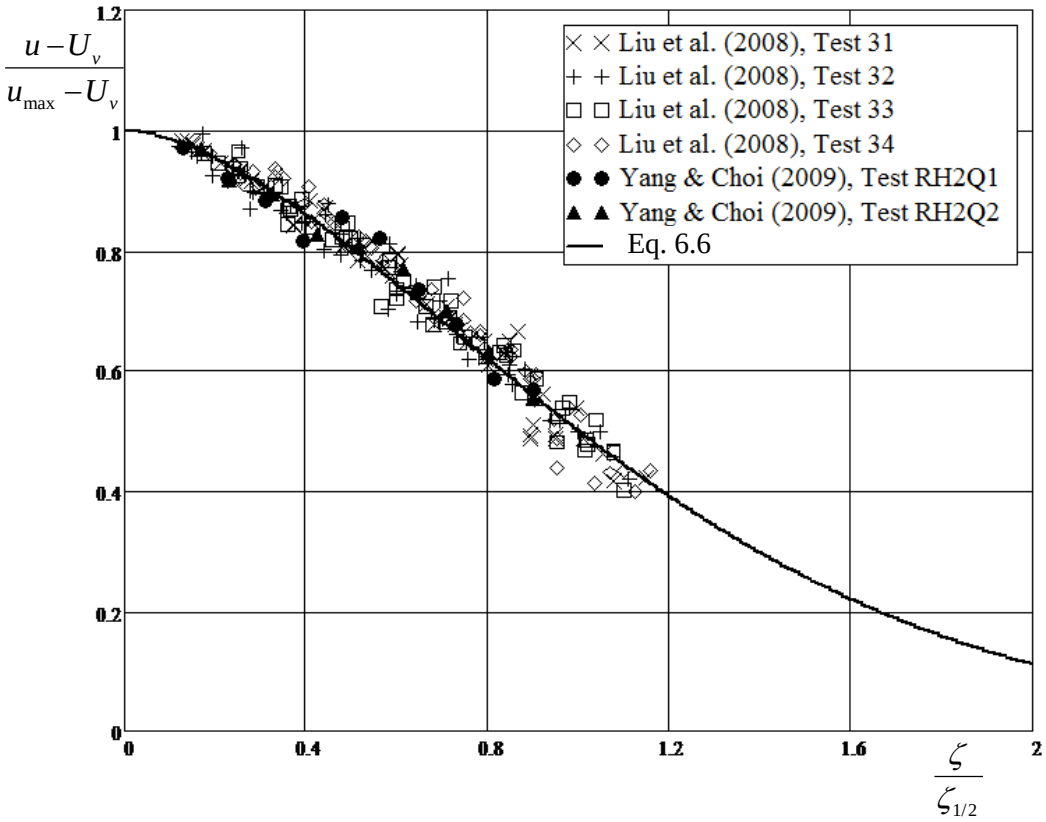

Fig. 6-13. Comparison of Eq. (6.6) with the previous measurements.

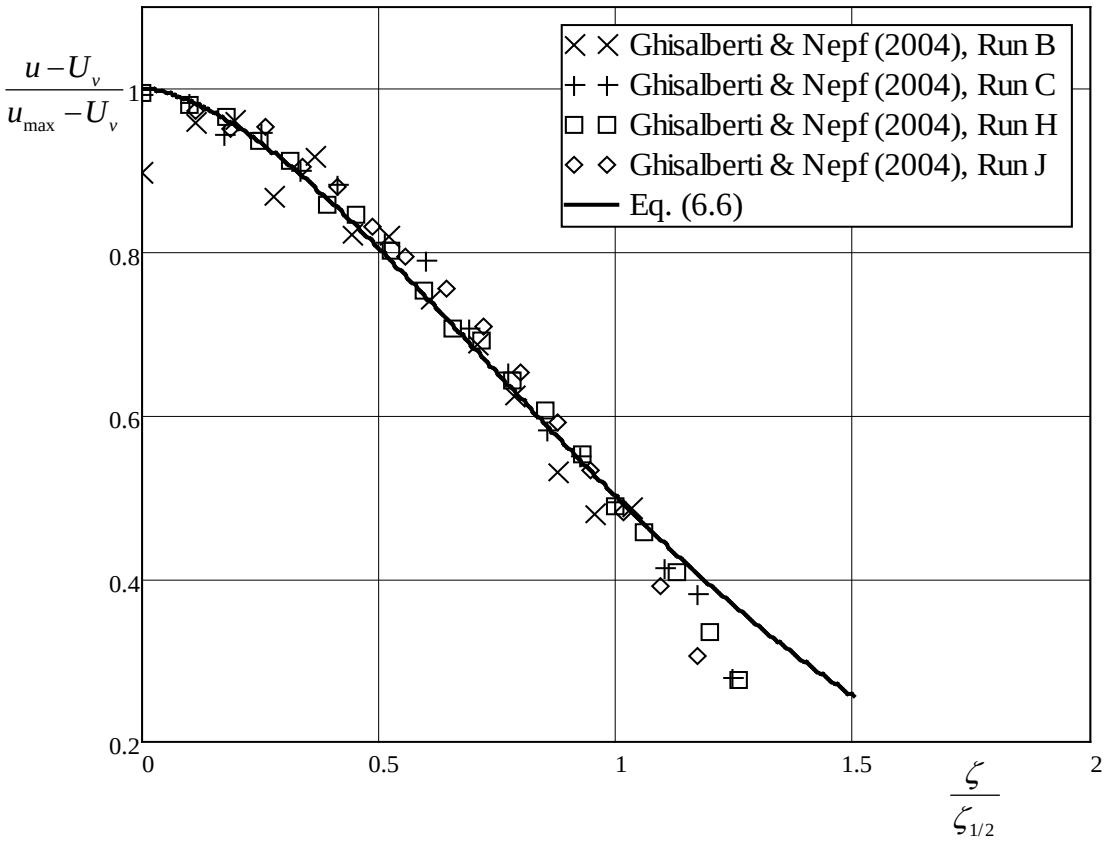

Fig. 6-14. Comparison of Eq. (6.6) with high flow depth experiments ($H/h_v >> 2$).

6.6 Conclusions

The presence of submerged vegetation functions as large-scale roughness that obstructs the near-bed flow and thus reduces the flow velocity. The flow through the near-bed vegetation layer differs from that of the surface layer above. The two-layer flow resembles the plane mixing layer in that an inflection point appears in the velocity profile. The resulted turbulent flow is inherently unstable and coherent. This analogy implies that the scaling

philosophy that underlies the logarithmic law is not applicable for depth-limited, vegetated open channel flows.

In this study, a length scale called half-thickness is proposed as the distance from the free surface to the location where the velocity difference reduces to one half of its maximum. Then, the velocity profile is scaled using the half-thickness and the maximum velocity defect. This scaling argument is better than others, yielding superior collapsing of velocity profiles measured by the authors and others under a wide range of flow and vegetation conditions. Finally, a viscosity model has been developed to theoretically describe the normalised velocity profile. The analysis compares well with the data collected from the laboratory experiments conducted in this study and also by others. It should be mentioned that this study is limited to vegetated open channel flows with the flow depth not greater than twice the vegetation height, and the vegetation simulated by the rigid, cylindrical rods. Further studies need to be conducted to examine if the proposed scaling is still applicable when the flow depth is relatively increased.

CHAPTER 7

CONCLUSIONS AND RECOMMENDATIONS

7.1 Conclusions

The presence of emergent vegetation in wetlands and rivers has impacts on physical and biological processes in aquatic environments. In vegetated open channel flows, the vegetation-induced drag reduces flow discharge in channels and increases the resistance. Numerous studies have focused on exploring, experimentally and analytically the effects of emergent and submerged vegetation on characteristics of open channel flows. However, the problem of describing the velocity profile and of evaluating flow resistance and sediment transport rates, remain challenging. This thesis's main focus was on evaluating the flow resistance induced by vegetation in emergent and submerged flow conditions. It developed an approach to estimate bulk flow velocity for rigid and flexible vegetation in submerged flow conditions. It also addressed problem how to normalise velocity profiles for depth-limited open channel flows with submerged vegetation.

A series of laboratory experiments was carried out to simulate vegetated open-channel flows. The vegetation was modeled by rigid rods with different configurations. Various flow depths were used to cover both emergent and submerged flow conditions. The streamwise and vertical components of flow velocity were measured with a two-dimensional Laser Doppler Anemometer (LDA) and a two-dimensional Electromagnetic Current Meter (EMCM). The total of 143 cases of emergent vegetation and 24 cases of submerged vegetation were considered. There was also an experiment with dye in order to visualize the coherent eddies in the roughness sublayer in depth-limited flow conditions.

The experimental results showed that the velocity profile is mostly uniform over the depth in the emergent cases. For submerged flows, the flow velocity inside the vegetation layer is significantly smaller than that inside the surface layer. A near-constant velocity dominates inside the vegetation layer, and increases near the interface. There is a sudden change in the shape of the velocity profile near the top edge of vegetation, indicating a two-layer velocity distribution for shallow flow conditions. The results also showed that, for both emergent and submerged cases, the flow velocity is strongly dependent on vegetation density. For depth-limited flow conditions over rigid vegetation, the experiments with dye illustrated the existence of vortices in the roughness sublayer which could cause flow instability near the vegetation interface. In addition, the distributions of the horizontal turbulent intensity, u_{rms}, attains

maximum just above the canopy, whereas the vertical turbulence intensity, w_{rms}, attains maximum just below the canopy.

This thesis introduced a new concept of hydraulic radius and demonstrated its benefit in unifying experimental data of resistance to emergent vegetated open channel flows for various bed and vegetation configurations. The vegetation hydraulic radius was defined by taking into account effects of vegetation size and density, as well as channel geometry. By drawing analogies between pipe flows and vegetated channel flows, the thesis proposed a new resistance function with the Reynolds number that is defined using a vegetation-related hydraulic radius [Eq. (4.23)]. The drag coefficient was shown to decreas monotonically with the Reynolds number, independent of vegetation density (Fig. 4-10). Furthermore, Ergun equation [Eq. (4.28)], if applied to emergent vegetated open channel flows, would underestimate drag coefficients for low Reynolds numbers and overestimate than for high Reynolds numbers. A new procedure was devised for correcting sidewall and bed effects that may appear significant in both laboratory and field conditions.

The thesis put forward a representative roughness height for the description of resistance of vegetated open channel flows, by considering the relative blockage caused by submerged vegetation. This roughness height is proportioned to both stem diameter and vegetation density [Eq. (5.8)]. It was shown to have better predictions in particular for the case of low flow rates, in comparison with the existing works. Also, all formulas, despite being derived with different

arguments under certain conditions, can be unified in a general form. The proposed formula [Eq. (5.16)] for the case of rigid and flexible vegetation delivered acceptable results.

Finally, The thesis proposed a length scale called half-thickness which normalises velocity profiles for depth-limited open channel flows with submerged vegetation using a plane mixing layer analogy. The new scaling is better than those based on logarithmic, velocity-defect and power laws in collapsing the velocity profiles under a wide range of flow and vegetation conditions. To justify the scaling argument, a simple viscosity model was developed [Eq. (6.7)].

7.2 Future work

The velocity profile in vegetated shallow flows was investigated for both cases of emergent and submerged flow conditions with different flow depths and vegetation configurations. However, more works is neccessary to achieve a better solution to describe the flow velocity. The current data were collected at a single location. It would be necessary to know the differences of the flow velocity at the measured location from the average flow velocity for the whole cross section. Advanced laser imaging techniques of Particle Image Velocimetry (PIV) can be employed as measurement methods. Numerical modeling can be also considered as a means to simulate flow velocity profile in the same settings. Also, turbulence structures of vegetated flow under shallow flow conditions would need to be analyzed in more detail.

In this work, experiments were conducted using rigid vegetation. In contrast, there are various species of vegetation in flexible type in the field measurements. Therefore, hydraulic responses to obstructing vegetation in a flow field may be different from the rigid vegetation experiments. The bending or waving of flexible vegetation could influence the flow field. The natural variation of the plant height, the surface density and the leaf foliage may also affect the hydraulic drag. Thus, it would be interesting to explore how flow structures and drag coefficients change with flexible vegetation.

Other experiments in future work will be considered o examine effects of vegetation on suspended sediment concentration profiles in vegetated shallow flow conditions. The impact of vegetation on the bed load transport and the bed form could also be investigated through experiments.

REFERENCES

Baptist, M. J., Babovic, V., Uthurburu, J. R., Keijzer, M., Uittenbogaard, R. E., Mynett, A., and Verwey, A. (2007). "On inducing equations for vegetation resistance." *Journal of Hydraulic Research*, 45(4), 435-450.

Baptist, M. J. (2005), Modelling floodplain biogeomorphology, *PhD Thesis*, ISBN 90-407-2582-9, 193 pp., Delft University of Technology, Faculty of Civil Engineering and Geosciences, Section Hydraulic Engineering.

Barfield, B. J., Tollner, E. W., and Hayes, J. C. (1979). "Filtration of sediment by simulated vegetation. I. Steady-state flow with homogeneous sediment." *Transactions American Society of Agricultural Engineers*, 22(3), 540-545.

Brunet, Y., Finnigan, J. J., and Raupach, M. R. (1994). "A wind-tunnel study of air-flow in waving wheat - single-point velocity statistics." *Boundary-Layer Meteorology*, 70(1-2), 95-132.

Carollo, F. G., Ferro, V., and Termini, D. (2002). "Flow velocity measurements in vegetated channels." *Journal of Hydraulic Engineering-ASCE*, 128(7), 664-673.

Chen, C. L. (1991). "Unified theory on power laws for flow resistance." *Journal of Hydraulic Engineering-ASCE*, 117(3), 371-389.

Cheng, H., and Castro, I. P. (2002). "Near wall flow over urban-like roughness." *Boundary-Layer Meteorology*, 104(2), 229-259.

Cheng, N. S. (2003). “Application of Ergun equation to computation of critical shear velocity subject to seepage.” *Journal of Irrigation and Drainage Engineering-ASCE*, 129(4), 278-283.

Cheng, N. S. (2007). "Power-law index for velocity profiles in open channel flows." *Advances in Water Resources*, 30(8), 1775-1784.

Cheng, N. S., and Chiew, Y. M. (1998). "Modified logarithmic law for velocity distribution subjected to upward seepage." *Journal of Hydraulic Engineering-ASCE*, 124(12), 1235-1241.

Cheng, N.-S., Chiew, Y.-M. (1999). "Incipient sediment motion with upward seepage." *Journal of Hydraulic Research*, 37 (5), 665-681.

Cheng, N.-S. (2003). "Application of Ergun equation to computation of critical shear velocity subject to seepage." *Journal of Irrigation and Drainage Engineering*, 129 (4), 278-283.

Cheng, N.-S., Hao, Z., Tan, S.K. (2008). "Comparison of quadratic and power law for nonlinear flow through porous media." *Experimental Thermal and Fluid Science*, 32 (8), 1538-1547.

Chow, V. T. (1959). *Open-Channel Hydraulics*, McGraw-Hill, New York.

Christensen, B.A. (1985). "Open channel and sheet flow over flexible roughness." *Proceedings of the 21st IAHR Congress in Melbourne, Australia*, 462-467.

Dantec (2000), "BSA Flow software installation and User's guide." Dantec Measurement Technology, Inc., Danmark.

Defina, A., and Bixio, A. C. (2005). "Mean flow and turbulence in vegetated open channel flow." *Water Resources Research*, 41(7), 1-12.

Dunn, C., F. Lopez, and M. Garcia (1996). "Mean flow and turbulence in a laboratory channel with simulated vegetation." *Hydraulic Engineering Series Report No. 51*, Hydrosystem Lab., University of Illinois, Urbana.

Ergun, S. (1952). "Fluid flow through packed columns." *Chemical. Engineering Progress*, 48 (2), 89-94.

Ferreira, R. M. L., Ricardo, A. M., and Franca, M. J. (2009). "Discussion of "Laboratory investigation of mean drag in a random array of rigid,

emergent cylinders" by Yukie Tanino and Heidi M. Nepf." *Journal of Hydraulic Engineering-ASCE*, 135(8), 690-693.

Finnigan, J. (2000). "Turbulence in plant canopies." *Annual Review of Fluid Mechanics*, 32, 519-571.

Ghisalberti, M., and Nepf, H. M. (2004). "The limited growth of vegetated shear layers." *Water Resources Research*, 40(7), W075021-W0750212.

Ghisalberti, M., and Nepf, H. (2005). "Mass transport in vegetated shear flows." *Environmental Fluid Mechanics*, 5(6), 527-551.

Ghisalberti, M., and Nepf, H. (2006). "The structure of the shear layer in flows over rigid and flexible canopies." *Environmental Fluid Mechanics*, 6(3), 277-301.

Ghisalberti, M. (2009). "Obstructed shear flows: similarities across systems and scales." *Journal of Fluid Mechanics*, 641, 51-61.

Ghisalberti, M., and Nepf, H. (2009). "Shallow flows over a permeable medium: the hydrodynamics of submerged aquatic canopies." *Transport in Porous Media*, 78(3), 385-402.

Gioia, G., and F. A. Bombardelli (2002). “Scaling and similarity in rough channel flows.” *Physical Review Letters*, 88(1), 145011-145014.

Gourlay, M. R. (1970). “Discussion of ‘Flow resistance in vegetated channels’ by N. Kouwen, T. E. Unny, and H. M. Hill.” *Journal of the Irrigation and Drainage Division of the American Society of Civil Engineers*, 96(3), 351-357.

Harman, I. N., and Finnigan, J. J. (2007). "A simple unified theory for flow in the canopy and roughness sublayer." *Boundary-Layer Meteorology*, 123(2), 339-363.

Huthoff, F., Augustijn, D. C. M., and Hulscher, S. (2007). "Analytical solution of the depth-averaged flow velocity in case of submerged rigid

cylindrical vegetation." *Water Resources Research*, 43(6), W06413, doi:06410.01029/02006WR005625.

Ikeda, S., and Kanazawa, M. (1996). "Three-dimensional organized vortices above flexible water plants." *Journal of Hydraulic Engineering-ASCE*, 122(11), 634-640.

Ishikawa, Y., Mizuhara, K., and Ashida, S. (2000). "Effect of density of trees on drag exerted on trees in river channels." *Journal of Forest Research*, 5(4), 271-279.

James, C. S., Birkhead, A. L., Jordanova, A. A., and O'Sullivan, J. J. (2004). "Flow resistance of emergent vegetation." *Journal of Hydraulic Research*, 42(4), 390-398.

James, C. S., Goldbeck, U. K., Patini, A., and Jordanova, A. A. (2008). "Influence of foliage on flow resistance of emergent vegetation." *Journal of Hydraulic Research*, 46(4), 536-542.

Jarvela, J. (2002). "Flow resistance of flexible and stiff vegetation: a flume study with natural plants." *Journal of Hydrology*, 269(1-2), 44-54.

Jarvela, J. (2003). “Influence of vegetation on flow structure in floodplains and wetlands.” *Proceedings, IAHR Symposium on River, Coastal and Estuarine Morphodynamics (RCEM 2003), IAHR*, Madrid, Spain, 845-856.

Jarvela, J. (2005). "Effect of submerged flexible vegetation on flow structure and resistance." *Journal of Hydrology*, 307(1-4), 233-241.

Klopstra, D., Barneveld, H. J., Van Noortwijk, J. M., and Van Velzen, E. H. "Analytical model for hydraulic roughness of submerged vegetation." *Proceedings, Congress of the International Association of Hydraulic Research, IAHR*, San Francisco, CA, USA, 775-780.

Kothyari, U. C., Hayashi, K., and Hashimoto, H. (2009). "Drag coefficient of unsubmerged rigid vegetation stems in open channel flows." *Journal of Hydraulic Research*, 47(6), 691-699.

Kouwen, N., and Unny, T. E. (1973). "Flexible roughness in open channels." *Journal of the Hydraulics Division-ASCE*, 99(HY5), 713-728.

Kouwen, N., Unny, T. E., and Hill, H. M. (1969). "Flow retardance in vegetated channels." *Journal of the Irrigation and Drainage Division-ASCE*, 95(IR2), 329-342.

Kubrak, E., J. Kubrak, and P. M. Rowinski (2008). "Vertical velocity distributions through and above submerged, flexible vegetation." *Hydrological Sciences Journal-Journal Des Sciences Hydrologiques*, 53(4), 905-920.

Kundu, P. K., Cohen, I. M., and Hu, H. H. (2004). *Fluid mechanics*, Elsevier Academic Press, Amsterdam, Boston.

Lee, J. K., Roig, L. C., Jenter, H. L., and Visser, H. M. (2004). "Drag coefficients for modeling flow through emergent vegetation in the Florida Everglades." *Ecological Engineering*, 22(4-5), 237-248.

Li, R.-M., and Shen, H. W. (1973). "Effect of tall vegetations on flow and sediment." *Journal of Hydraulic Division-ASCE*, 99(HY5), 793-814.

Liu, D., Diplas, P., Fairbanks, J. D., and Hodges, C. C. (2008). "An experimental study of flow through rigid vegetation." *Journal of Geophysical Research-Earth Surface*, 113(F4), F04015.

Meijer, and M, D. (1998). "Flume studies of submerged vegetation." *Technical Report PR121*, HKV Consultants, Lelystad, the Netherlands.

Meijer, D. G., and E. H. van Velzen (1999). "Prototype-scale flume experiments on hydraulic roughness of submerged vegetation." paper presented at *XXVIII IAHR Conference*, Graz, Austria.

Murphy, E., M. Ghisalberti, and H. Nepf (2007). “Model and laboratory study of dispersion in flows with submerged vegetation.” *Water Resources Research*, 43(5), W05438, doi:05410.01029/02006WR005229.

Nepf, H., and Ghisalberti, M. (2008). "Flow and transport in channels with submerged vegetation." *Acta Geophysica*, 56(3), 753-777.

Nepf, H. M., and Vivoni, E. R. (1998). "Drag and diffusivity within emergent vegetation." *Proceedings of the 1998 ASCE Wetlands Engineering River Restoration Conference*, Denver, CO, USA.

Nepf, H. M. (1999). "Drag, turbulence, and diffusion in flow through emergent vegetation." *Water Resources Research*, 35(2), 479-489.

Nepf, H. M., Sullivan, J. A., and Zavistoski, R. A. (1998). "A model for diffusion within emergent vegetation." *Limnology and Oceanography*, 42(8), 1735-1745.

Nepf, H. M., and Vivoni, E. R. (2000). "Flow structure in depth-limited, vegetated flow." *Journal of Geophysical Research - Oceans*, 105(C12), 28547-28557.

Nepf, H. M., White, B., Lightbody, A., and Ghisalberti, M. (2007). “Transport in aquatic canopies.” *Book chapter of Flow and Transport Processes with Complex Obstructions. NATO Science Series II: Mathematics, Physics and Chemistry*, edited by Gayev Y.A. and Hunt. J.C.R., Springer, ISBN: 978-1-4020-5383-2, 236, 221-250.

Nezu, I., and Nakagawa, H. (1993). "Turbulence in open-channel flows." *IAHR Monograph Series*, Balkema Publishers, Rotterdam, Netherlands.

Nezu, I., and Onitsuka, K. (2001). "Turbulent structures in partly vegetated open-channel flows with LDA and PIV measurements." *Journal of Hydraulic Research*, 39(6), 629-642.

Nezu, I., and Sanjou, M. (2008). "Turburence structure and coherent motion in vegetated canopy open-channel flows." *Journal of Hydro-Environment*

Research, 2(2), 62-90.

Nikora, V.a , McEwan, I.a , McLean, S.b , Coleman, S.c , Pokrajac, D.a , and Walters, R.d. (2007) "Double-averaging concept for rough-bed open-channel and overland flows: Theoretical background." *Journal of Hydraulic Engineering*, 133 (8), 873-883.Nikuradse, J. (1933). "Stromungsgesetze in rauhen Rohren, Forschung auf dem Gebiete des Ingenieurwesens." Forschungsheft 361. VDI Verlag, Berlin, Germany (in German). (English translation: Laws of flow in rough pipes, NACA TM 1292, 1950).

Okamoto, T., and I. Nezu (2010). "Flow resistance law in open-channel flows with rigid and flexible vegetation." *River Flow 2010*, edited by A. Dittrich, et al., pp. 261-268, Bundesanstalt für Wasserbau, Karlsruhe, Germany.

Dantec (2000), "BSA Flow software installation and User's guide." Dantec Measurement Technology, Inc., Danmark.

Omega (n.d). "*Introduction to Magnetic Flow Meters."* Retrieved from http://www.omega.com/prodinfo/magmeter.html.

Poggi, D., Porporato, A., Ridolfi, L., Albertson, J. D., and Katul, G. G. (2004). "The effect of vegetation density on canopy sub-layer turbulence." *Boundary-Layer Meteorology*, 111(3), 565-587.

Pope, S. B. (2000). *Turbulent flows*, Cambridge University Press, Cambridge.

Prandtl, L. (1925). "Bericht über Untersuchungen zur ausgebildeten Turbulenz." *Zeitschrift für angewandte Mathematik und. Mechanik*, 5, 136-139.

Qian, N., and Wan, Z. (1999). *Mechanics of sediment transport*, American Society of Civil Engineers, Reston, Va.

Raupach, M. R., Antonia, R. A., and Rajagopalan, S. (1991). "Rough-wall turbulent boundary layers." *Applied Mechanics Reviews*, 44(1), 1-25.

Raupach, M. R., Finnigan, J. J., and Brunet, Y. (1996). "Coherent eddies and turbulence in vegetation canopies: The mixing-layer analogy." *Boundary-Layer Meteorology*, 78(3-4), 351-382.

Raupach, M. R., and Thom, A. S. (1981). "Turbulence in and above plant canopies." *Annual Review of Fluid Mechanics*, 13, 97-129.

Shimizu, Y., T. Tsujimoto, H. Nakagawa, and T. Kitamura (1991). "Experimental study on flow over rigid vegetation simulated by cylindrical with equi-spacing." *Proceedings of the Japan Society of Civil Engineers*, 438/II-17, 31-40 (In Japanese).

Shimizu, Y. and T. Tsujimoto, 1994. "Numerical analysis of turbulent open-channel

flow over a vegetation layer using a k-ε turbulence model." *Journal of hydroscience and hydraulic engineering*, JSCE, 11(2), 21-36.

Stephan, U., and Gutknecht, D. (2002). "Hydraulic resistance of submerged flexible vegetation." *Journal of Hydrology*, 269(1-2), 27-43.

Stoesser, T., Kim, S. J., and Diplas, P. (2010). "Turbulent flow through idealized emergent vegetation." *Journal of Hydraulic Engineering-ASCE*, 136(12), 1003-1017.

Stokes, G.G. (1851). "On the effect of the internal friction of fluids on the motion of pendulums." *Transactions of the Cambridge Philosophical Society*, 9, 8-106.

Stone, B. M. (1997). "Hydraulics of Flow in Vegetated Channels." *Master Thesis*, Clarkson University.

Stone, B. M., and Shen, H. T. (2002). "Hydraulic resistance of flow in channels with cylindrical roughness." *Journal of Hydraulic Engineering-ASCE*, 128(5), 500-506.

Takemura, T., and Tanaka, N. (2007). "Flow structures and drag characteristics

of a colony-type emergent roughness model mounted on a flat plate in uniform flow." *Fluid Dynamics Research*, 39(9-10), 694-710.

Tanino, Y., and Nepf, H. M. (2008). "Laboratory investigation of mean drag in a random array of rigid, emergent cylinders." *Journal of Hydraulic Engineering*, 134(1), 34-41.

Tanino, Y., and Nepf, H. M. (2010). "Laboratory investigation of mean drag in a random array of rigid, emergent cylinders (Unpublished raw data)."

Temple, D. M. (1986). "Velocity distribution coefficients for grass-lined channels." *Journal of Hydraulic Engineering-ASCE*, 112(3), 193-205.

Thom, A. S. (1971). "Momentum absorption by vegetation." *Quart. J. Roy. Meteorol. Soc.*, 97, 414-428.

Tsihrintzis, V. A. (2001). "Variation of roughness coefficients for unsubmerged and submerged vegetation - Discussion." *Journal of Hydraulic Engineering-ASCE*, 127(3), 241-244.

Tsujimoto, T., and Kitamura, T. (1990). "Velocity profile of flow in vegetated-bed channels." *KHL Communication 1990*, 1, 43-55.

Vanoni, V. A., and Brooks, N. H. (1957). "Laboratory studies of the roughness and suspended load of alluvial streams." *Report E-68*, Sedimentation Laboratory, California Institute of Technology, Pasadena, California, USA.

White, B. L., and Nepf, H. M. (2007). "Shear instability and coherent structures in shallow flow adjacent to a porous layer." *Journal of Fluid Mechanics*, 593, 1-32.

Wu, F. S. (2008). "Characteristics of flow resistance in open channels with non-submerged rigid vegetation." *Journal of Hydrodynamics*, 20(2), 239-245.

Wu, F. C., Shen, H. W., and Chou, Y. J. (1999). "Variation of roughness coefficients for unsubmerged and submerged vegetation." *Journal of Hydraulic Engineering-ASCE*, 125(9), 934-942.

Yan, J. (2008). "Experimental study of flow resistance and turbulence characteristics of open channel flow with vegetation." *PhD Thesis, Hohai University, China*.

Yang, W. (2008). "Experimental study of turbulent open-channel flows with submerged vegetation." *PhD Thesis, Yonsei University, Korea*.

Yang, W., and Choi, S. U. K. (2009). "Impact of stem flexibility on mean flow and turbulence structure in depth-limited open channel flows with submerged vegetation." *Journal of Hydraulic Research*, 47(4), 445-454.

Yen, B. C. (2002). "Open channel flow resistance." *Journal of Hydraulic Engineering-ASCE*, 128(1), 20-39.

Zima, L., and Ackermann, N. L. (2002). "Wave generation in open channels by vortex shedding from channel obstructions." *Journal of Hydraulic Engineering-ASCE*, 128(6), 596-603.

Zinke, P. (2010). "Flow resistance parameters for nature emergent vegetation derived from a porous media model." River Flow 2010, A. Dittrich, K. Koll, J. Aberle, and P. Geisenhainer, eds., Bundesanstalt für Wasserbau (BAW), Karlsruhe, Germany, 461-468.

APPENDIX

Appendix. Compilation of Experimental Data of Open Channel Flows with Submerged Vegetation

(A) Rigid vegetation

	No.	Run	Q (m^3/s)	B (m)	H (m)	S	λ	d (m)	h_v (m)	N ($/m^2$)
Shimizu et al. (1991)	R1	R21	0.002073	0.5	0.0636	0.00066	0.00785	0.001	0.041	9995
	R2	R22	0.003486	0.5	0.073	0.00108	0.00785	0.001	0.041	9995
	R3	R23	0.004786	0.5	0.0883	0.0009	0.00785	0.001	0.041	9995
	R4	R24	0.006058	0.5	0.0948	0.001	0.00785	0.001	0.041	9995
	R5	R25	0.007736	0.5	0.1054	0.00099	0.00785	0.001	0.041	9995
	R6	R31	0.003537	0.5	0.0631	0.00164	0.00785	0.001	0.041	9995
	R7	R32	0.00518	0.5	0.0747	0.00213	0.00785	0.001	0.041	9995
	R8	R33	0.006841	0.5	0.0842	0.00201	0.00785	0.001	0.041	9995
	R9	R34	0.008558	0.5	0.0941	0.00183	0.00785	0.001	0.041	9995
	R10	R35	0.010552	0.5	0.1061	0.00176	0.00785	0.001	0.041	9995
	R11	R41	0.004784	0.5	0.0659	0.00233	0.00785	0.001	0.041	9995
	R12	R42	0.006306	0.5	0.0735	0.00263	0.00785	0.001	0.041	9995
	R13	R43	0.008508	0.5	0.0847	0.00304	0.00785	0.001	0.041	9995
	R14	R44	0.010512	0.5	0.0953	0.00256	0.00785	0.001	0.041	9995
	R15	R45	0.014154	0.5	0.1026	0.0032	0.00785	0.001	0.041	9995
	R16	R51	0.006129	0.5	0.0659	0.00455	0.00785	0.001	0.041	9995
	R17	R52	0.007541	0.5	0.0739	0.00455	0.00785	0.001	0.041	9995
	R18	R53	0.009802	0.5	0.0841	0.00435	0.00785	0.001	0.041	9995
	R19	R54	0.012944	0.5	0.0956	0.00435	0.00785	0.001	0.041	9995
	R20	R55	0.016022	0.5	0.1052	0.00476	0.00785	0.001	0.041	9995
	R21	A11	0.005035	0.4	0.095	0.001	0.00442	0.0015	0.046	2501
	R22	A12	0.003511	0.4	0.0749	0.001	0.00442	0.0015	0.046	2501
	R23	A31	0.007334	0.4	0.0936	0.003	0.00442	0.0015	0.046	2501
	R24	A32	0.005274	0.4	0.0735	0.003	0.00442	0.0015	0.046	2501
	R25	A34	0.00216	0.4	0.05	0.003	0.00442	0.0015	0.046	2501
	R26	A35	0.002806	0.4	0.0568	0.003	0.00442	0.0015	0.046	2501
	R27	A71	0.011832	0.4	0.0895	0.007	0.00442	0.0015	0.046	2501
	R28	A72	0.007761	0.4	0.0727	0.007	0.00442	0.0015	0.046	2501
Dunn et al. (1996)	R29	1	0.179	0.91	0.335	0.0036	0.005436	0.00635	0.1175	172
	R30	2	0.088	0.91	0.229	0.0036	0.005436	0.00635	0.1175	172
	R31	3	0.046	0.91	0.164	0.0036	0.005436	0.00635	0.1175	172
	R32	4	0.178	0.91	0.276	0.0076	0.005436	0.00635	0.1175	172
	R33	5	0.098	0.91	0.203	0.0076	0.005436	0.00635	0.1175	172
	R34	6	0.178	0.91	0.267	0.0036	0.001362	0.00635	0.1175	43
	R35	7	0.095	0.91	0.183	0.0036	0.001362	0.00635	0.1175	43
	R36	8	0.18	0.91	0.391	0.0036	0.012269	0.00635	0.1175	387
	R37	9	0.058	0.91	0.214	0.0036	0.012269	0.00635	0.1175	387
	R38	10	0.18	0.91	0.265	0.0161	0.012269	0.00635	0.1175	387
	R39	11	0.177	0.91	0.311	0.0036	0.003067	0.00635	0.1175	97
	R40	12	0.181	0.91	0.233	0.0108	0.003067	0.00635	0.1175	97
Meijer (1998) [see Baptist (2005)]	R41	1	1.0395	3	1.98	0.00109	0.012868	0.008	1.5	256
	R42	2	1.39101	3	1.99	0.0018	0.012868	0.008	1.5	256
	R43	3	1.39284	3	2.19	0.00095	0.012868	0.008	1.5	256
	R44	4	1.56366	3	2.19	0.00125	0.012868	0.008	1.5	256
	R45	5	1.7061	3	2.35	0.00081	0.012868	0.008	1.5	256
	R46	6	2.35563	3	2.33	0.00154	0.012868	0.008	1.5	256
	R47	7	1.9125	3	2.5	0.00065	0.012868	0.008	1.5	256
	R48	8	2.72688	3	2.47	0.00143	0.012868	0.008	1.5	256
	R49	9	1.86327	3	2.01	0.00106	0.003217	0.008	1.5	64
	R50	10	2.52657	3	2.01	0.00193	0.003217	0.008	1.5	64
	R51	11	2.2902	3	2.2	0.00101	0.003217	0.008	1.5	64
	R52	12	3.07476	3	2.19	0.00188	0.003217	0.008	1.5	64
	R53	13	2.6226	3	2.35	0.00093	0.003217	0.008	1.5	64
	R54	14	3.45807	3	2.31	0.00187	0.003217	0.008	1.5	64
	R55	15	2.90904	3	2.48	0.00094	0.003217	0.008	1.5	64
	R56	16	3.9483	3	2.46	0.00178	0.003217	0.008	1.5	64
	R57	17	1.12344	3	1.51	0.00107	0.012868	0.008	0.9	256

	R58	18	1.6188	3	1.52	0.00204	0.012868	0.008	0.9	256
	R59	19	1.79733	3	1.81	0.00085	0.012868	0.008	0.9	256
	R60	20	2.5542	3	1.8	0.00165	0.012868	0.008	0.9	256
	R61	21	2.52681	3	2.09	0.00071	0.012868	0.008	0.9	256
	R62	22	3.61779	3	2.09	0.00138	0.012868	0.008	0.9	256
	R63	23	3.72	3	2.48	0.00055	0.012868	0.008	0.9	256
	R64	24	5.96304	3	2.46	0.00149	0.012868	0.008	0.9	256
	R65	25	1.74858	3	1.51	0.00103	0.003217	0.008	0.9	64
	R66	26	2.52624	3	1.52	0.00205	0.003217	0.008	0.9	64
	R67	27	2.50323	3	1.81	0.00085	0.003217	0.008	0.9	64
	R68	28	3.52974	3	1.78	0.0018	0.003217	0.008	0.9	64
	R69	29	3.3831	3	2.1	0.00075	0.003217	0.008	0.9	64
	R70	30	4.72152	3	2.06	0.00164	0.003217	0.008	0.9	64
	R71	31	4.77945	3	2.47	0.00071	0.003217	0.008	0.9	64
	R72	32	6.68382	3	2.47	0.00143	0.003217	0.008	0.9	64
	R73	33	0.86598	3	1.02	0.00078	0.012868	0.008	0.45	256
	R74	34	1.30977	3	0.99	0.00164	0.012868	0.008	0.45	256
	R75	35	2.08833	3	1.51	0.00059	0.012868	0.008	0.45	256
	R76	36	3.06	3	1.5	0.00138	0.012868	0.008	0.45	256
	R77	37	3.7422	3	1.98	0.00058	0.012868	0.008	0.45	256
	R78	38	5.62374	3	1.99	0.00142	0.012868	0.008	0.45	256
	R79	39	5.91876	3	2.46	0.0007	0.012868	0.008	0.45	256
	R80	40	7.17867	3	2.49	0.0009	0.012868	0.008	0.45	256
	R81	41	1.34028	3	1.02	0.00075	0.003217	0.008	0.45	64
	R82	42	1.983	3	1	0.00187	0.003217	0.008	0.45	64
	R83	43	2.808	3	1.5	0.00069	0.003217	0.008	0.45	64
	R84	44	4.7745	3	1.5	0.00199	0.003217	0.008	0.45	64
	R85	45	5.73	3	2	0.00099	0.003217	0.008	0.45	64
	R86	46	7.314	3	2	0.00159	0.003217	0.008	0.45	64
	R87	47	6.56952	3	2.48	0.00063	0.003217	0.008	0.45	64
	R88	48	8.97966	3	2.41	0.00127	0.003217	0.008	0.45	64
Stone and Shen (2002) [see Stone (1997)]	R89	S9	5.70E-03	0.45	0.151	2.32E-03	0.061	0.013	0.124	460
	R90	S22	3.20E-03	0.45	0.155	9.10E-04	0.061	0.013	0.124	460
	R91	S23	4.80E-03	0.45	0.155	1.59E-03	0.061	0.013	0.124	460
	R92	S24	8.20E-03	0.45	0.155	4.06E-03	0.061	0.013	0.124	460
	R93	S25	0.011	0.45	0.155	7.61E-03	0.061	0.013	0.124	460
	R94	S26	0.017	0.45	0.155	0.017	0.061	0.013	0.124	460
	R95	S27	0.026	0.45	0.155	0.032	0.061	0.013	0.124	460
	R96	S28	2.40E-03	0.45	0.155	5.50E-04	0.061	0.013	0.124	460
	R97	S51	2.70E-03	0.45	0.153	5.90E-04	0.061	0.013	0.124	460
	R98	S52	4.30E-03	0.45	0.155	1.44E-03	0.061	0.013	0.124	460
	R99	S53	7.10E-03	0.45	0.155	3.34E-03	0.061	0.013	0.124	460
	R100	S54	0.029	0.45	0.155	0.044	0.061	0.013	0.124	460
	R101	S29	4.50E-03	0.45	0.206	4.50E-04	0.061	0.013	0.124	460
	R102	S30	6.00E-03	0.45	0.207	6.30E-04	0.061	0.013	0.124	460
	R103	S31	8.70E-03	0.45	0.205	9.40E-04	0.061	0.013	0.124	460
	R104	S32	0.012	0.45	0.205	1.98E-03	0.061	0.013	0.124	460
	R105	S33	0.018	0.45	0.206	4.45E-03	0.061	0.013	0.124	460
	R106	S34	0.029	0.45	0.207	0.012	0.061	0.013	0.124	460
	R107	S35	0.023	0.45	0.207	7.42E-03	0.061	0.013	0.124	460
	R108	S36	6.90E-03	0.45	0.207	8.10E-04	0.061	0.013	0.124	460
	R109	S46	5.00E-03	0.45	0.206	5.90E-04	0.061	0.013	0.124	460
	R110	S47	6.60E-03	0.45	0.209	5.40E-04	0.061	0.013	0.124	460
	R111	S48	8.00E-03	0.45	0.206	9.00E-04	0.061	0.013	0.124	460
	R112	S49	9.20E-03	0.45	0.207	1.17E-03	0.061	0.013	0.124	460
	R113	S50	0.011	0.45	0.212	1.34E-03	0.061	0.013	0.124	460
	R114	S37	0.01	0.45	0.311	3.60E-04	0.061	0.013	0.124	460
	R115	S38	0.011	0.45	0.308	5.40E-04	0.061	0.013	0.124	460
	R116	S39	0.016	0.45	0.308	7.60E-04	0.061	0.013	0.124	460
	R117	S40	0.021	0.45	0.311	9.30E-04	0.061	0.013	0.124	460
	R118	S41	0.013	0.45	0.314	4.00E-04	0.061	0.013	0.124	460
	R119	S42	0.028	0.45	0.308	1.88E-03	0.061	0.013	0.124	460
	R120	S43	0.013	0.45	0.308	3.50E-04	0.061	0.013	0.124	460
	R121	S44	0.011	0.45	0.308	4.70E-04	0.061	0.013	0.124	460
	R122	S45	0.015	0.45	0.311	5.40E-04	0.061	0.013	0.124	460
	R123	S66	3.80E-03	0.45	0.155	3.50E-04	0.022	0.013	0.124	166
	R124	S67	4.90E-03	0.45	0.155	5.80E-04	0.022	0.013	0.124	166
	R125	S68	7.10E-03	0.45	0.155	1.03E-03	0.022	0.013	0.124	166

R126	S69	8.90E-03	0.45	0.155	1.70E-03	0.022	0.013	0.124	166
R127	S70	0.011	0.45	0.155	2.75E-03	0.022	0.013	0.124	166
R128	S71	0.017	0.45	0.155	5.23E-03	0.022	0.013	0.124	166
R129	S72	0.028	0.45	0.155	0.014	0.022	0.013	0.124	166
R130	S90	0.018	0.45	0.155	5.68E-03	0.022	0.013	0.124	166
R131	S91	0.021	0.45	0.155	8.38E-03	0.022	0.013	0.124	166
R132	S94	0.023	0.45	0.155	0.01	0.022	0.013	0.124	166
R133	S95	0.015	0.45	0.155	4.52E-03	0.022	0.013	0.124	166
R134	S99	6.60E-03	0.45	0.155	9.80E-04	0.022	0.013	0.124	166
R135	S109	8.90E-03	0.45	0.155	2.07E-03	0.022	0.013	0.124	166
R136	S110	7.10E-03	0.45	0.155	1.18E-03	0.022	0.013	0.124	166
R137	S119	0.013	0.45	0.155	3.14E-03	0.022	0.013	0.124	166
R138	S120	0.019	0.45	0.155	6.79E-03	0.022	0.013	0.124	166
R139	S121	0.023	0.45	0.155	9.52E-03	0.022	0.013	0.124	166
R140	S73	4.60E-03	0.45	0.207	2.30E-04	0.022	0.013	0.124	166
R141	S74	5.90E-03	0.45	0.207	2.70E-04	0.022	0.013	0.124	166
R142	S75	6.90E-03	0.45	0.207	3.60E-04	0.022	0.013	0.124	166
R143	S76	8.10E-03	0.45	0.207	6.30E-04	0.022	0.013	0.124	166
R144	S77	9.40E-03	0.45	0.207	5.30E-04	0.022	0.013	0.124	166
R145	S78	0.011	0.45	0.207	7.10E-04	0.022	0.013	0.124	166
R146	S79	0.017	0.45	0.207	1.53E-03	0.022	0.013	0.124	166
R147	SS0	0.029	0.45	0.207	4.28E-03	0.022	0.013	0.124	166
R148	S92	0.025	0.45	0.207	3.82E-03	0.022	0.013	0.124	166
R149	S93	0.021	0.45	0.207	2.34E-03	0.022	0.013	0.124	166
R150	S97	6.80E-03	0.45	0.207	3.50E-04	0.022	0.013	0.124	166
R151	S98	0.015	0.45	0.207	1.23E-03	0.022	0.013	0.124	166
R152	S108	7.70E-03	0.45	0.207	5.40E-04	0.022	0.013	0.124	166
R153	S126	0.013	0.45	0.207	8.90E-04	0.022	0.013	0.124	166
R154	S127	0.019	0.45	0.207	1.95E-03	0.022	0.013	0.124	166
R155	S128	0.024	0.45	0.207	3.63E-03	0.022	0.013	0.124	166
R156	S81	0.011	0.45	0.308	4.50E-04	0.022	0.013	0.124	166
R157	S82	9.50E-03	0.45	0.308	9.00E-05	0.022	0.013	0.124	166
R158	S83	0.013	0.45	0.308	3.60E-04	0.022	0.013	0.124	166
R159	S84	0.015	0.45	0.308	4.50E-04	0.022	0.013	0.124	166
R160	S85	0.017	0.45	0.308	5.40E-04	0.022	0.013	0.124	166
R161	S86	0.027	0.45	0.308	7.90E-04	0.022	0.013	0.124	166
R162	S101	0.029	0.45	0.308	1.47E-03	0.022	0.013	0.124	166
R163	S122	0.012	0.45	0.308	2.20E-04	0.022	0.013	0.124	166
R164	S123	0.019	0.45	0.308	4.00E-04	0.022	0.013	0.124	166
R165	S124	0.024	0.45	0.308	6.60E-04	0.022	0.013	0.124	166
R166	S146	6.60E-03	0.45	0.155	9.80E-04	5.50E-03	3.18E-03	0.124	692
R167	S147	7.60E-03	0.45	0.155	1.16E-03	5.50E-03	3.18E-03	0.124	692
R168	S148	0.01	0.45	0.155	1.87E-03	5.50E-03	3.18E-03	0.124	692
R169	S149	0.014	0.45	0.155	4.57E-03	5.50E-03	3.18E-03	0.124	692
R170	S150	0.019	0.45	0.155	4.43E-03	5.50E-03	3.18E-03	0.124	692
R171	S151	0.028	0.45	0.155	0.011	5.50E-03	3.18E-03	0.124	692
R172	S153	5.50E-03	0.45	0.155	5.40E-04	5.50E-03	3.18E-03	0.124	692
R173	S154	0.011	0.45	0.155	2.05E-03	5.50E-03	3.18E-03	0.124	692
R174	S155	3.90E-03	0.45	0.154	2.60E-04	5.50E-03	3.18E-03	0.124	692
R175	S156	0.022	0.45	0.155	6.76E-03	5.50E-03	3.18E-03	0.124	692
R176	RS146	6.10E-03	0.45	0.155	7.60E-04	5.50E-03	3.18E-03	0.124	692
R177	RS147	7.50E-03	0.45	0.155	8.40E-04	5.50E-03	3.18E-03	0.124	692
R178	RS148	0.01	0.45	0.155	1.73E-03	5.50E-03	3.18E-03	0.124	692
R179	RS154	0.011	0.45	0.155	1.87E-03	5.50E-03	3.18E-03	0.124	692
R180	RS156	0.022	0.45	0.155	6.94E-03	5.50E-03	3.18E-03	0.124	692
R181	S157	3.70E-03	0.45	0.207	2.70E-04	5.50E-03	3.18E-03	0.124	692
R182	S158	6.70E-03	0.45	0.208	1.70E-04	5.50E-03	3.18E-03	0.124	692
R183	S159	0.011	0.45	0.209	5.30E-04	5.50E-03	3.18E-03	0.124	692
R184	S160	0.014	0.45	0.206	1.06E-03	5.50E-03	3.18E-03	0.124	692
R185	S161	0.028	0.45	0.206	3.72E-03	5.50E-03	3.18E-03	0.124	692
R186	S167	0.022	0.45	0.207	2.31E-03	5.50E-03	3.18E-03	0.124	692
R187	S168	0.024	0.45	0.206	2.73E-03	5.50E-03	3.18E-03	0.124	692
R188	S170	0.019	0.45	0.208	1.62E-03	5.50E-03	3.18E-03	0.124	692
R189	S171	8.90E-03	0.45	0.205	2.60E-04	5.50E-03	3.18E-03	0.124	692
R190	S172	0.027	0.45	0.205	3.65E-03	5.50E-03	3.18E-03	0.124	692
R191	S173	0.054	0.45	0.205	0.015	5.50E-03	3.18E-03	0.124	692
R192	S162	0.016	0.45	0.308	4.00E-04	5.50E-03	3.18E-03	0.124	692
R193	S163	0.022	0.45	0.308	5.70E-04	5.50E-03	3.18E-03	0.124	692

	R194	S164	0.027	0.45	0.308	8.80E-04	5.50E-03	3.18E-03	0.124	692
	R195	S165	0.042	0.45	0.308	2.03E-03	5.50E-03	3.18E-03	0.124	692
	R196	S166	0.065	0.45	0.308	5.22E-03	5.50E-03	3.18E-03	0.124	692
	R197	S169	0.024	0.45	0.311	5.30E-04	5.50E-03	3.18E-03	0.124	692
	R198	S174	9.80E-03	0.45	0.308	9.00E-05	5.50E-03	3.18E-03	0.124	692
	R199	S175	0.017	0.45	0.308	1.70E-04	5.50E-03	3.18E-03	0.124	692
	R200	S176	0.027	0.45	0.308	8.80E-04	5.50E-03	3.18E-03	0.124	692
	R201	S177	0.054	0.45	0.311	3.08E-03	5.50E-03	3.18E-03	0.124	692
	R202	S207	0.011	0.45	0.155	1.08E-03	5.50E-03	6.35E-03	0.124	174
	R203	S208	0.027	0.45	0.155	7.03E-03	5.50E-03	6.35E-03	0.124	174
	R204	S209	0.02	0.45	0.155	4.13E-03	5.50E-03	6.35E-03	0.124	174
	R205	S211	0.017	0.45	0.155	2.55E-03	5.50E-03	6.35E-03	0.124	174
	R206	S212	9.50E-03	0.45	0.155	8.30E-04	5.50E-03	6.35E-03	0.124	174
	R207	S210	8.70E-03	0.45	0.205	2.60E-04	5.50E-03	6.35E-03	0.124	174
	R208	S213	0.014	0.45	0.205	6.10E-04	5.50E-03	6.35E-03	0.124	174
	R209	S214	0.02	0.45	0.205	1.27E-03	5.50E-03	6.35E-03	0.124	174
	R210	S215	0.028	0.45	0.205	2.39E-03	5.50E-03	6.35E-03	0.124	174
	R211	S216	0.039	0.45	0.205	4.94E-03	5.50E-03	6.35E-03	0.124	174
	R212	S217	0.058	0.45	0.205	9.51E-03	5.50E-03	6.35E-03	0.124	174
	R213	S21S	0.021	0.45	0.31	3.40E-04	5.50E-03	6.35E-03	0.124	174
	R214	S219	0.028	0.45	0.31	4.50E-04	5.50E-03	6.35E-03	0.124	174
	R215	S220	0.04	0.45	0.31	1.17E-03	5.50E-03	6.35E-03	0.124	174
	R216	S221	0.057	0.45	0.31	2.57E-03	5.50E-03	6.35E-03	0.124	174
Poggi et al.	R217	D1	0.162	0.6	0.9	0.00004	0.000842	0.004	0.12	67
(2004)	R218	D2	0.162	0.6	0.9	0.00007	0.001684	0.004	0.12	134
	R219	D3	0.162	0.6	0.9	0.00011	0.003368	0.004	0.12	268
	R220	D4	0.162	0.6	0.9	0.00018	0.006736	0.004	0.12	536
	R221	D5	0.162	0.6	0.9	0.00032	0.013471	0.004	0.12	1072
Murphy et al.	R222	A	0.0048	0.38	0.467	9.9E-06	0.011781	0.006	0.14	417
(2007)	R223	C	0.0074	0.38	0.467	0.000025	0.016022	0.006	0.14	567
	R224	D	0.0048	0.38	0.467	0.000012	0.016022	0.006	0.14	567
	R225	E	0.0143	0.38	0.467	0.000075	0.01885	0.006	0.14	667
	R226	G	0.0048	0.38	0.467	0.000013	0.01885	0.006	0.14	667
	R227	H	0.0143	0.38	0.467	0.0001	0.037699	0.006	0.14	1333
	R228	I	0.0094	0.38	0.467	0.000034	0.037699	0.006	0.14	1333
	R229	A6	0.0017	0.38	0.298	0.000003	0.011781	0.006	0.07	417
	R230	B6	0.0094	0.38	0.298	8.04E-05	0.011781	0.006	0.07	417
	R231	C6	0.0048	0.38	0.298	2.42E-05	0.011781	0.006	0.07	417
	R232	A1	0.0017	0.38	0.236	1.06E-05	0.011781	0.006	0.07	417
	R233	B1	0.0094	0.38	0.236	0.000116	0.011781	0.006	0.07	417
	R234	C1	0.0048	0.38	0.236	4.27E-05	0.011781	0.006	0.07	417
	R235	A2	0.0017	0.38	0.14	1.73E-05	0.011781	0.006	0.07	417
	R236	B2	0.0094	0.38	0.14	0.000487	0.011781	0.006	0.07	417
	R237	C2	0.0048	0.38	0.14	0.000301	0.011781	0.006	0.07	417
	R238	A3	0.0017	0.38	0.105	0.000124	0.011781	0.006	0.07	417
	R239	C3	0.0048	0.38	0.105	0.000666	0.011781	0.006	0.07	417
	R240	A5	0.0017	0.38	0.088	0.000284	0.011781	0.006	0.07	417
	R241	C5	0.0048	0.38	0.088	0.00134	0.011781	0.006	0.07	417
	R242	C6D	0.0048	0.38	0.298	2.03E-05	0.037699	0.006	0.07	1333
	R243	C2D	0.0048	0.38	0.14	0.000366	0.037699	0.006	0.07	1333
	R244	A2D	0.0017	0.38	0.14	4.74E-05	0.037699	0.006	0.07	1333
	R245	A3D	0.0017	0.38	0.105	0.000232	0.037699	0.006	0.07	1333
Liu et al. (2008)	R246	L1.4	0.0114	0.3	0.097	0.003	0.006136	0.00635	0.076	194
	R247	L1.5	0.0114	0.3	0.101	0.003	0.012272	0.00635	0.076	388
	R248	L1.6	0.0114	0.3	0.087	0.003	0.003068	0.00635	0.076	97
	R249	L3.1	0.0114	0.3	0.114	0.003	0.015708	0.00635	0.076	496
	R250	L3.2	0.0114	0.3	0.115	0.003	0.015708	0.00635	0.076	496
	R251	L3.3	0.0114	0.3	0.118	0.003	0.015708	0.00635	0.076	496
	R252	L3.4	0.0114	0.3	0.119	0.003	0.015708	0.00635	0.076	496
	R253	L3.5	0.0114	0.3	0.114	0.003	0.015708	0.00635	0.076	496
	R254	L3.6	0.0114	0.3	0.119	0.003	0.015708	0.00635	0.076	496
Nezu and Sanjou	R255	A-10	0.0072	0.4	0.15	0.000777	0.1848	0.008	0.05	3676
(2008)	R256	B-10	0.0072	0.4	0.15	0.000652	0.0924	0.008	0.05	1838
	R257	C-10	0.0072	0.4	0.15	0.000544	0.0476	0.008	0.05	947
	R258	C-21	0.0025	0.4	0.0625	0.001553	0.0476	0.008	0.05	947
	R259	C-22	0.003	0.4	0.075	0.001165	0.0476	0.008	0.05	947
	R260	C-23	0.004	0.4	0.1	0.000653	0.0476	0.008	0.05	947
	R261	C-24	0.005	0.4	0.125	0.00046	0.0476	0.008	0.05	947

	R262	C-25	0.006	0.4	0.15	0.000364	0.0476	0.008	0.05	947
	R263	C-26	0.008	0.4	0.2	0.000196	0.0476	0.008	0.05	947
Yan (2008)	R264	e1	0.0144	0.42	0.12	0.0128	0.056549	0.006	0.06	2000
	R265	e2	0.0232	0.42	0.18	0.0048	0.056549	0.006	0.06	2000
	R266	e3	0.031	0.42	0.24	0.0022	0.056549	0.006	0.06	2000
	R267	e4	0.0378	0.42	0.3	0.0012	0.056549	0.006	0.06	2000
	R268	f1	0.0146	0.42	0.12	0.0072	0.028274	0.006	0.06	1000
	R269	f2	0.0227	0.42	0.18	0.0031	0.028274	0.006	0.06	1000
	R270	f3	0.0302	0.42	0.24	0.0015	0.028274	0.006	0.06	1000
	R271	f4	0.0368	0.42	0.3	0.0011	0.028274	0.006	0.06	1000
	R272	g1	0.0151	0.42	0.12	0.0037	0.014137	0.006	0.06	500
	R273	g2	0.0227	0.42	0.18	0.0026	0.014137	0.006	0.06	500
	R274	g3	0.0302	0.42	0.24	0.0011	0.014137	0.006	0.06	500
	R275	g4	0.0368	0.42	0.3	0.00065	0.014137	0.006	0.06	500
Yang (2008)	R276	RH2Q1	0.0075	0.45	0.075	0.00141	0.004398	0.002	0.035	1400
	R277	RH2Q2	0.0105	0.45	0.075	0.00269	0.004398	0.002	0.035	1400
					(B) Flexible vegetation					
Kouwen et al. (1969)	F1	1	0.002756	0.61	0.1506	0.0005	0.098175	0.005	0.1	5000
	F2	2	0.016956	0.61	0.2527	0.001	0.098175	0.005	0.1	5000
	F3	3	0.085496	0.61	0.3819	0.003	0.098175	0.005	0.085	5000
	F4	4	0.009081	0.61	0.1519	0.005	0.098175	0.005	0.1	5000
	F5	7	0.013163	0.61	0.1509	0.01	0.098175	0.005	0.1	5000
	F6	8	0.082736	0.61	0.2422	0.0094	0.098175	0.005	0.05	5000
	F7	9	0.043805	0.61	0.3503	0.001	0.098175	0.005	0.1	5000
	F8	10	0.04087	0.61	0.25	0.0049	0.098175	0.005	0.1	5000
	F9	11	0.038064	0.61	0.4	0.0005	0.098175	0.005	0.1	5000
	F10	12	0.019398	0.61	0.3	0.0005	0.098175	0.005	0.1	5000
	F11	13	0.006479	0.61	0.1496	0.003	0.098175	0.005	0.1	5000
	F12	14	0.006717	0.61	0.2002	0.0005	0.098175	0.005	0.1	5000
	F13	15	0.049593	0.61	0.3	0.003	0.098175	0.005	0.095	5000
	F14	16	0.009643	0.61	0.2001	0.001	0.098175	0.005	0.1	5000
	F15	17	0.047949	0.61	0.199	0.01	0.098175	0.005	0.06	5000
	F16	18	0.028379	0.61	0.3498	0.0005	0.098175	0.005	0.1	5000
	F17	19	0.073151	0.61	0.2998	0.005	0.098175	0.005	0.075	5000
	F18	20	0.028914	0.61	0.3	0.001	0.098175	0.005	0.1	5000
	F19	21	0.01647	0.61	0.2	0.003	0.098175	0.005	0.1	5000
	F20	22	0.02257	0.61	0.2	0.005	0.098175	0.005	0.1	5000
	F21	24	0.113978	0.61	0.3486	0.005	0.098175	0.005	0.06	5000
	F22	25	0.05568	0.61	0.3986	0.001	0.098175	0.005	0.09	5000
	F23	26	0.01264	0.61	0.2527	0.0005	0.098175	0.005	0.1	5000
	F24	27	0.075324	0.61	0.3508	0.003	0.098175	0.005	0.09	5000
	F25	28	0.031014	0.61	0.2594	0.003	0.098175	0.005	0.1	5000
	F26	29	0.142281	0.61	0.383	0.0049	0.098175	0.005	0.055	5000
	F27	30	0.003729	0.61	0.1491	0.001	0.098175	0.005	0.1	5000
Dunn et al. (1996)	F28	13	0.179	0.91	0.367052	0.0036	0.005449	0.00635	0.152	172
	F29	14	0.18	0.91	0.231752	0.0101	0.005445	0.00635	0.115	172
	F30	15	0.093	0.91	0.257085	0.0036	0.005432	0.00635	0.132	172
	F31	16	0.179	0.91	0.230072	0.0036	0.001366	0.00635	0.097	43
	F32	17	0.078	0.91	0.278509	0.0036	0.012284	0.00635	0.161	388
	F33	18	0.179	0.91	0.283482	0.0101	0.012297	0.00635	0.121	388
Jarvela (2003)	F34	R4-1	0.04	1.1	0.306	0.0015	0.07389	0.0028	0.205	12000
	F35	R4-2	0.1	1.1	0.3084	0.0036	0.07389	0.0028	0.155	12000
	F36	R4-3	0.04	1.1	0.4065	0.0005	0.07389	0.0028	0.23	12000
	F37	R4-4	0.1	1.1	0.4041	0.0013	0.07389	0.0028	0.19	12000
	F38	R4-5	0.143	1.1	0.407	0.002	0.07389	0.0028	0.16	12000
	F39	R4-6	0.04	1.1	0.5044	0.0002	0.07389	0.0028	0.245	12000
	F40	R4-7	0.1	1.1	0.495	0.0006	0.07389	0.0028	0.22	12000
	F41	R4-8	0.1	1.1	0.7065	0.0002	0.07389	0.0028	0.26	12000
	F42	R4-9	0.143	1.1	0.7037	0.0003	0.07389	0.0028	0.215	12000
	F43	S3-1	0.04	1.1	0.4003	0.0004	0.003619	0.003	0.295	512
	F44	S3-2	0.1	1.1	0.3961	0.001	0.003619	0.003	0.2	512
	F45	S3-3	0.143	1.1	0.3942	0.0018	0.003619	0.003	0.17	512
Yang (2008)	F46	FH1Q1	0.0075	0.45	0.055	0.00361	0.004398	0.002	0.0226	1400
	F47	FH2Q1	0.0075	0.45	0.075	0.00151	0.004398	0.002	0.0275	1400
	F48	FH2Q2	0.0105	0.45	0.075	0.00266	0.004398	0.002	0.0253	1400
	F49	FH3Q1	0.0075	0.45	0.11	0.0007	0.004398	0.002	0.0339	1400
	F50	FH3Q2	0.0105	0.45	0.11	0.00079	0.004398	0.002	0.0309	1400

Kubrak et al. (2008)	F51	1.1.1	0.0433	0.58	0.2661	0.0087	0.005346	0.000825	0.163	10000
	F52	1.1.2	0.0384	0.58	0.2576	0.0087	0.005346	0.000825	0.163	10000
	F53	1.1.3	0.0333	0.58	0.2475	0.0087	0.005346	0.000825	0.164	10000
	F54	1.1.4	0.0274	0.58	0.2275	0.0087	0.005346	0.000825	0.164	10000
	F55	1.2.1	0.0422	0.58	0.2236	0.0174	0.005346	0.000825	0.161	10000
	F56	1.2.2	0.0385	0.58	0.2184	0.0174	0.005346	0.000825	0.162	10000
	F57	1.2.3	0.0333	0.58	0.2068	0.0174	0.005346	0.000825	0.161	10000
	F58	1.2.4	0.0274	0.58	0.1951	0.0174	0.005346	0.000825	0.162	10000
	F59	2.1.1	0.0525	0.58	0.2386	0.0087	0.001336	0.000825	0.153	2500
	F60	2.1.2	0.0425	0.58	0.2136	0.0087	0.001336	0.000825	0.154	2500
	F61	2.1.3	0.0332	0.58	0.1935	0.0087	0.001336	0.000825	0.155	2500
	F62	2.2.1	0.0751	0.58	0.2131	0.0174	0.001336	0.000825	0.132	2500
	F63	2.2.2	0.065	0.58	0.1925	0.0174	0.001336	0.000825	0.131	2500
	F64	2.2.3	0.0547	0.58	0.1799	0.0174	0.001336	0.000825	0.133	2500
	F65	3.1.1	0.0605	0.58	0.2386	0.0087	0.001336	0.000825	0.151	2500
	F66	3.1.2	0.0504	0.58	0.2234	0.0087	0.001336	0.000825	0.152	2500
	F67	3.1.3	0.0408	0.58	0.2005	0.0087	0.001336	0.000825	0.153	2500
	F68	3.2.1	0.0693	0.58	0.1962	0.0174	0.001336	0.000825	0.132	2500
	F69	3.2.2	0.0555	0.58	0.1876	0.0174	0.001336	0.000825	0.139	2500
	F70	4.1.1	0.0609	0.58	0.2421	0.0087	0.001336	0.000825	0.151	2500
	F71	4.1.2	0.05	0.58	0.2246	0.0087	0.001336	0.000825	0.153	2500
	F72	4.1.3	0.0408	0.58	0.2053	0.0087	0.001336	0.000825	0.156	2500
	F73	4.2.1	0.0693	0.58	0.2077	0.0174	0.001336	0.000825	0.138	2500
	F74	4.2.2	0.0466	0.58	0.1932	0.0174	0.001336	0.000825	0.142	2500
	F75	4.2.3	0.0553	0.58	0.1806	0.0174	0.001336	0.000825	0.143	2500
Okamoto and Nezu (2010)	F76	L1.1	0.021	0.4	0.15	0.002409	0.0478	0.008	0.03	951
	F77	L1.2	0.018	0.4	0.15	0.002211	0.0478	0.008	0.034	951
	F78	L1.3	0.015	0.4	0.15	0.001996	0.0478	0.008	0.036	951
	F79	L1.4	0.012	0.4	0.15	0.001646	0.0478	0.008	0.04	951
	F80	L1.5	0.0102	0.4	0.15	0.001414	0.0478	0.008	0.042	951
	F81	L1.6	0.009	0.4	0.15	0.001127	0.0478	0.008	0.044	951
	F82	L1.7	0.0072	0.4	0.15	0.000775	0.0478	0.008	0.046	951
	F83	L1.8	0.006	0.4	0.15	0.00056	0.0478	0.008	0.049	951
	F84	L2.1	0.0294	0.4	0.21	0.001489	0.0478	0.008	0.04	951
	F85	L2.2	0.0252	0.4	0.21	0.001366	0.0478	0.008	0.045	951
	F86	L2.3	0.021	0.4	0.21	0.001287	0.0478	0.008	0.051	951
	F87	L2.4	0.0168	0.4	0.21	0.001058	0.0478	0.008	0.056	951
	F88	L2.5	0.0143	0.4	0.21	0.000864	0.0478	0.008	0.058	951
	F89	L2.6	0.0126	0.4	0.21	0.000737	0.0478	0.008	0.06	951
	F90	L2.7	0.0101	0.4	0.21	0.000505	0.0478	0.008	0.063	951
	F91	L2.8	0.0084	0.4	0.21	0.000382	0.0478	0.008	0.068	951
	F92	L3.1	0.027	0.4	0.27	0.000623	0.0478	0.008	0.054	951
	F93	L3.2	0.0216	0.4	0.27	0.000541	0.0478	0.008	0.06	951
	F94	L3.3	0.0184	0.4	0.27	0.000486	0.0478	0.008	0.065	951
	F95	L3.4	0.0162	0.4	0.27	0.000439	0.0478	0.008	0.071	951
	F96	L3.5	0.013	0.4	0.27	0.000333	0.0478	0.008	0.075	951
	F97	L3.6	0.0108	0.4	0.27	0.000238	0.0478	0.008	0.078	951
	F98	L4.1	0.0315	0.4	0.315	0.00041	0.0478	0.008	0.064	951
	F99	L4.2	0.0252	0.4	0.315	0.00039	0.0478	0.008	0.068	951
	F100	L4.3	0.0214	0.4	0.315	0.000376	0.0478	0.008	0.076	951
	F101	L4.4	0.0189	0.4	0.315	0.000331	0.0478	0.008	0.081	951
	F102	L4.5	0.0151	0.4	0.315	0.000249	0.0478	0.008	0.084	951
	F103	L4.6	0.0126	0.4	0.315	0.00019	0.0478	0.008	0.096	951